EXPERIMENTAL INVESTIGATION OF NANOFLUID BEHAVIOR IN MICROCHANNELS

A THESIS SUBMITTED TO
THE GRADUATE SCHOOL OF NATURAL AND APPLIED SCIENCES
OF
MIDDLE EAST TECHNICAL UNIVERSITY

BY

EYLÜL ŞİMŞEK

IN PARTIAL FULFILLMENT OF THE REQUIREMENTS
FOR
THE DEGREE OF MASTERS OF SCIENCE
IN
MECHANICAL ENGINEERING

JUNE 2016

Approval of the thesis:

EXPERIMENTAL INVESTIGATION OF NANOFLUID BEHAVIOR IN MICROCHANNELS

submitted by **EYLÜL ŞİMŞEK** in partial fulfillment of the requirements for the degree of the **Master of Science in Mechanical Engineering Department, Middle East Technical University** by,

Prof. Dr. Gülbin Dural Ünver _____
Dean, Graduate School of **Natural and Applied Sciences**

Prof. Dr. Tuna Balkan _____
Head of Department, **Mechanical Engineering**

Assoc. Prof. Dr. Tuba Okutucu Özyurt _____
Supervisor, **Mechanical Engineering Dept., METU**

Examining Committee Members:

Prof. Dr. Zafer Dursunkaya _____
Mechanical Engineering Dept., METU

Assoc. Prof. Dr. Tuba Okutucu Özyurt _____
Mechanical Engineering Dept., METU

Assoc. Prof. Dr. H. Emrah Ünalan _____
Metallurgical and Materials Engineering Dept., METU

Asst. Prof. Dr. F. Nazlı Dönmezer _____
Mechanical Engineering Dept., METU

Assoc. Prof. Dr. Barbaros Çetin _____
Mechanical Engineering Dept., Bilkent University

Date: 28/06/2016

I hereby declare that all information in this document has been obtained and presented in accordance with academic rules and ethical conduct. I also declare that, as required by these rules and conduct, I have fully cited and referenced all material and results that are not original to this work.

Name, Last name :

Signature :

ABSTRACT

EXPERIMENTAL INVESTIGATION OF NANOFLUID BEHAVIOR IN MICROCHANNELS

Şimşek, Eylül

M.Sc., Department of Mechanical Engineering

Supervisor : Assoc. Prof. Dr. Tuba Okutucu Özyurt

June 2016, 113 pages

The present study investigates thermal and hydrodynamic performance of nanofluids in copper microchannels. Experiments are performed using spherical gold nanoparticles, and silver nanowires suspended in deionized (DI) water under constant heat flux condition. Polyvinylpyrrolidone (PVP) is used as the surfactant. In gold nanofluid experiments, effects of nanoparticle size (10, 50 and 100 nm), volumetric concentration (0.00064% - 0.0052%) and flow rate (100-140 μL/min) on the nanofluid performance are investigated in 70 μm × 50 μm rectangular microchannels. In silver nanofluid experiments, microchannels of 200 μm × 50 μm, 100 μm × 50 μm and 70 μm × 50 μm cross-sectional area are used. To investigate the surfactant effect, experiments are repeated with DI water, and a PVP – DI water solution. Among the investigated cases, the silver nanofluid showed the best thermal performance.

Both silver and gold nanofluids yielded higher convective heat transfer coefficient than PVP – DI water solution, however the golf nanofluid occasionally showed better thermal performance compared to DI water. Nanofluid stability is also observed. This study contributes to the literature by considering the surfactant effect on stability, as well as thermal and hydrodynamic performance of nanofluids. Silver nanowires are experimented for the first time in the literature in microchannel heat sinks. Results indicated that surfactants may significantly lower the heat removal by nanofluids. A long term stability is achieved for both gold and silver nanofluids. The particle size and the flow rate are two very important parameters that affect thermal performance. The nanofluid with silver nanowires is proved to be promising in microchannel cooling applications.

Keywords: Microchannel Cooling, Silver Nanofluid, Gold Nanofluid, Stability of Nanofluid

ÖZ

MİKROKANALLARDA NANOAKIŞKAN DAVRANIŞININ DENEYSEL İNCELENMESİ

Şimşek, Eylül

Yüksek Lisans, Makina Mühendisliği Bölümü

Tez Yöneticisi : Doç. Dr. Tuba Okutucu Özyurt

Haziran 2016, 113 sayfa

Bu çalışmada nanoakışkanların bakır mikrokanallardaki termal ve hidrodinamik performansı incelenmiştir. Deneyler, iyondan arındırılmış suyun içinde süspansiyon halinde bulunan küresel altın nanoparçacıklar ve gümüş nanoteller ile sabit ısı akısında gerçekleştirilmiştir. Yüzey aktif madde olarak da Polyvinylpyrrolidone (PVP) kullanılmıştır. Altın nanoakışkan ile yapılan deneylerde, parçacık boyutunun (10, 50, 100 nm), hacim bazlı konsantrasyonun (0.00064% - 0.0052%) ve akış hızının (100-140 μL/min) nanoakışkan performansındaki etkisi 70 μm × 50 μm'lik dikdörtgen mikrokanalda incelenmiştir. Gümüş nanoakışkan deneylerinde, 200 μm × 50 μm, 100 μm × 50 μm ve 70 μm × 50 μm kesit alanine sahip kanallar kullanılmıştır. Yüzey aktif maddenin etkisini incelemek için deneyler deiyonize su ve PVP – deiyonize su çözeltisi ile tekrarlanmıştır. İncelenen durumlar arasında, gümüş nanoakışkanın en iyi termal performansı göstermiştir.

Hem gümüş nanoakışkanlar hemde altın nanoakışkanların PVP - deiyonize su çözeltisinden daha yüksek taşınımlı ısı aktarım katsayısına sahip olduğu, fakat altın nanoakışkanın bazı durumlarda deiyonized sudan daha iyi termal performans gösterdiği gözlenmiştir. Nanokakışkanların stabilizasyonu da gözlenmiştir. Bu çalışma yüzey aktif maddenin nanoakışkanın stabilizasyonunda, ve de termal ve hidrodinamik performansındaki etkisini incelemesi ile literature katkıda bulunmuştur. Gümüş nanoteller mikrokanal ısı alıcılarında ilk defa kullanılmıştır. Sonuçlara göre yüzey aktif maddeler nanoakışkanlar tarafından uzaklaştırılan ısı miktarında önemli bir düşüşe sebep olabileceğini göstermiştir. Altın ve gümüş nanoakışkanlarda uzun süreli stabilizasyon başarılmıştır. Parçacık boyutu ve akış hızının termal performansı etkileyen en önemli iki faktördür. Gümüş nanoteller içeren nanoakışkanların mikrokanal soğutma uygulamalarında gelecek vaadettiği kanıtlanmıştır.

Anahtar Kelimeler: Mikrokanal ile Soğutma, Gümüş Parçacıklı Nanoakışkan, Altın Parçacıklı Nanoakışkan, Nanoakışkan Stabilizasyonu.

To my beautiful mother, Selma Şimşek

ACKNOWLEDGEMENTS

I would like to express my deepest gratitude to my supervisor Assoc. Prof. Dr. Tuba Okutucu Özyurt for her guidance. I greatly appreciate for her support throughout my master study. I have learned a lot from her in these three years. I am grateful to be a member of Dr. Tuba Okutucu's Micro and Nanoscale Energy Transport and Conversion Research Group and work with the members of this group.

I would like to express my thanks to Aziz Koyuncuoğlu who helped me alot throughout my study. He always answer my questions even my emails that were too long. He contributed my study a lot. I would also like to thank to Rahim Jafari who helped me to get familiar with the experimental setup.

I would like to thank to Şahin Çoşkun for his support in the nanofluid preparation and visualization. He never refused my requests. I learned a lot from him. I would also like to thank to Doğa Doğanay for his support.

I would like to thank my workmates alot, Heat Laboratory become a home for me rather than a laboratory. I would like to thank Onur Özkan, who is my first roommate and my biggest supporter. I would like to thank Göker Türkakar, I have learnt alot about academic life and I was very happy during our shares. I would like to thank Mine Kaya who become a sister rather than a friend, I love to work with her. I would like to thank Serhat Bilyaz for being great friend and his support during this three year. I would like to thank Berke Harmancı for being a great roommate. I would like to thank Mustafa Yalçın a lot, he helped me to solve all problems that I have faced about experimental setup. This research has been financially supported by the Scientific and Technological Research Council of Turkey under grant number TÜBİTAK 108M515.

TABLE OF CONTENTS

LIST OF FIGURES

FIGURES

LIST OF TABLES

TABLES

NOMENCLATURE

Symbols		
A	Area	μm^2 , m^2
C	Constant	-
c_p	Specific heat	kj/kgK
d	Diameter	μm
D_h	Hydraulic diameter	μm
f	Friction factor	-
$\overline{h}$	Convective heat transfer coefficient	W/m^2K
H	Height	μm
I	Current	A
k	Thermal conductivity	W/mK
l	Axial distance	m
L	Length	mm, cm
$\dot{m}$	Mass flow rate	kg/s
n	Empirical shape factor	
P	Pressure	Pa
$\dot{P}$	Pumping power	W
Pe	Peclet number	-
Pr	Prandtl number	-
q	Heat	W
q''	Heat flux	W/m^2
r_h	Hydraulic diameter	μm
R	Resistance	Ohm

Re	Reynolds number	-
T	Temperature	ºC
u	Mean velocity	m/s
V	Voltage	V
$\dot{V}$	Volumetric flow rate	m^3/s
W	Width	mm , μm
x	Entry length	m
Greek Symbols		
γ	Aspect ratio (height/width)	-
μ	Dynamic viscosity	$N.s/m^2$
ρ	Density	kg/m^3
χ	Particle volume fraction	-
ψ	Sphericity	-
Subscripts		
bf	Base fluid	
e	Electrical	
f	Fluid	
fd	Fully developed	
h	Hydrodynamic	
i	Inlet	
max	Maximum	
measured	Experimentally measured value	
minor	Minor losses	
N	Number of resistance	
nf	Nanofluid	
np	Nanoparticle	
norm	Normalized	
PCB	Printed circuit board	
r	Room temperature	
o	Outlet	
t	Thermal	

Abbreviations	
CMOS	Complementary metal oxide semiconductors
DAQ	Data acquisition system
EG	Ethylene glycol
FM	Figure of merit
LMTD	Log mean temperature difference
PCB	Printed circuit board
PEC	Performance energetic coefficient
PVP	Polyvinylpyrrolidone
RTD	Resistive temperature detector
SDBS	Sodium dodecylbenzene sulfonate
SEM	Scanning electron microscope
SOCT	Sodium octanoate
STEM	Scanning transmission electron microscope
TEM	Transmission electron microscope

CHAPTER 1

INTRODUCTION

1.1. Motivation

The use of microchannel heat sinks is an attractive option for removing high heat fluxes that accumulate in small volumes in disciplines including, but not limited to, microelectronics, optics and lasers. Microchannel cooling was first demonstrated by Tuckerman and Pease when they pumped water through microchannels to remove up to 790 W/cm^2 heat flux from a silicon substrate [1]. Water is the most commonly used working fluid in microchannels owing to its high heat capacity, although other fluids are also in use. In addition to single phase flow applications, multiphase flow is also being considered for its potential to remove even higher heat fluxes [2]. However, the flow instabilities, unpredictable heat transfer rates, and increased pressure drop caused by fluid acceleration during phase change, remain as significant challenges that require further investigation. Nanofluid was first proposed as a promising new working fluid which could improve the heat sink performance, reduce pumping requirements, or both [3]. For cooling applications, nanofluids are obtained by adding high thermal conductivity nanoparticles (1-100 nm in diameter) to a lower thermal conductivity base fluid as a way to increase the mean thermal conductivity of the fluid for enhanced heat transfer. Thermal conductivity values of different materials are given in Table 1.

Table 1. Thermal conductivity values at 300 K

Materials	Thermal Conductivity (W/mK)
Water	0.613
Ethylene Glycol	0.252
Engine Oil	0.145
Gold (Au)	317
Silver (Ag)	235
Copper (Cu)	401
Aluminum (Al)	237

Thermal conductivity values of solids are order of magnitudes higher than liquids. Aluminum oxide (Al_2O_3), copper (Cu), copper oxide (CuO), gold (Au), silver (Ag), titanium dioxide (TiO_2), and carbon nanotubes (CNT)'s are the most commonly used nanoparticle materials while the most common liquids used as base fluids were listed as deionized water, engine oil (EO), acetone, and ethylene glycol (EG).

The methods used to prepare nanofluids can be classified as one-step method and two-step method. In one-step method, the synthesis of the nanoparticles and their dispersion within the base fluid are made in the same step, while in two-step methods, the nanoparticles are synthesized first, and their dispersion within the base fluid is done in a separate step. Experimental results prove that nanofluids have better heat transfer performance than their corresponding base fluids which was also supported by theoretical studies [4–6].

The motivation of this study is to understand the thermal and hydrodynamic behavior of nanofluids in a CMOS compatible copper microchannel. If higher heat transfer performance can be achieved with the usage of the nanofluid, cooling with nanofluids in the microchannel can be a good solution for cooling especially for industrial applications.

Stability of the nanofluid is also investigated which is important to enlarge application areas of nanofluids. Moreover, the effect of surfactant on the heat transfer performance and pumping power of nanofluids in microchannels is studied. Also different coolants are prepared to enlarge the viewpoint of the study. Convection heat transfer coefficient and pumping power are compared for the flow of each coolant through the microchannels.

1.2. Literature Review

A large number of experimental and theoretical studies on nanofluid flow in microchannels have been reported in the literature. A brief information on a few experimental studies investigating nanofluid behavior is provided in Table 2. In Table 2, A, L, W, H, D_h and d are the cross-sectional area, length, width, height, hydraulic diameter and nanoparticle diameter, respectively.

In forced convection heat transfer studies, mostly metal oxide nanoparticles are investigated rather than pure metallic nanoparticles [7]. Nitiapiruk et al. [8] performed experiments with TiO_2 – water nanofluid in microchannels and used different thermophysical models in the calculation of Nusselt number and friction factor. Volumetric concentrations of the TiO_2 nanofluid samples were changing between 0.5% - 2%. Constant heat fluxes were applied to microchannels of 40 channels each with 283 μm width, 800 μm height and 50 mm length. After the experiments, three different models were used to calculate the thermal conductivity and viscosities of the TiO_2 nanofluids. It was observed that Nusselt numbers calculated by different models were very close to each other so that different models can conveniently be used to estimate the thermal conductivity of the nanofluids. Moreover, TiO_2 nanofluids yielded higher heat transfer coefficients than by water for all volumetric concentrations.

Peyghambarzadeh et al. [9] examined the performance of two different nanofluids (water based CuO and Al_2O_3) in a heat sink that consists of 17 rectangular microchannels with a cross section area of 400 μm × 560 μm.

A constant heat flux is applied to the system and the average heat transfer coefficient with respect to Reynolds number is plotted to compare the performances of the two nanofluids. It is observed that both nanofluids had better thermal performances compared to pure water. Up to a critical Reynolds number, the ratio of nanofluid Nusselt number to that of the base fluid (*Nu* ratio) increased with Reynolds number, however, Reynolds numbers higher than a limiting value caused a decrease in the *Nu* ratio. This limiting Reynolds number value should not be exceeded so that the use of nanofluids can be justified at high heat removal rates.

Rimbault et al. [10] performed experiments with a CuO- water nanofluid that flowed through a rectangular microchannel. The CuO nanoparticle size was 29 nm with three different volumetric concentrations (0.24%, 1.03%, 4.5%). In this study, the performance energetic coefficient (PEC) is defined to evaluate nanofluid's overall energetic performance which is the ratio of the heat transfer to the pumping power. Results showed that the CuO nanofluid with 4.5% concentration has the lowest heat transfer coefficient and PEC. The best performance was observed at 1.03% concentration.

Effect of pure metallic nanoparticles such as gold and silver are investigated in limited studies. The performance of spherical silver nanoparticles in DI water in micro-pin fin heat sinks is studied [11]. A relatively low volumetric concentration (0.00197% - 0.0121%) of the silver nanoparticles is used in the experiments. In addition, a solution with the surfactant is prepared to compare its thermal and hydrodynamic performance relative to pure DI water, and to the silver nanofluid. It is observed that the nanofluid yielded higher heat transfer coefficient than the surfactant and DI water solution. On the other hand, the silver nanofluid caused higher pressure drop relative to the surfactant – DI water solution.

Table 2. Summary of some experimental studies using nanofluids for cooling

Ref.	Channel Dimensions	Base fluid	Particle type	Particle Size /Shape	Nanofluid Concentration	Stability Enhancement Method	Investigated Parameters	Boundary Conditions	Results
[9]	*A*: 400 µm x 560 µm *L* : 50 mm	Water	CuO Al_2O_3	CuO : d_{avg}:40 nm Semi-spherical Al_2O_3 : d_{avg}: 20nm Spherical	0.1 vol.% - 1 vol.%	pH adjustment, high speed magnetic stirrer, ultrasonic agitation	Thermal performance	Constant heat flux	Both nanofluids had better thermal performances compared to pure water
[12]	*W*: 8 mm *L*: 12 mm *H*: 100 µm	Water	SiO_2	*d* : 20 nm	0.2 wt.% 0.5 wt.% 1 wt.%	Ultrasonic bath, probe type sonicator	Thermal performance at different flow rates	Constant bottom wall temperature	There is a critical flow rate for nanofluids which should not be exceeded to have higher heat transfer than the base fluid.
[13]	d_{h1} : 571 µm d_{h2} : 762 µm d_{h3} : 1454 µm	Ethanol	Al_2O_3	Particle size < 50 nm	0.01 vol.%- 0.5 vol.%	Ultrasonic bath	Friction factor and heat transfer coefficient in single and two phase flow of nanofluids	Constant heat flux	In two phase flow, oscillations in the pressure drop and enhancement in heat transfer coefficient are observed.
[14]	*L* : 50 mm *W* : 14 mm *H*: 295 µm	Water	Al_2O_3 Ag Hybrid (Al_2O_3+Ag)	d_1: 30 nm d_2: 50 nm d_3 :70nm d_4: 90 nm	3 vol.%	-	Heat transfer coefficient	Constant heat flux	Hybrid nanofluids can be used for similar heat transfer performance with less cost.
[15]	D_h : 218 µm D_h : 303 µm	Water Ethylene Glycol	Alumina	*d* :45 nm	0.25 vol. % 0.5 vol. % 1 vol. %	Sonication, pH variation	Effect of volumetric concentration and base fluid on heat transfer performance	Constant heat flux	Nusselt number increases with increasing volumetric concentration, alumina - water nanofluid has better performance than alumina – EG nanofluid.

Although the nanofluid usage seems advantageous, it has some important limitations which should be considered. One of the limitations in the usage of nanofluids is the difficulty of maintaining a long term stability.

In a recent study the stability of nanofluids have been reviewed [16]. Extensive research has been performed to understand the stability of nanofluids, as well as parameters that alter the stability. Firstly, the nanofluid stability is affected by the chemical structure of the base fluid and the particle. The particle morphology also has an important effect [17]. While investigating the stability of nanofluids, interaction between the base fluid and the nanoparticle should be considered. Therefore, the selection of base fluid and the material of the nanoparticle are crucial. Secondly, the production method of the nanofluid can change the stability of the nanofluids. The one step method has the known advantage over the two step method due to reduction in agglomeration. Factors that influence the stability are listed by Li et al. [18] as nanoparticle concentration, dispersants, particle diameter, and properties such as density and dynamic viscosity of nanofluids. In addition, the sonication time, pH of the solvent, the zeta potential, the fluid temperature and the sunlight exposure are factors that affect dispersion stability of nanofluids [19]. Surely, all these parameters should be investigated comprehensively. However, it is observed that the most frequently examined parameters are the nanoparticle concentration and the surfactant amount.

Nanoparticle aggregation and sedimentation, can be detected by measuring the zeta potential, transmission electron microscope (TEM) and sediment photography capturing which are commonly used indicators in nanofluid stability evaluation in the literature.

Ultra Violet Spectrophotometer: UV–Vis spectrophotometry is one of the mostly used instruments to assess the stability of nanofluids. The principle used in the UV-Vis spectrophotometry is that intensity of light differs while light is passing through a fluid due to scattering and absorption. In UV-Vis spectrophotometer, sediment volume versus sedimentation time is measured to evaluate the stability of nanofluids [20].

In UV-Vis spectrophotometry, any type of base fluid can be used whereas zeta potential measurements have a constraint for the viscosity of the base liquid. Owing to this characteristic, stability can be determined by UV-Vis spectrophotometer for various nanofluids with different base fluids.

Sediment Photography Capturing: In the sediment photography capturing (SPC) method, photographs of nanofluids are taken to visualize sedimentation after a certain time interval. Photographs help the visualization of whether any color difference or settlement occurs in the nanofluid. Although SPC is an effective tool for the observation of nanofluid stability, it is not enough alone so it is carried out together with another method [20].

Transmission Electron Microscopy (TEM): Transmission Electron Microscopy is a common method used to observe characteristics of nanoparticles in the base fluid before and after dispersion [21]. Standard transmission electron microscopy consists of five steps. In the first step, there should be a stable nanofluid in suspension form. Secondly, a drop from the suspension is sampled as a specimen to be placed on the TEM holder. Thirdly, the specimen is put in the vacuum oven. Specimen is then heated in the oven to obtain a dry sample. In this step, the specimen could also be dried naturally in the air but this takes longer time. After this step, the solid particles are coated by Palladium (Pd) and Gold (Au). Lastly, the solid particles are placed in the vacuum chamber of the TEM for their pictures to be taken [22]. In TEM, due to the usage of dried samples, a realistic placement of the nanoparticles in nanofluids cannot be obtained [20].

If the stability of the nanofluids cannot be achieved, agglomerations start immediately after the production of the nanofluid. These agglomerations cause the formation of large scale particles and it will be hard to estimate the particle size inside the nanofluid. The non-uniform particle size distributions and large particles may cause some operational problems in the system. One of the common methods used in the literature is the addition of a surfactant into the nanofluid. This approach is simple and efficient for the long term stability relative to the other methods.

The aim in the usage of surfactant in nanofluids is basically to minimize the agglomeration of the particles and prevent possible particle-particle interactions.

There are several stability enhancement methods used in the literature in an attempt to understand how to increase stability and how stability affects the thermal conductivity. Some of these methods are used in the production step to produce stable nanofluids, whereas some are used to break down the agglomerations after the production steps. Adding a surfactant, varying pH, sonication, using an ultrasonic probe, high shear homogenization and magnetic stirrer are commonly used stability enhancement methods. One of these techniques or a combination of them may be used to obtain stable nanofluids.

Addition of surfactant: Surfactant addition is an easy method to enhance the stability of nanofluids by altering the surface properties. When a liquid is in contact with a solid, there occurs interaction between the solid boundaries and the liquid. If the fluid molecules are attracted to the solid boundaries, then the boundary gets wetted which is called wettability. On the contrary, fluid molecules may be repulsed by the solid boundaries, in which case the fluid does not wet the boundaries. In nanofluids, there is interference between nanoparticles and base fluid. By adding a surfactant to the nanofluid, an increase is observed in the contact of two materials which means an increase in the wettability. Surfactants that are mainly used in literature are gum arabaic, sodium octanoate (SOCT), salt, oleic acid, sodium dodecyl benzene sulfonate (SDBS) and polyvinyl pyrrolidone (PVP). Critical points in the addition of surfactant to the nanofluids are the selection and the amount of the surfactant. The proper amount of the surfactant should be used so that it will provide sufficient coating on nanoparticle surfaces to compensate Van der Waal forces [20].

Varying pH: Setia et al. stated that by switching pH value of the base fluid, the surface charges of the nanoparticles and the interaction between the nanoparticle and the base fluid is changed [20]. The same pH value does not have the same effect on different nanofluids because every nanofluid has a different optimum pH value.

Sonication: Sonication is a method which differs from the other methods mentioned above because external forces are applied to the nanofluids to breakdown the agglomeration of nanoparticles [23].

The working principle of sonication is that compression waves are created by electrical signals which are oscillating at a high frequency [20]. In the end, agglomerations break into small pieces which may increase the stability of the nanofluids. Similar to the optimum pH value, an optimum sonication time is needed to enhance the stability.

Ultrasonic probe, magnetic stirrer, homogenizer and high shear mixer have similar principles with that of sonication. These methods are used by different researchers to increase the stability of nanofluids. Hwang et al. [24] made experiments to compare the physical stability enhancement methods. It is seen that the stirrer is not an effective way to break down agglomeration. In another comparison study, it is concluded that ultrasonic probe is the most effective dispersion method due to its higher energy density [25]. Lee et al. [26] investigated the stability by visualization over a time period. In this study, water based-Al_2O_3 nanofluids which have 1% and %2 volumetric concentrations are used. Photographs of the nanofluids are taken immediately after mixing and after 30 days. In this period, nanofluids are waited in the glass beakers. From the photographs of 1% and 2% samples, it can be observed that there is settlement and color difference between the top and the bottom of the glass beaker in both nanofluids. Hence, it can be concluded that the stability of nanofluids changes with time. This settlement can cause some problems in the long term usage such as thermal performance reduction in the system.

On the other hand, the effect of surfactant usage on the heat transfer performance of the nanofluids has not been investigated and the surfactant layer on the particle surface has not been taken into account in the theoretical models. The mechanisms that were addressed so far in the literature need to be improved by the addition of surfactants since the particle-particle and particle-liquid interaction change in their presence.

If a surfactant exists in the nanofluid, an additional interface between the liquid and the nanoparticle will form. Especially the morphology of the interfacial layer changes with the surfactant layer. This additional layer is expected to change the thermophysical properties of the solution too. In recent models, the thermal conductivity of a nanofluid is formulated by considering a liquid layer [27,28].

However, the surfactant layer thickness has not been considered in these models. Yang et al. [29] conducted a study that accounts surfactant layer during the calculation of the thermal conductivity of the nanofluid. This study is an extended version of the Leong et al. [30] by defining interfacial layer as a combination of the surfactant layer base fluid molecules. Thermal conductivity results obtained from this model is compared with the experimental studies which used nanofluids with low volumetric concentration and surfactant as a stability enhancement technique.

The surfactant layer thickness and its geometry are variable parameters since the surfactant encapsulates the nanoparticles. If the nanoparticle size is large, the surfactant layer thickness will be large too and neglecting the surfactant layer in the calculations may cause great errors therefore this study is important because addition of surfactant layer into the model will decrease the error amount.

In the experimental studies reported in the literature, the heat transfer performance of the nanofluid is compared with the base fluid rather than surfactant added base fluid. The amount of surfactant in the solution is usually neglected. However the addition of the surfactant may significantly change the thermophysical properties of nanofluids.

There is only one experimental study [31] that compares the thermal performance of water, a water and gum Arabic solution and a water based carbon nanotube suspension with gum Arabic as the surfactant. The density, viscosity and thermal conductivity of these fluids were measured. Also their heat transfer performance in a concentrated tube heat exchanger was investigated by calculating corresponding Nusselt numbers. In this heat exchanger, oil was the hot fluid exchanging heat with three alternative coolants.

In the low temperature band, the thermal conductivity of the gum Arabic solution was nearly equal to that of water, whereas the carbon nanotube suspension in water with gum Arabic had higher thermal conductivity. Results of their experiments showed that carbon nanotubes yielded the highest Nusselt number, and the lowest Nusselt number was obtained with pure water.

Other than the mentioned study by Rashmi et al. [31] experiments with different surfactant/nanoparticle types, concentrations and in different Reynolds number ranges are yet to be performed. In addition, more theoretical studies are needed to support experimental results.

1.3. Scope and Outline

The main objective of this study is to investigate the thermal and hydrodynamic behavior of nanofluids in microchannels experimentally. Experiments have been performed to understand whether promising results will be obtained from nanofluids in cooling applications and effects of different parameters on this behavior have been examined. The outline of this study is given below.

In Chapter 2, the experimental setup is presented and the setup elements are explained. Then the experimental procedure is explained step by step. Later, in the data analysis part, the flow regimes and governing equations are given.

In Chapter 3, the results of the gold nanofluid experiments are given. At the beginning of this chapter, preparation of the coolants are explained. Moreover, stability investigation of the coolants used in the experiments are performed. In the end of this chapter, results for the heat transfer and hydrodynamic performance are reported and interpreted.

In Chapter 4, silver nanofluid experiments are explained. Again, the preparation of the coolants for this experiment is mentioned. Stability of the silver nanofluids are visualized. The assumptions made in the data analysis are clearly stated. Finally, the results of the gold nanofluid experiments and their discussion are given.

In Chapter 5, a summary of the present study is given. Afterwards, conclusions obtained from the results of gold and silver nanofluid experiments are given in order. In the end of this chapter, future work that can be considered after this work are given.

CHAPTER 2

EXPERIMENTAL SETUP AND PROCEDURE

This chapter consists of three parts: experimental setup, experimental procedure and data analysis. In Section 2.1, components of the experimental setup are shown and their working principles are described. In Section 2.2, the procedure of the experiments is explained step by step in detail. In the last section of Chapter 2, methods that have been used to analyze experimental data are explained and a comparison between these methods have been made.

2.1. Experimental Setup

Cooling experiments with microchannels have been conducted using the setup shown in Figure 1 which was previously used for water experiments in [32]. The setup consists of:

a) Constant DC power supply (Agilent DC power supply N5771A, 300V, 5A)

b) Single output DC power supply (Agilent DC power supply, 30V, 3A)

c) Digital syringe pump (NewEra NE-4000)

d) Data acquisition system (Agilent LXI data acquisition 34972A)

e) Computer

f) Microchannel test section

One of the DC supplies (Agilent DC power supply N5771A) in the setup provides voltage across the heaters of the microchannel and across the resistances of the electrical circuit.

The other DC power supply (Agilent DC power supply, 30V) provides lower voltage values and is used in the setup to feed the pressure transducers which are located at the inlet and outlet of the channels. Digital syringe pump supplies fluid at a constant volumetric flow rate to cool the on-chip heaters. A data acquisition system (DAQ) is used to record data and transfer it to the computer for data analysis during the experiments.

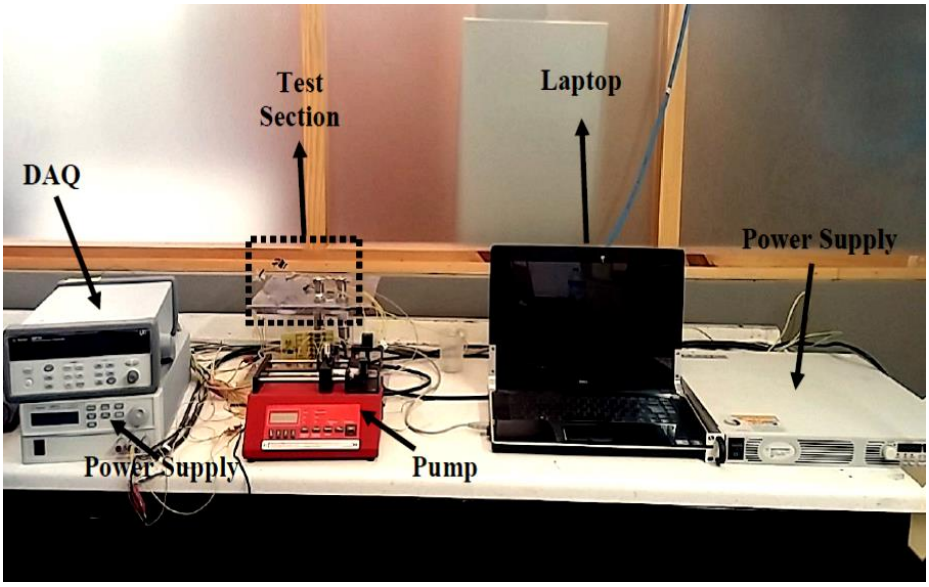

Figure 1. A photograph of the experimental setup used in this work

The microchannel test section consists of a monolithic microchannel chip and electrical circuit. An enlarged view of the test section is shown Figure 2 for clarity. In this electrical circuit, there is a printed circuit board (PCB), the heaters' resistances and a large resistance (500 Ω).

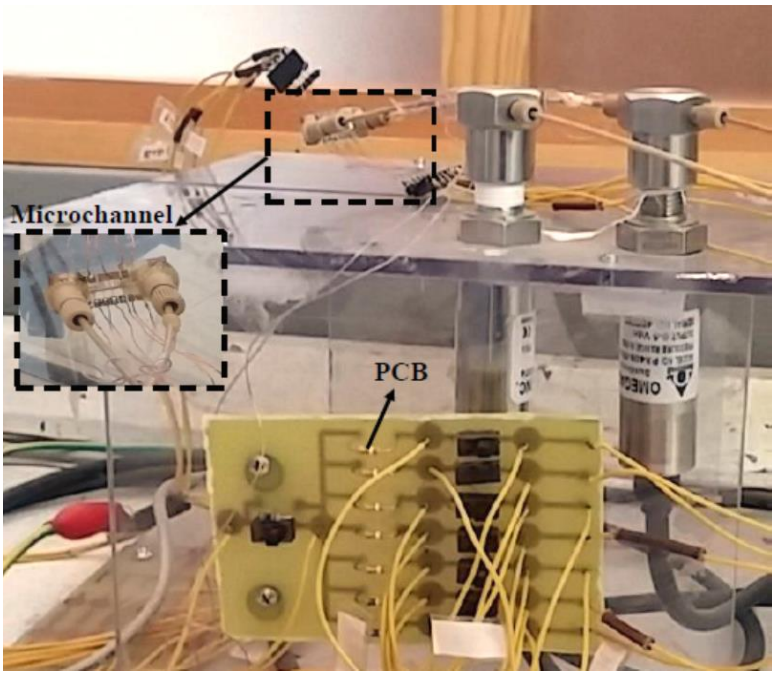

Figure 2. A photograph of the microchannel test section used in this study

This electrical circuit is attached to a holder and designed to enable the measurement of current flow through the heaters during the experiments and the calibrations. On the PCB, there are seven parallel branches each consisting of one on/off switch for the heater resistance and one resistance for current/voltage measurement which are connected as parallel to each other. The entire branch is in series with a larger resistance. The circuit is simply shown in Figure 3. The larger resistance is added in the circuit so that the supplied current can be decreased to minimize the heat generation during the calibration. The on/off switches are used to control the heater resistances and large resistance so that during the calibration larger resistance can be added to the circuit, however during the experiments it is eliminated to have higher current flow through the circuit.

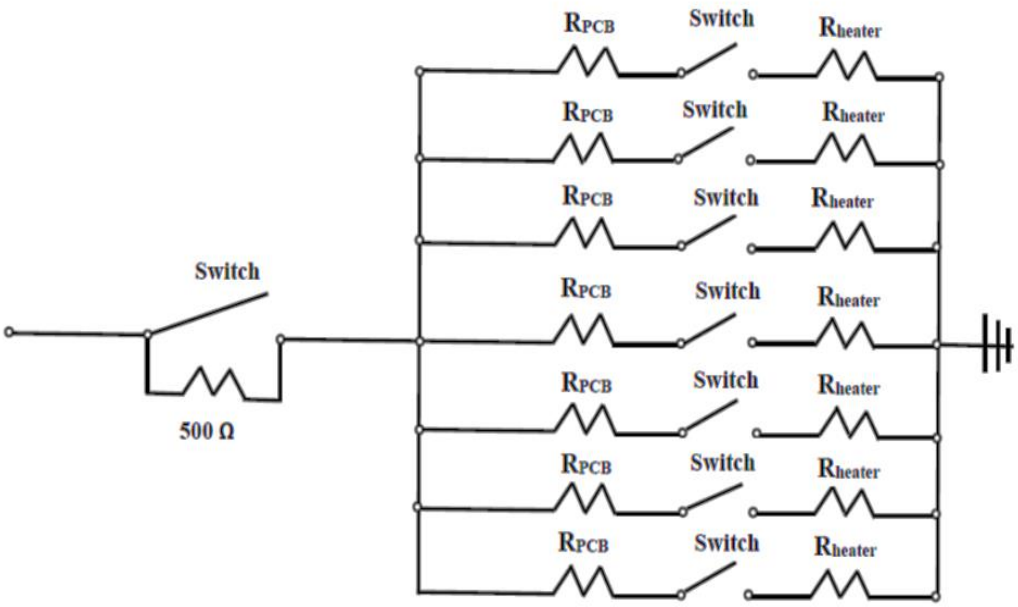

Figure 3. Schematic diagram of the electrical circuit

The resistances on the PCB are nearly the same at room temperature and they are equal to 4 Ω. The heater resistance values vary between 20 – 80 Ω. The resistances of the heaters located in the same microchannel are nearly equal so that each branch's resistance values are close to each other. For this reason, voltage difference across each branch is equal to each other enabling an equal current flow in each branch. This way, an equal voltage and current is supplied to the heaters so that each heater located in the microchannel provides equal power along the channel length. During the experiments, voltage values across each resistance on the PCB, and the heater resistance are recorded. However in the DAQ that has been used in this experiment, only two direct current measurements can be recorded. Therefore, only the currents passing through branch 3 and branch 5 can be recorded. The other current values are calculated by the help of this electrical circuit. The details of the current calculation is explained in Section 2.3.

Extensive research has been performed on the fabrication of microchannels because they can be remove concentrated heat fluxes in electronic circuits due to their high surface area to volume ratios.

Furthermore, microchannels may be located close to the source of the heating which will help decrease the thermal resistance. Different microchannel fabrication techniques suggested in the literature such as silicon etching are described in [33].

Microchannel chips that are used in this study has been fabricated by Koyuncuoglu [33]. Microchannels have been fabricated by electroplating method in which a metal microchannel can be manufactured on the top of the complementary metal oxide semiconductor (CMOS) circuit. The fabrication steps can be explained as follows. In the first step, titanium heaters are fabricated onto a glass substrate beneath the microchannel along the channel length. These titanium heaters are put at the bottom of the channels to demonstrate the heat generated by a circuit. Totally seven heaters which are made from titanium have been placed at the bottom layer of the channel. During the fabrication, titanium heaters are used for two main purposes: to generate heat, and to measure the temperatures in these points as resistance temperature detectors. The resistances of titanium heaters change linearly with respect to temperature which enables the temperature measurements throughout the channel. Right before the first and after the last heaters, resistance temperature detectors (RTD) are laid for assessing the fluid inlet and outlet temperatures. A thin parylene layer was coated over the heaters so that there will not be interaction between the microchannel and heaters. Parylene material is selected because of its low electrical conductivity for electrical insulation. Moreover, pads and led of the titanium heaters are coated with gold to minimize connection resistances.

In the second stage, a gold seed layer is deposited and microchannels are fabricated using copper electroplating method. By copper electroplating, copper is coated on the exposed surface at the seed layer. The details of the fabrication technique is described in [34]. The duration of the electroplating alters the heat transfer area of the microchannel.

In this fabrication method, the side walls are made from copper material and the bottom wall material is gold. However, the top wall of the channel differs according to the duration of the electroplating. If the duration of the electroplating process is increased, copper may partially or fully cover the channel top wall which may cause an additional heat transfer wall area [32].

In this study, rectangular microchannels of 50 μm height, 1.42 cm length and 200 μm, 100 μm and 70 μm width have been fabricated. Wall thickness of the channels are equal to 20 μm. It is observed that the 70 μm × 50 μm channel has no gap at the top wall so that it has 3 copper walls and a gold bottom wall, which means that it has four heated walls. The 100 μm × 50 μm and 200 μm × 50 μm microchannels may have a gap at the top wall, so that the gap should be extracted during the calculation of the heated area. A schematic of a single channel cross section which has a parylene gap has been demonstrated in Figure 4.

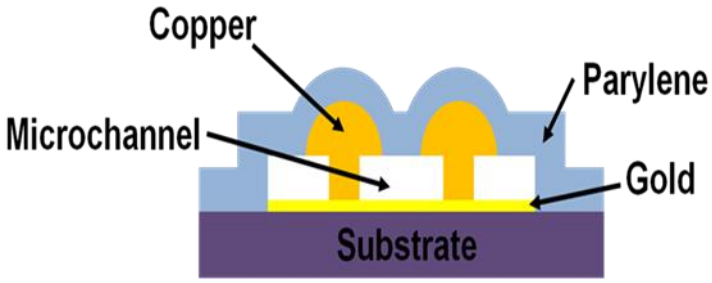

Figure 4. Schematic of a single channel cross section [32]

2.2. Procedure

Before starting experiments, microchannels are prepared for the experiments. After the fabrication, the channels are put in an acetone bath. Channels are kept in acetone for a day to eliminate photoresist remains in the channels.

Microchannels are checked by an optical microscope to make sure that there is no any photoresist remaining which may cause blockage of the fluid flow through the channel. This step is visualized in Figure 5.

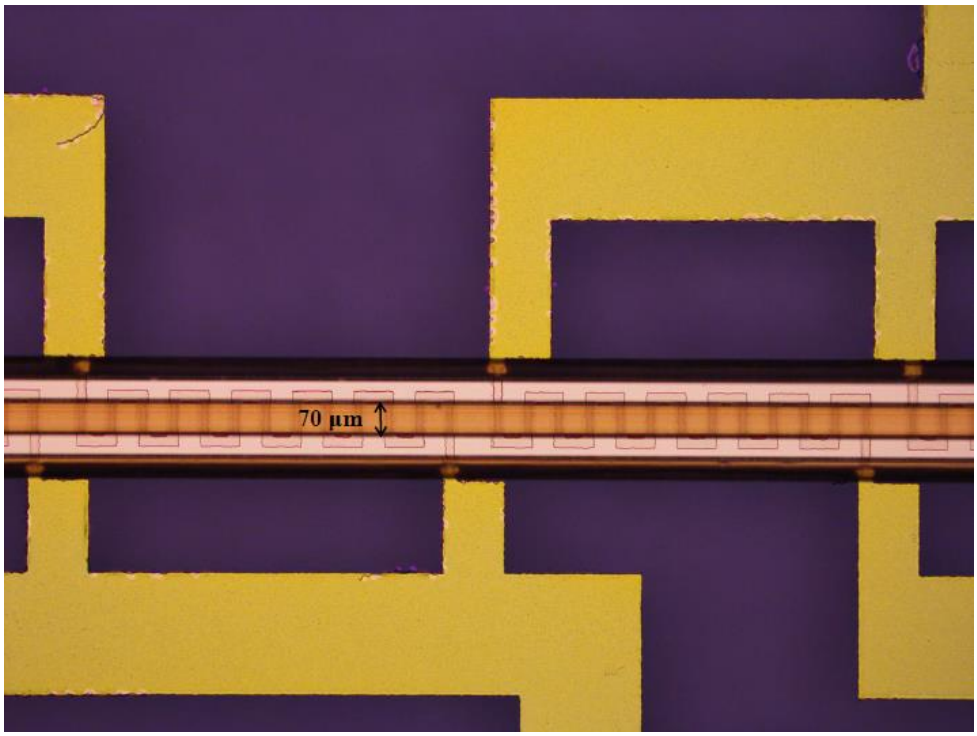

Figure 5. Optical microscope image of the microchannel

If the flow is observed through the microchannels, then no further placement in the acetone bath is required. Then Upchurch nanoports are glued by epoxy to the inlet and outlet of the microchannels. The amount of the glue should be adjusted very carefully. A low amount of glue will cause a fluid leakage, however if excess glue is used it will cause blockage of the channel. Therefore the amount of the epoxy should be carefully adjusted. A channel with glued nanoports is shown in Figure 6. In the end of the preparation, electrical connections of the microchannels are soldered.

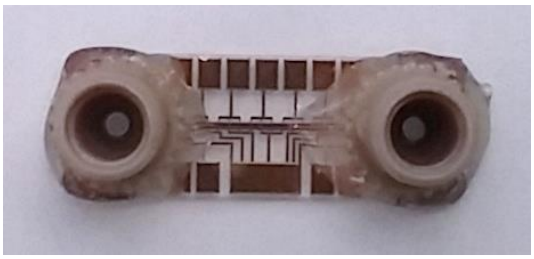

Figure 6. A photograph of the microchannel with inlet and outlet ports

At the beginning of the experiments, the calibration of the microchannel is performed to determine the temperature-resistance behavior of the heaters and RTD of the channel. During the calibration, the microchannel test section is covered by a removable enclosure and a very low voltage (0.2 V which is the minimum voltage output of the power supply used in this setup) is applied to the heaters. Large resistance that is located at the electrical circuit is at the on position, so that overall resistance of the circuit becomes very large that cause very low current to flow through the circuit. This low voltage and current is applied to the circuit to eliminate burning of the heaters or any damage to the heaters because there is not any flow during the calibration.

The temperature inside the enclosure changed between 20 to 80°C and steady state conditions are achieved at 6 different temperatures in this range. From the data handled during the calibration, the resistance values of the heaters at different temperatures are obtained and the corresponding calibration curves are plotted. During the calibration, two thermocouples (T-type) are located in the enclosure for the measurement of air temperature at different locations, hence a total of 4 thermocouples (including the inlet and outlet thermocouples) are used. The average of the four temperature readings are taken to estimate a uniform temperature throughout the enclosure. In Figure 7, the calibration curves of the seven heaters are presented. The RTD calibration curves are shown in Figure 8. From the calibration curves, a linear relationship between the temperature and the resistance of the heaters and the RTDs can be found. Therefore the temperature at the different positions of the microchannel can be estimated.

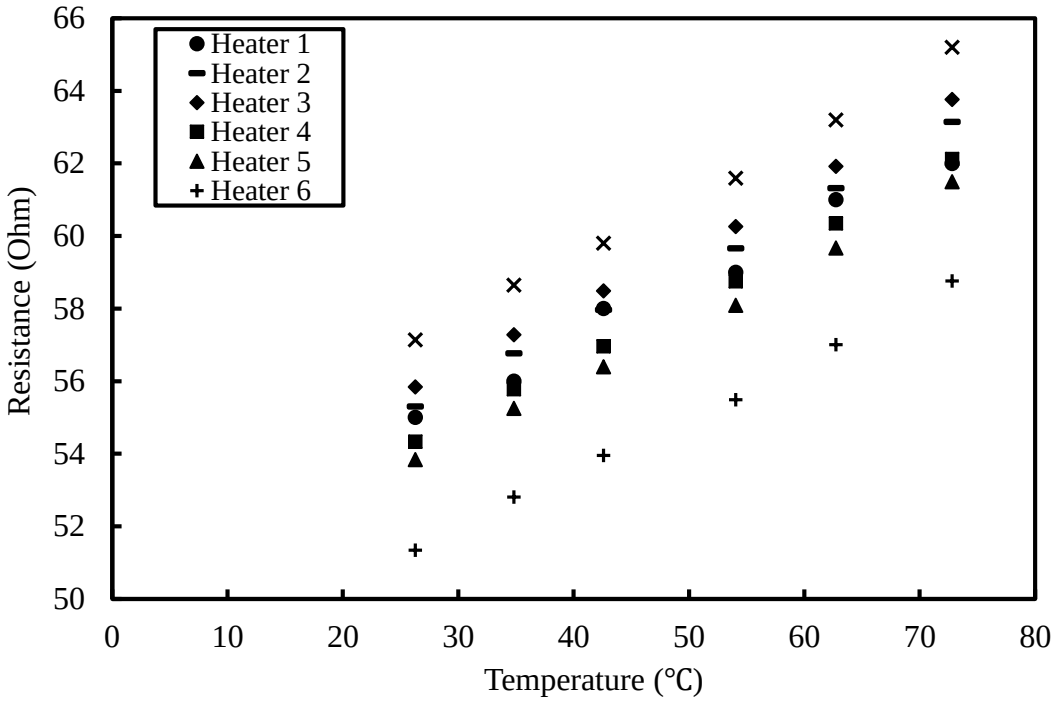

Figure 7. Heater calibration curves of 70 μm × 50 μm channel

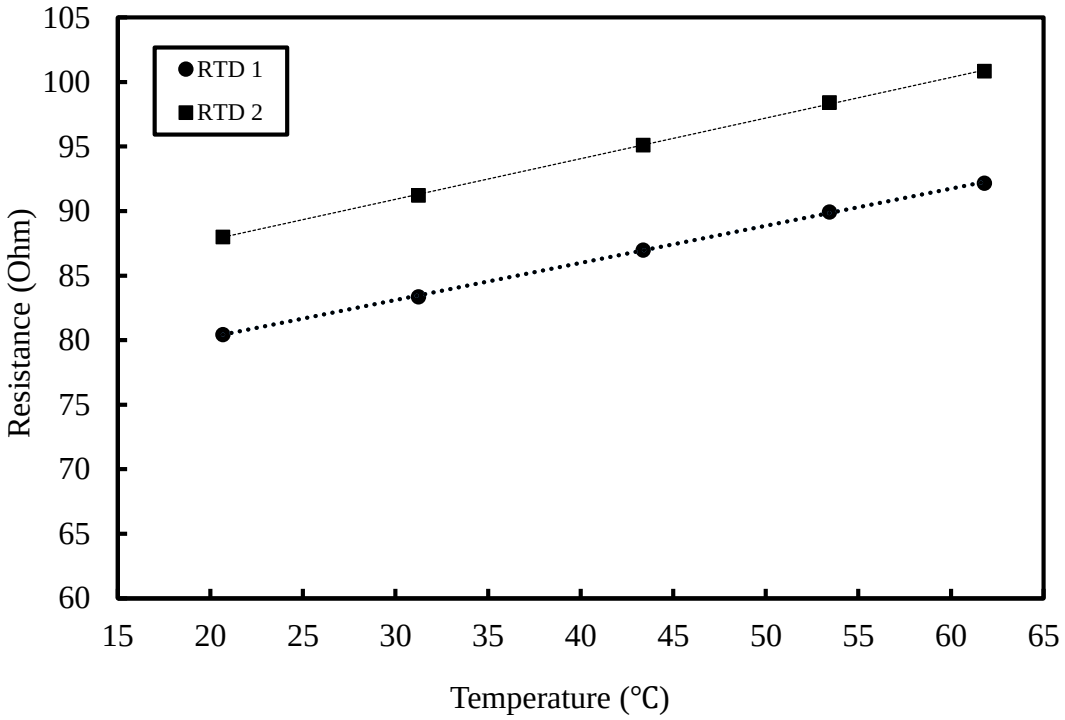

Figure 8. RTD calibration curves of 70 μm × 50 μm channel

All heaters have very close resistance values and they have a similar resistance – temperature trend. Similar to the heaters, RTDs have close resistance values. The rate of increase of the resistance values with an increase in temperature are very close to each other. To see this trend, normalized resistance values of the heaters and RTDs are defined in Equation (1).

$$R_{\text{norm}} = \frac{R}{R_{\text{i}}} \tag{1}$$

In this equation, R_{norm} is the normalized resistance value, R is the resistance value at any temperature and R_{i} is the resistance value at room temperature. The change in normalized resistance values of microchannel heaters with temperature is given in Figure 9. The normalized resistance values for three sample heaters are given in the figure.

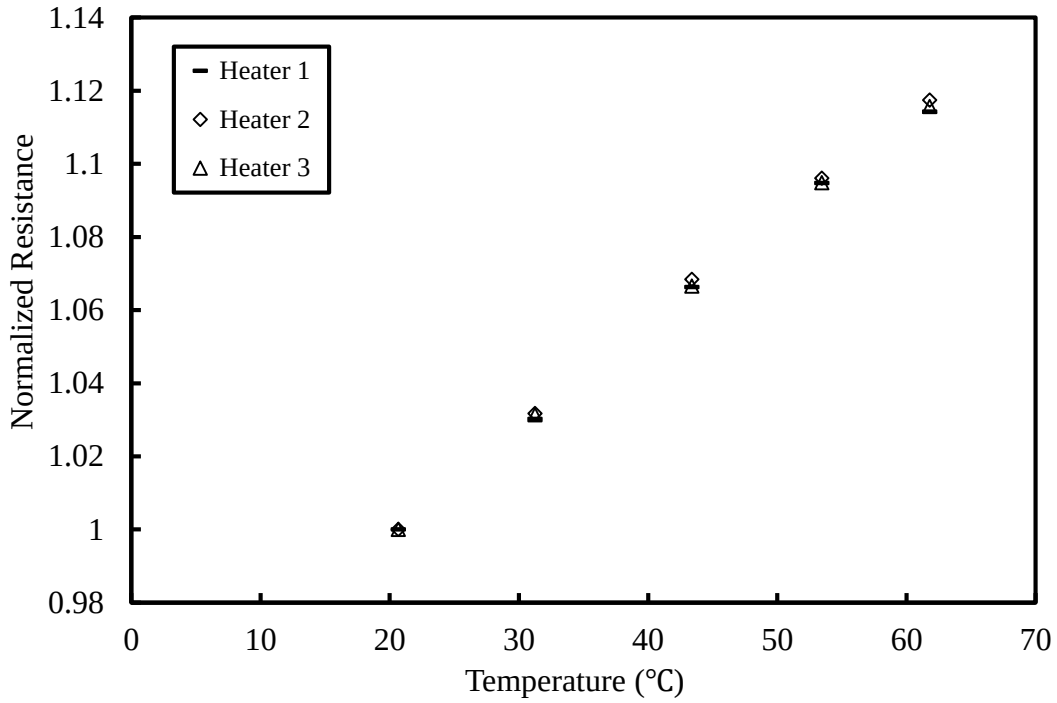

Figure 9. Normalized resistance curve of the 70 μm × 50 μm channel heaters

The normalized resistance values of the RTDs are given in Figure 10. Although RTD values at room temperature are different, their normalized resistance values are the same.

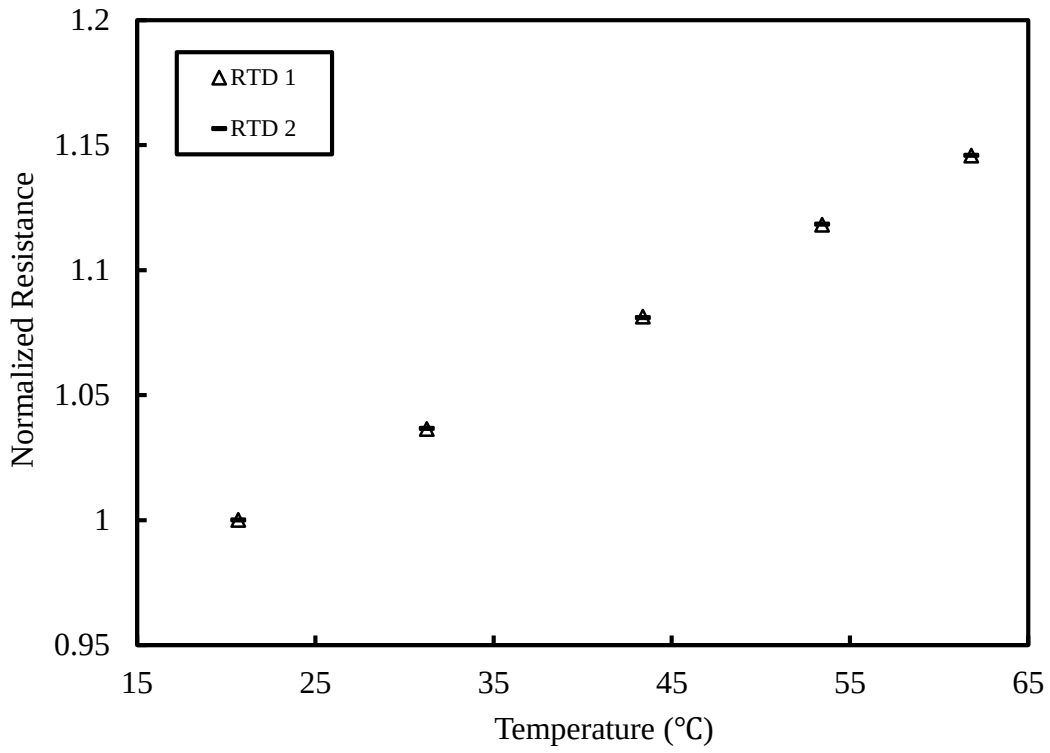

Figure 10. Normalized resistance curve of the 70 μm × 50 μm channel RTDs

Before starting the tests, the heater resistances of the microchannels are checked using a multimeter to make sure that their values are close to each other. Even if the resistances are not exactly the same, they should be close to each other. After mounting the microchannel on the test section, all resistance values of the electrical circuit is also checked using the DAQ. All resistance values are recorded within a short time interval. If there is a large difference between the heaters' resistance values, this may indicate a short circuit in the resistances or any touch between the heaters' soldering points.

In the experiments, firstly, deionized (DI) water is pumped through the microchannel test section and data is recorded by a DAQ before applying any voltage to the system. This test is performed to ensure that there is not any liquid leakage or disconnection in the electrical connections of the channel which may cause damage to the channel.

Also the resistance values are checked using DAQ after the voltage is applied to the heaters. Again, a voltage may cause a damage in the microchannel heaters, therefore their resistance values should be checked before performing further experiments.

Experiments started with DI water. Then a solution of the surfactant that is used in the nanofluids in DI water is tested. Lastly, the experiments are performed with nanofluids with surfactant. This order is preferred to eliminate the contamination of channel walls by the nanoparticles or the surfactant. Furthermore, between two tests, the experimental apparatus is cleaned with pure water. The same experimental procedure is repeated for all fluids. The homogeneity of all three are maintained by pre-sonication in an ultrasonic bath for 5 to 10 minutes. After achieving a homogenous solution, the coolant is pumped with a constant volumetric flow rate through the test section.

A voltage is applied across the heater circuit to yield a constant heat flux. During the experiments, the voltage, current, temperature and pressure values are recorded by the DAQ system. The temperature of the fluid at the inlet and outlet of the microchannel is measured by a T-type thermocouple and the pressure drop across the microchannel is measured by Omega absolute pressure transducers. The cooling performance of the fluid for a constant surface heat flux is observed and convective heat transfer coefficient is calculated in the low Reynolds number range. The effects of different parameters such as the volumetric flow rate, the amount of surfactant, the size and the volumetric concentration of the nanofluid on the thermal and hydrodynamic performance are investigated. The flow rate range has been arranged according to the pressure drop limitation of the pump. As the channel dimension gets smaller, obtaining high flow rates gets harder. Due to the pressure limitations of the pump, the total pressure drop throughout the channel should not exceed 75 kPa.

2.3. Data Analysis

In the data analysis part of this study, methods to interpret experimental data are explained. This section is divided in two parts.

Firstly the determination of the heat transfer coefficient is stated and the steps during the calculation of average convective heat transfer coefficient are stated. In the second part, analysis that is needed to evaluate the hydrodynamic performance of the microchannel is given.

2.3.1. Data analysis for thermal performance in the microchannel

In the thermal analysis part, convective heat transfer coefficient for different cases are calculated. To determine the convective heat transfer coefficient, regardless of method used, the channel wall temperatures and the inlet and outlet temperatures of the fluid should be known. Then the heat flux and convective heat transfer coefficient can be calculated. The calculation steps are explained in detail in this section.

Firstly, the wall temperatures of the channels should be determined. As an initial stage in the determination of the wall temperatures, heater temperatures need to be calculated. The heater temperatures can be calculated from the recorded data and calibration curve that have been plotted before the experiments. During the experiments, the voltage across the heaters and resistors on the PCB are recorded by DAQ, but the current flowing through only two branches can be measured directly. The currents passing from the 3rd (PCB3) and 5th (PCB5) branches of the circuit are recorded directly by DAQ which is shown in Figure 3. With the recorded voltage and current values, the resistance on the PCB and heaters located at the 3rd and 5th branches can be calculated directly from Equation (2).

$$R = \frac{V}{I} \tag{2}$$

In this equation R is the resistance, V is the voltage and I is the current. Since the currents flowing through other branches cannot be measured directly with DAQ an approach should be followed to determine these current values.

The resistances on the PCB have been recorded before the experiments as mentioned in Section 2.2. However, the resistance values on the PCB will change during the experiment due to the change in the temperature. Resistance values of PCB3 and PCB5 can be calculated during the experiment and before the experiment, so that the percentage change during the experiment can be calculated for both.

If we assume that the changes in the other PCB resistances are the same as the average change of these two resistances (R_{PCB3} and R_{PCB5}), we can calculate other PCB resistance values during the experiment with the following equation:

$$R_{\mathrm{PCB}} = R_{\mathrm{PCB,r}} \times \left[1 + \frac{\frac{R_{\mathrm{PCB,3}} - R_{\mathrm{PCB,3r}}}{R_{\mathrm{PCB,3r}}} + \frac{R_{\mathrm{PCB,5}} - R_{\mathrm{PCB,5r}}}{R_{\mathrm{PCB,5r}}}}{2}\right] \quad (3)$$

In Equation (3), R_{PCB} is the resistance value on the PCB during the experiment, $R_{\mathrm{PCB,r}}$ is the resistance value on the PCB at the room temperature, $R_{\mathrm{PCB,3}}$ is the resistance value of PCB3, $R_{\mathrm{PCB,3r}}$ is the resistance of PCB3 at room temperature, $R_{\mathrm{PCB,5}}$ is the resistance value of PCB5 and $R_{\mathrm{PCB,5r}}$ is the resistance of PCB5 at room temperature.

After the calculation of resistance on the PCB, the current passing through the PCB can be calculated from Equation (4).

$$I = \frac{V_{\mathrm{PCB}}}{R_{\mathrm{PCB}}} \quad (4)$$

In this equation, V_{PCB} is the voltage across the PCB resistance which is recorded by DAQ during the experiment and R_{PCB} is the resistance of the PCB that has been calculated from Equation (3).

Since the heater resistance and the one on the PCB are parallel to each other at each branch, the current passing through the PCB is equal to the current passing through the heater. The heater resistances are calculated from Equation (5).

$$R_{\mathrm{heater,N}} = \frac{V_{\mathrm{heater,N}}}{I} \tag{5}$$

In Equation (5), $R_{\mathrm{heater,N}}$ is the resistance of the heater during the experiment (N is the heater number other than 3 and 5 since these two heater resistances can be calculated directly), V_{heater} is the voltage across the heater recorded from the DAQ and I is the current that passes through the heater which is found from Equation (4). The temperatures of the heaters can be estimated from the calibration curves of the channels that are illustrated in Figure 7.

After this point, the temperature of the channel walls can be estimated. There are mainly two layers between the heaters and the channel which are parylene layer and gold layer. The thickness of the parlyene layer is 0.4 μm and the gold layer thickness is 0.45 μm.

Due to the low thermal resistance at the gold layer, the temperature drop in this layer is neglected, only temperature drop through the parylene layer is considered. Assuming one dimensional heat conduction through the parylene, the temperature at the channel wall is estimated from Equation (6).

$$T_{\text{wall,N}} = T_{\text{heater,N}} - q''_{\text{heater,N}} \times \frac{l_{\text{parylene}}}{k_{\text{parylene}}} \quad (6)$$

In this equation, $T_{\text{wall,N}}$ is the wall temperature of the channel near heater N, $T_{\text{heater,N}}$ is the heater temperature that has been found from the heater's calibration curve, $q''_{\text{heater,N}}$ is the heat flux generated by the heater, l_{parylene} is the parylene thickness and k_{parylene} is the thermal conductivity of the parylene. $q''_{\text{heater,N}}$ is calculated from Equation (7).

$$q''_{\text{heater,N}} = \frac{V_{\text{heater,N}} \times I_{\text{heater,N}}}{A_{\text{heater}}} \quad (7)$$

After the evaluation of the wall temperatures along the channel, the second step is the determination of the inlet and outlet temperatures of the fluid. The inlet fluid temperature of the fluid is taken as the thermocouple reading which is located near the inlet of the channel. The exact location of the inlet thermocouple does not really affect the temperature since up to the inlet reservoir of the microchannel, there is not any heating of the fluid. However, the outlet fluid temperature cannot be determined with this methodology because the outlet thermocouple cannot be exactly at the outlet of microchannel due to fittings. In this work, it is assumed that the fluid temperature increased at the same rate as the wall temperature in the fully developed region of the flow [34]. This method is illustrated in Figure 11.

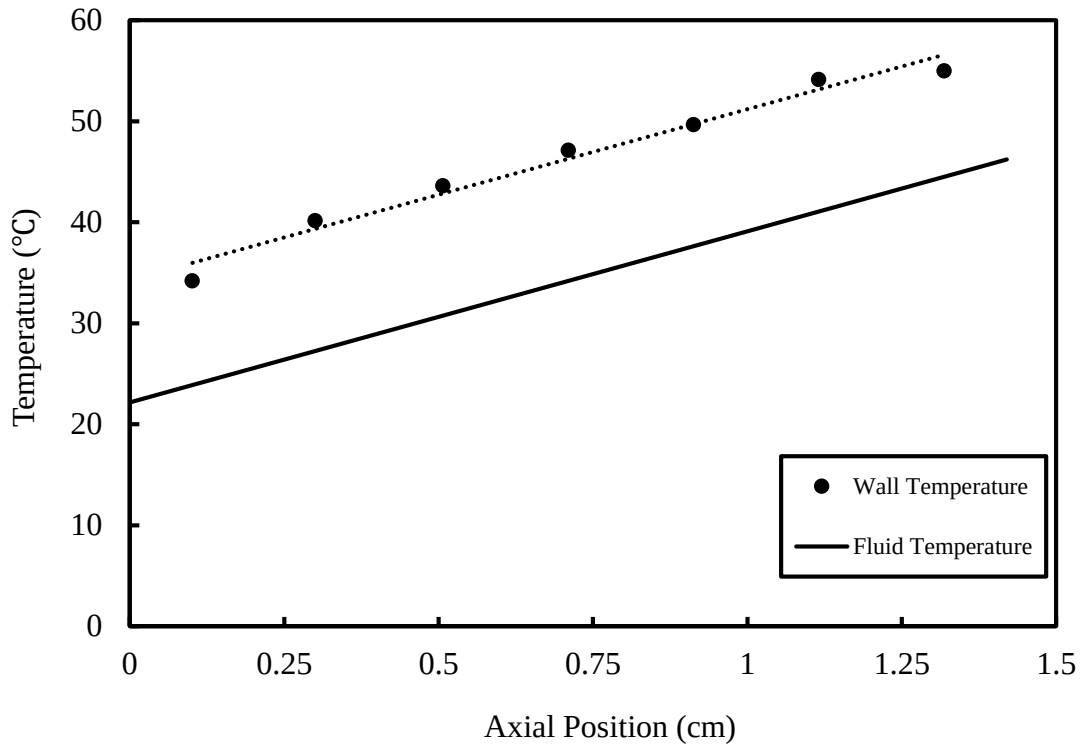

Figure 11. Fully developed method

After the estimation of all required temperatures, the final step is the calculation of the average convective heat transfer. In the literature, mainly two approaches exist to estimate the temperature difference for the calculation of the heat transfer coefficient: the logaritmic mean temperature difference method (LMTD) and the average method. In the LMTD, the heat transfer coefficient is calculated by comparing the average wall temperature to the inlet and outlet fluid temperatures [35,36].

In the average method, the average wall temperature along the entire channel is compared to the average fluid temperature in the entire channel [37]. These two methods result in slightly different heat transfer coefficients. In this work, both methods are used to calculate the heat transfer coefficient.

In the LMTD method, the average heat transfer coefficient, $\bar{h}$, is calculated through Equation (8) – (10).

$$\Delta T_{\mathrm{LM}} = \frac{\left(T_w - T_{\mathrm{f,i}}\right) - \left(T_{\mathrm{w}} - T_{\mathrm{f,o}}\right)}{\ln\left(\frac{T_w - T_{\mathrm{f,i}}}{T_{\mathrm{w}} - T_{\mathrm{f,o}}}\right)} \tag{8}$$

$$q = \dot{m} c_p (T_{\mathrm{f,i}} - T_{\mathrm{f,o}}) \tag{9}$$

$$\bar{h} \equiv \frac{q}{A(\Delta T_{\mathrm{LM}})} \tag{10}$$

In Equation (8), T_w is the mean wall temperature, $T_{\mathrm{f,i}}$ is the fluid inlet temperature and $T_{\mathrm{f,o}}$ is the fluid outlet temperature. The inlet fluid temperature is measured by a thermocouple at the inlet of the microchannel and the outlet fluid temperature is found by extrapolation using fully developed flow assumption.

Additionally, the inlet and outlet RTDs are used for double checking the coolant inlet and outlet temperatures. Expectedly, the RTDs slightly overestimate the fluid inlet and outlet temperatures due to conduction from the adjacent resistance heaters.

In Equation (9), $\dot{m}$ is the mass flow rate and c_{p} is the specific heat. In Equation (10), q is the heat gained by the coolant, A is the microchannel wall area (all four sides with or without a gap) and ΔT_{LM} is calculated from Equation (8).

In the average method, $\bar{h}$ is calculated by using average wall temperature and the mean fluid temperature.

$$\bar{h} \equiv \frac{q}{A(T_{\mathrm{w}} - T_{\mathrm{f}})} \tag{11}$$

In Equation (11), T_{f} is the mean fluid temperature. Again, the fluid inlet temperature is measured by a thermocouple and the fluid outlet temperature is estimated as before. The mean fluid temperature is the average of the inlet and outlet fluid temperatures

In this study, mainly LMTD method with fully developed assumption is used. The steps which are followed during the calculation of convective heat transfer is given in Figure 12.

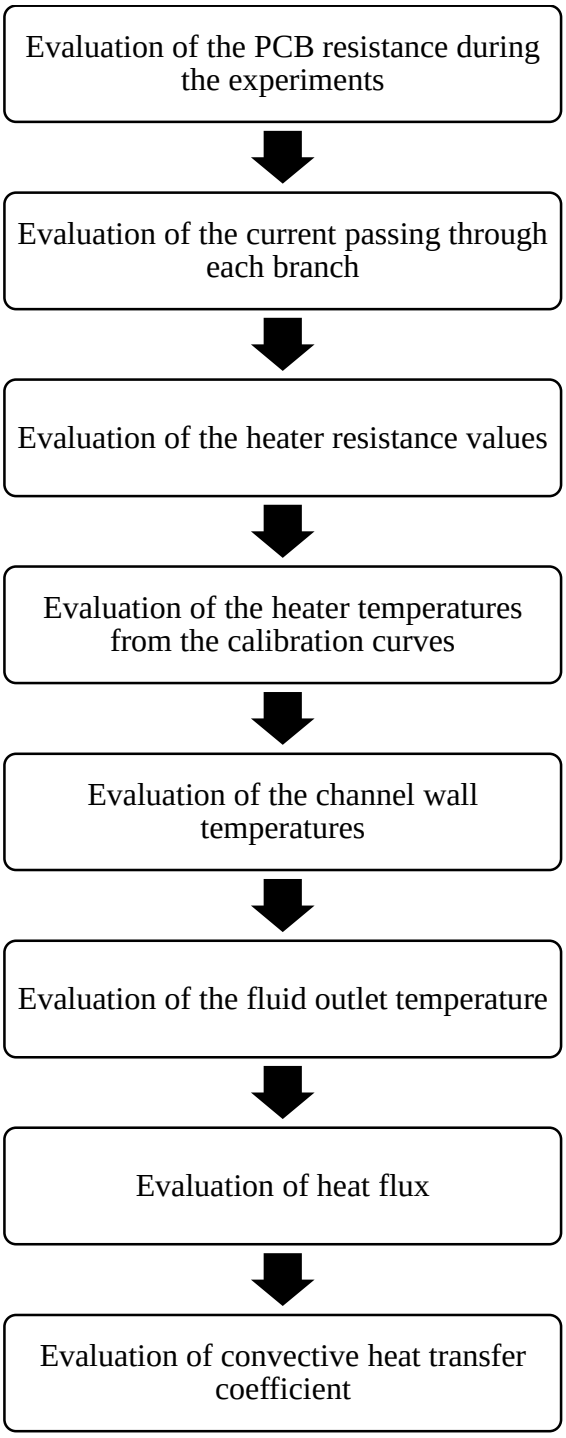

Figure 12. Steps followed in the data analysis

2.3.2. Data analysis for hydrodynamic performance of the microchannel

In the hydrodynamic analysis part of this study, the pressure drop, pumping power and friction factor values are evaluated. The pressure drop during the experiments is measured by pressure transducers located near the inlet and outlet of the channel.

In the pressure drop calculations, the pressure drop in the tubing between the pressure transducer on the microchannel is neglected but losses due to contraction and expansion at the microchannel inlet and outlet are calculated. Then, the pressure drop from the inlet to the outlet of the microchannel is calculated using Equations (12) - (14) [35].

$$\Delta P = \Delta P_{measured} - \Delta P_{\text{minor}} \tag{12}$$

$$\Delta P_{\text{minor}} = K_{\text{in}} \left(\frac{\rho_{\text{in}} u_{\text{in}}^2}{2} \right) + K_{\text{out}} \left(\frac{\rho_{\text{out}} u_{\text{out}}^2}{2} \right) \tag{13}$$

$$\Delta P_{\text{minor}} = 0.5 \left(\frac{\rho_{\text{in}} u_{\text{in}}^2}{2} \right) + \left(\frac{\rho_{\text{out}} u_{\text{out}}^2}{2} \right) \tag{14}$$

In these equations, ΔP is the pressure drop, K_{in} is *k*-factor for sudden contraction, K_{out} is the *k*-factor for sudden expansion and ρ is the density. K_{in} and K_{out} factors are found from [38] with an aspect ratio between 0.1 to 1 and the area ratio (microchannel to contraction/expansion cross-sectional area) is assumed to be zero since microchannel area is very small.

Pumping power, $\dot{P}$, is calculated from the Equation (15).

$$\dot{P} = \dot{V}(\Delta P) \tag{15}$$

Friction factor is calculated from Equation (16).

$$f = \frac{2 \times \Delta P \times D_{\mathrm{h}}}{L \times \rho \times u^2} \tag{16}$$

In this equation, D_{h} is the hydraulic diameter, L is the channel length, ρ is the average density of the fluid and u is the mean velocity of the fluid.

For comparison of the experimental results with theoretical ones, the friction factor for fully developed flow has been calculated using Equation (17) [37].

$$f = \frac{4.7 + \frac{19.64(\gamma^2 + 1)}{(\gamma + 1)^2}}{Re} \tag{17}$$

In this equation, f is the friction factor, and γ is the aspect ratio (height / width) of the channel.

CHAPTER 3

GOLD NANOFLUID EXPERIMENTS AND RESULTS

In this chapter, convection heat transfer and pressure drop characteristics of gold nanofluids flowing through CMOS compatible monolithic microchannel heat sinks in a low Reynolds number range ($30 < Re < 50$) are experimentally investigated. The cross-sectional area of the copper microchannel used in this part of the experiment is $50\ \mu m \times 70\ \mu m$. The effects of the flow rate, particle size and the volumetric concentration of the gold nanofluid on the heat transfer coefficient and the pressure drop are investigated. A figure of merit for the heat sink performance is defined and calculated for each experiment. To determine the true heat transfer enhancement due to the added nanoparticles, the experiments are repeated with DI water, PVP - DI water solution, and the water based gold nanofluid with added PVP. In Section 3.1, preparation of the PVP - DI water solution and the water based gold nanofluid is explained in detail. In Section 3.2, stability of the coolants used in the gold nanofluid experiments are investigated. In Section 3.3, the estimation of the thermophysical properties of the coolants are presented. Results for the thermal and hydrodynamic behavior of the gold nanofluids are given in Section 3.4 and Section 3.5.

3.1. Preparation of the Coolants

Three coolants, DI water, PVP - DI water solution and DI water based gold nanofluid, are prepared for this set of experiments.

Among the three coolants used in the experiments, DI water is used to validate the experimental setup and to make a comparison with the other fluids. A solution of DI water with PVP is prepared to examine the surfactant effect on the heat transfer performance. The PVP amount in this solution is not selected arbitrarily. To make an accurate comparison between the gold-PVP-water nanofluid and the PVP - DI water solution, the weight based surfactant concentration in both fluids are kept the same. The custom made gold nanofluids have been purchased from Nanocomposix Inc. and they contained an unknown amount of the surfactant PVP. Hence, to estimate the amount of surfactant in the nanofluid, the thickness of the surfactant layer over the nanoparticle is visualized and measured by a Scanning Electron Microscope (SEM). In the preparation of the PVP – DI water solution, surfactant amount in the nanofluid is calculate in the 100 nm gold nanofluid because surfactant layer thickness can be visualize only in this particle size.

The thickness of the surfactant layer decreases as the particle size decreases, thus visualization of this layer thickness becomes hard due to the available resolution of the devices. The maximum magnification of the scanning transmission electron microscope (STEM) at METU Central Laboratory has been used. The gold nanoparticles can be seen clearly however, the surfactant layer cannot be distinguished from the particle as shown in Figure 13.

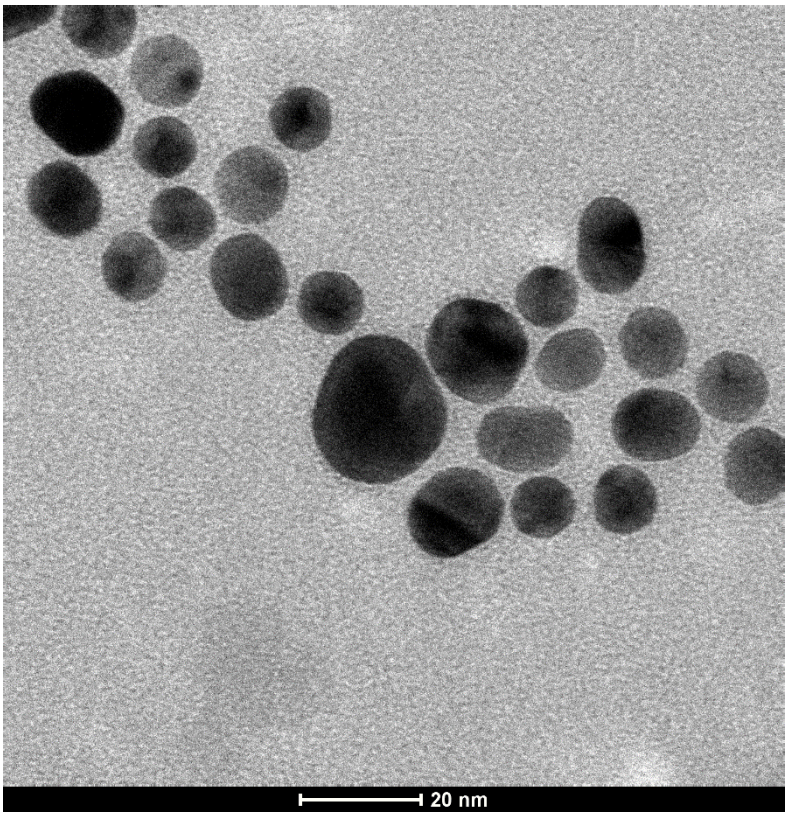

Figure 13. STEM images of dried 10 nm gold nanofluid

In Figure 14 the SEM image of the nanofluid with about 100 nm particle diameter is shown where the particles and surrounding surfactant layer can be observed. The image shows a homogenous particle dispersion within the nanofluid. The particle size distribution is relatively uniform changing between 100-130 nm. The surfactant layer thickness is about 12 nm which is nearly 10% of the nanoparticle size. This implies that neglecting the surfactant layer may not be a good assumption. After the calculation of the amount of PVP in the nanofluid, the same amount of PVP is dissolved in DI water and put in an ultrasonic bath to prepare a homogenous solution.

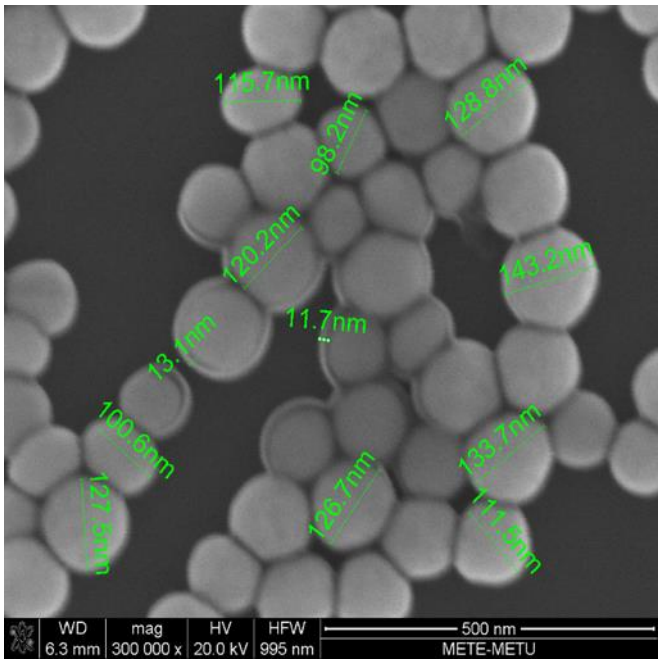

Figure 14. SEM image of dried 100 nm gold nanofluid

Nanofluids are composed of spherical gold nanoparticles suspended in DI water with PVP used as the surfactant to stabilize the mixture. A variety of gold particle diameters ranging from 10–100 nm have been tested.

The purity of the gold particles were stated by the manufacturer to be 99.99%. Nanofluids concentrations ranging from 0.125 to 1 mg/mL (0.00064 – 0.005% volume) have been prepared by diluting the original nanofluids with DI water. Higher concentrations of the nanofluids have not been prepared due to the recommendation of the supplier because at higher concentrations the nanofluids were prone to agglomeration. The SEM images of this study has been taken at METU METE NANOLAB of Dr. H. Emrah Ünalan.

3.2. Stability of the Coolants

One major problem in the long term usage of nanofluids is maintaining a stable suspension.

The stability of the nanofluid can be defined as having a homogenous composition throughout so that there is not any sedimentation or agglomeration of the nanoparticles. Different techniques can be used to indicate and enhance the stability of the nanofluids [39]. In this study, an ultrasonic bath is used to enhance the stability and a SEM is used to visualize the nanoparticles. The ultrasonic bath is used every time before the experiments to break down possible agglomeration if any.

The SEM images of nanofluids are taken before and after the experiments for all gold nanofluids used in these experiments (100 nm, 50 nm, 10 nm gold nanoparticles). Before starting the experiments, SEM images present the size of the particle and the position of the particles with respect to each other. After the experiment, the repeated SEM imaging reveals whether any agglomeration during the flow occurs. Although the gold nanofluids used in this study have been purchased approximately four years ago, particles were nearly at their initial sizes and there were not any agglomerations. Thus, the present study is also important for proving the long term stability of the used nanofluids for potential applications. In Figure 15(a), a SEM image of 100 nm gold nanofluid which is taken before the experiment is shown.

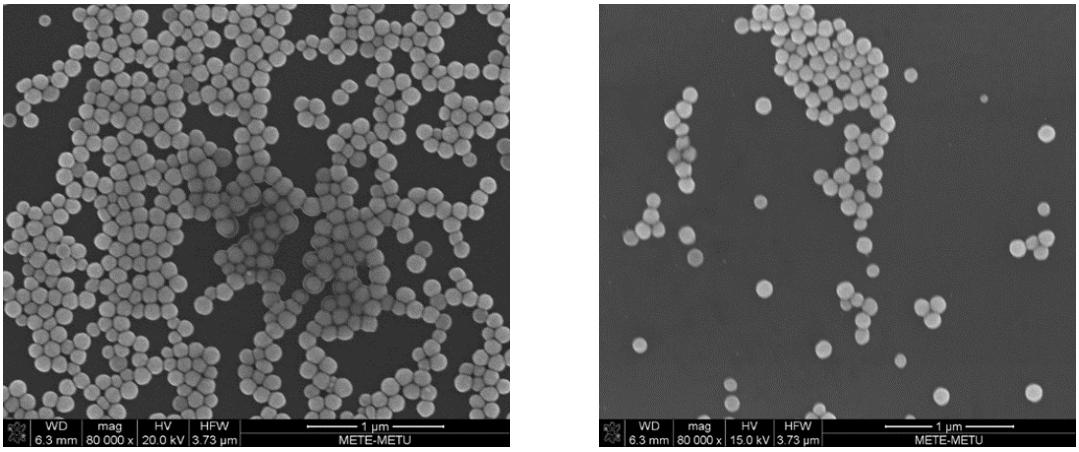

(a) (b)

Figure 15. SEM images of a dried 100 nm gold nanofluid (a) before (b) after the experiment

The particles are really close to each other, however there is not any agglomeration which will result in formation of large particles. A fairly uniform distribution of the nanoparticles can be observed from the image. The morphology of the nanoparticles after the heating is given in Figure 15 (b). It should be noted that the magnification in Figure 15 (a) and (b) are the same, therefore a realistic comparison can be made. It is observed that nanoparticle size does not change after the heating. It may be concluded that heating in the microchannel did not cause an agglomeration of the particles.

SEM images of 50 nm gold nanofluid which are taken before and after the experiment are shown in Figure 16. The particle sizes varied between 45 – 65 nm before and after the experiment which may be the evidence that there is not any larger particle formation. The distance between the particles are very small but they do not stick to each other and there is not any agglomeration which is an indicator of the stability.

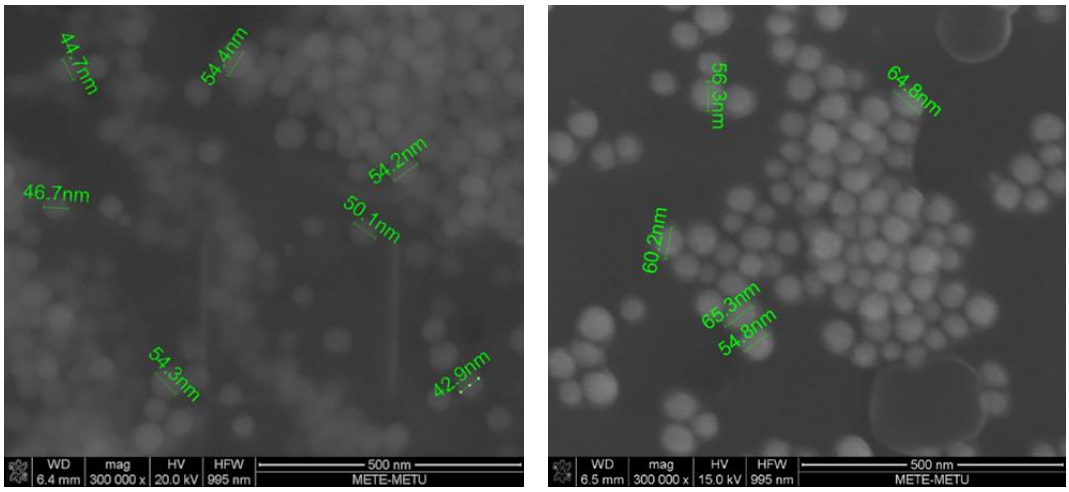

(a) (b)

Figure 16. SEM images of the dried 50 nm gold particle nanofluid (a) before (b) after heating

Lastly, the stability of the 10 nm gold nanofluid is tried to be visualized with the SEM. However due to the small size of the nanoparticles, the SEM device could not be focused on this small particles and even the highest resolution was not sufficient. This SEM image of the 10 nm gold nanofluid is shown in Figure 17. As a solution of this problem, visualization of this 10 nm gold nanofluid has been realized in the METU Central Laboratory.

A scanning transmission electron microscope (STEM) is used to obtain the images of the 10 nm gold nanofluid. In Figure 18, STEM images of the 10 nm gold nanofluid is shown. The particles can be clearly seen in these figures. It is observed that there is uniform distribution of the particles. From Figure 19, rarely, the formation of larger particles is observed. These larger particles are nearly 26 nm, and the particle size distribution is changing between 10 nm – 30 nm as shown in Figure 20.

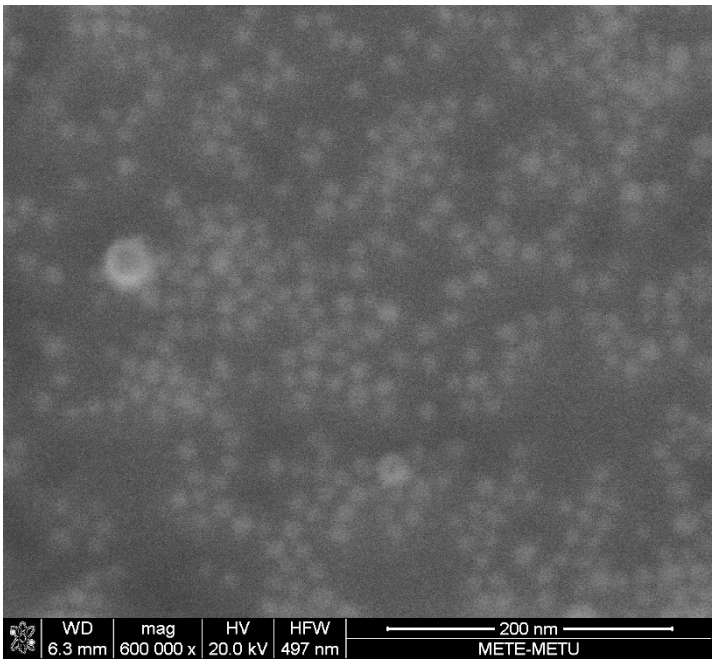

Figure 17. SEM image of the dried 10 nm gold particle nanofluid

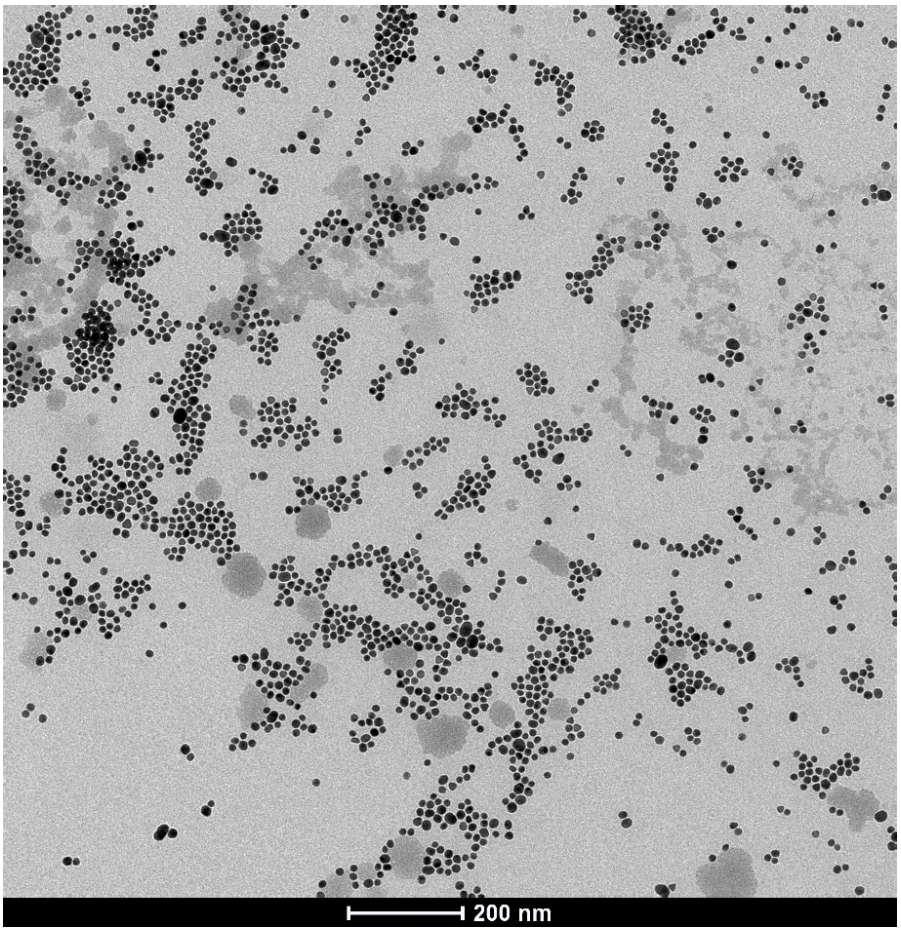

Figure 18. STEM image of dried 10 nm gold nanofluid

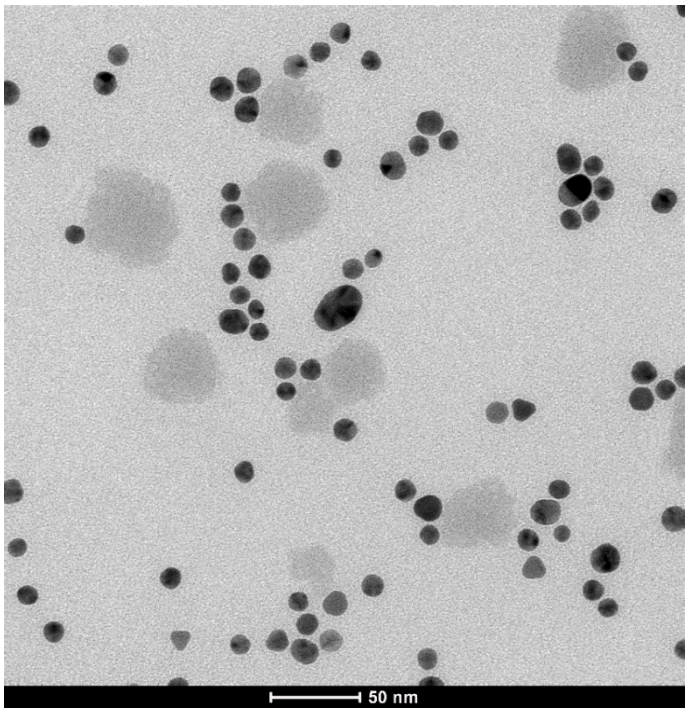

Figure 19. STEM image of the dried 10 nm gold nanofluid

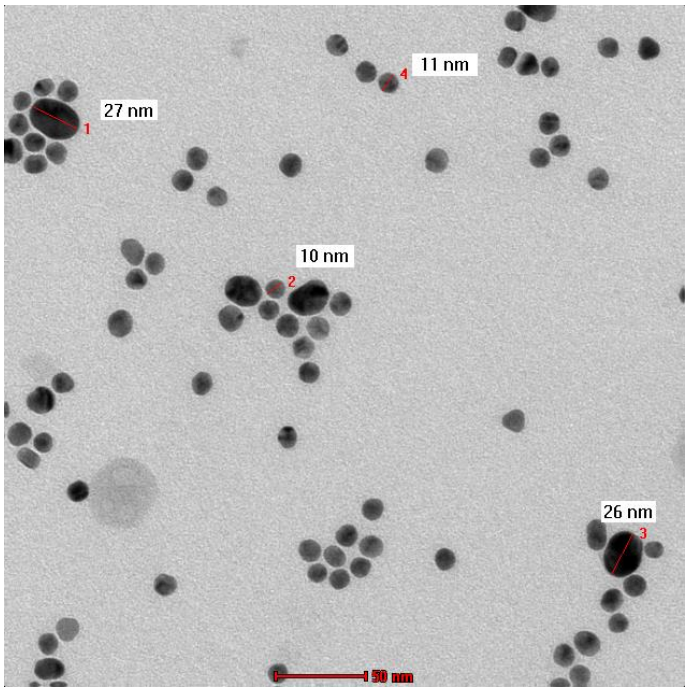

Figure 20. STEM images of the dried 10 nm gold nanofluid

The nanoparticle diameters and surfactant layer thicknesses are shown for gold particles with 100 nm nominal diameter. In Figure 21(a), the particle diameter and the surfactant layer could be measured separately and it is observed that the surfactant layer changes between 7 to 25 nm. However in Figure 21(b), the total particle diameter including the surfactant layer could be visualized. Hence, the measured dimensions differ in the two figures. The nanofluid of 50 nm particles has also been visualized in SEM. The particle size distribution was uniform before and after the heating, but the surfactant layer could not be observed due to the smaller particle size relative to 100 nm ones.

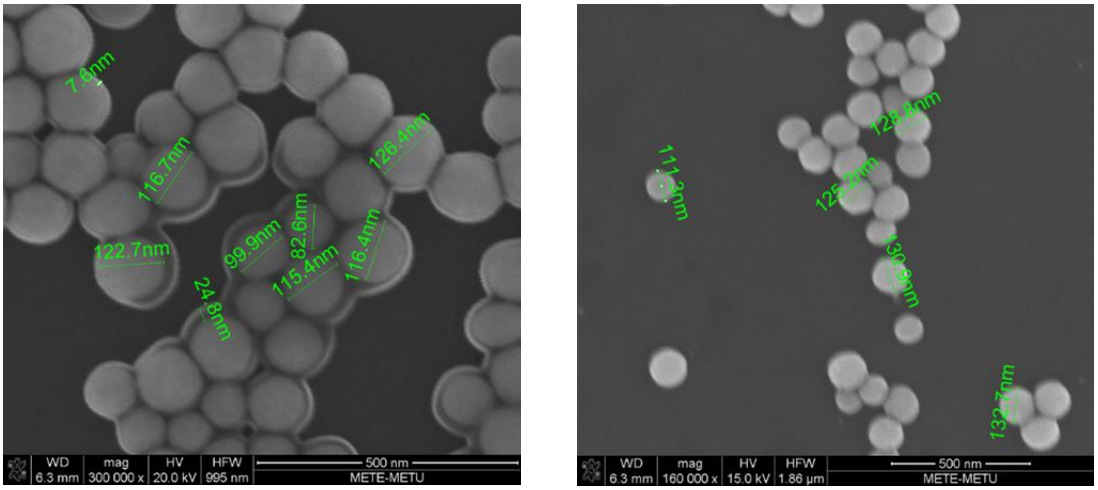

(a) (b)

Figure 21. SEM images of a dried 100 nm gold nanofluid (a) before and (b) after the experiment

The stability of nanofluids can also be investigated by sediment photography capturing method. In this method, photographs of the same nanofluid sample are taken periodically.

In Figure 22, photographs of 10 nm gold nanofluids that are taken (a) 4 years ago (b) recently are shown. No color change or agglomeration of the particles is observed in the nanofluid.

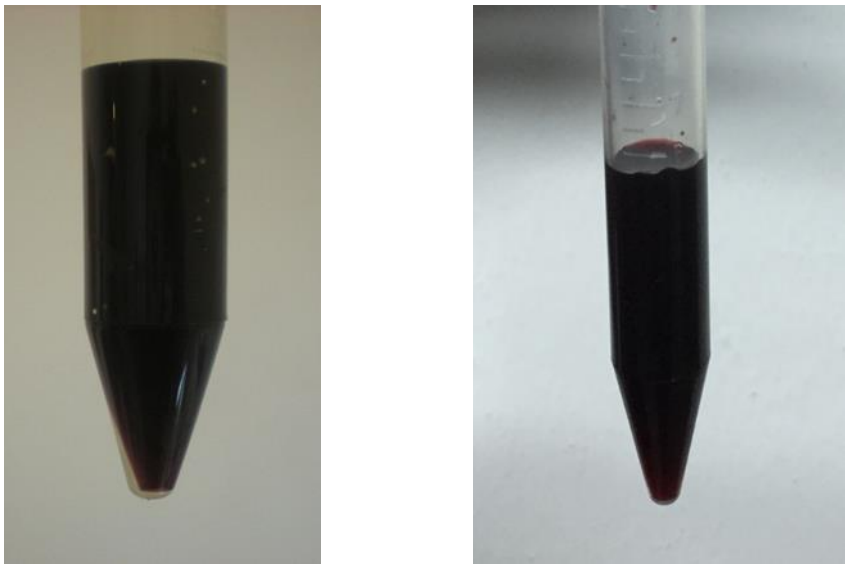

(a) (b)

Figure 22. Photographs of gold nanofluid with 10 nm nanoparticles at a concentration of 1 mg/ml (a) 4 years ago (b) today

3.3. Assumptions

The main assumptions made during the gold nanofluid experiments and data analysis may be stated as follows:

- In the experiments, data are taken when the system reaches a steady state. The steady state of the system can be checked by the recorded outlet fluid temperature. As the heating starts, an increase in the temperature of the fluid is observed. This will cause some fluctuations in the outlet temperature of fluid. Therefore, the data is recorded when a stable outlet fluid temperature is reached.

- During the calculation of the microchannel wall temperature, one dimensional heat conduction across the parylene layer without any heat loss is assumed.
- A uniform flow rate of the fluid through the microchannel is assumed.
- The heat flux supplied by the seven heaters are assumed to be uniform throughout the channel.

The flow is assumed to be fully developed both thermally and hydrodynamically. For rectangular microchannels, the thermal entry length is given in [38]:

$$x_{\mathrm{fd,t}} = 0.1 ReP r D_{\mathrm{h}} \tag{18}$$

where $x_{fd,t}$ is thermal entry length. The thermal entry length calculated from Equation (18) shows that the maximum thermal entry length is only 8% of the total microchannel length. Therefore, thermally fully developed flow condition is realized in this study. The entrance region become significant in high Reynolds number flows, however in this study the Reynolds numbers are very low hence the entrance region effects can safely be neglected.

The hydrodynamic entry length is calculated using:

$$x_{\mathrm{fd,h}} = 0.05 ReD_{\mathrm{h}} \tag{19}$$

where $x_{\mathrm{fd,h}}$ is hydrodynamic entry length. The maximum hydrodynamic entry length calculated from Equation (19) was less than 7% of the total microchannel length. Therefore, hydrodynamically fully developed flow is assumed in this study.

- Heating from all four sides is considered in the heat transfer area calculations of the 50 μm x 70 μm single channel microchannel. Electroplating duration is the parameter that alters number of the heated wall sides. The channels are checked under the microscope to observe whether the top wall is covered with copper or a gap exist. It is observed that the copper covers the channel top which yields an additional heat transfer wall area.

- Well dispersed solutions are prepared before the experiments, thus uniform dispersion of the nanoparticles inside the base fluid is assumed. This assumption is also valid since there is not any agglomeration seen in the images of the nanofluids given in Figure 18 - 21. This uniformity is achieved by the addition of surfactant by the manufacturer and the usage of ultrasonic bath.

- It is assumed that the pump has 100 % efficiency.

3.4. Thermophysical properties of the coolants used in the experiments

The thermophysical properties of DI water are evaluated at the average of inlet and outlet temperatures and considering the pressure difference by Engineering Equation Solver (EES).

Thermophysical properties of the PVP - DI water solution are obtained by the help of the literature and making some important assumptions. Firstly, the density of PVP - DI water solution is obtained from [40]. A density- temperature graph is plotted and the density values for PVP - DI water solution at the inlet/outlet temperatures are found. The specific heat of the solution is obtained by assuming that the heat loss to surroundings in PVP - DI water solution experiments during the application of voltage is equal to that in DI water experiments. Then, the heat given to the fluid is known and the specific heat of the solution is calculated. The viscosity of the PVP - DI water solution is obtained from [41]. The viscosity with respect to volumetric fraction is plotted and the viscosity values at the volumetric concentration of PVP - DI water solution is calculated.

For the third fluid used in the experiments, namely PVP added gold nanofluids, the effects of particle size and concentration have been considered. When nanoparticles are added in a fluid, its effective bulk properties (density, specific heat, viscosity, thermal conductivity) change depending on the amount of the nanoparticles added. The effective density and the specific heat of gold nanofluids are calculated by Equation (20) and (21).

$$\rho_{\mathrm{nf}} = (1-\chi)\rho_{\mathrm{bf}} + \chi\rho_{\mathrm{np}} \tag{20}$$

$$\left(\rho c_{\mathrm{p}}\right)_{\mathrm{nf}} = (1-\chi)\left(\rho c_{\mathrm{p}}\right)_{\mathrm{bf}} + \chi\left(\rho c_{\mathrm{p}}\right)_{\mathrm{np}} \tag{21}$$

In these equations, ρ is the density, χ is the particle volume fraction and the subscripts nf, bf and np stand for nanofluid, base fluid (DI water solution in this case), and nanoparticle, respectively.

The viscosity of the nanofluid as a function of volume fraction is described by Equation (22).

$$\frac{\mu_{\mathrm{nf}}}{\mu_{\mathrm{bf}}} = 1 + C_{\mu}\chi \tag{22}$$

where μ is the dynamic viscosity and C_{μ} is a constant corresponding to the increase in viscosity with volume fraction. The Einstein theory for the viscosity of particles in a low concentration nanofluid predicts a value of 2.5 for C_{μ} [42]. The viscosity of gold nanofluids are calculated from Equation (22) by taking C_{μ} as 2.5.

Thermal conductivity determination is more complicated than other thermophysical properties. In general, the increase in thermal conductivity of a nanofluid as a function of volume fraction is described by equation (23).

$$\frac{k_{\mathrm{nf}}}{k_{\mathrm{bf}}} = 1 + C_{\mathrm{k}}\chi \tag{23}$$

In this equation, k is thermal conductivity and C_{k} is a constant corresponding to the increase in thermal conductivity with volume fraction. For well dispersed spherical particles and particle volume fractions below 5%, the effective medium theory developed by Maxwell provides a lower bound to the nanofluid thermal conductivity and results in a value of 3 for C_{k} when the nanoparticle thermal conductivity is much higher than the fluid thermal conductivity [43,44]. Other effective medium theories, such as the Hamilton-Crosser approach, extend Maxwell's theory to non-spherical particles [45]. Maxwell theory is used in the evaluation of thermal conductivity of gold nanofluids since gold nanoparticles are in spherical shape.

3.5. Convective Heat Transfer Coefficient Results

Previous tests of nanofluids in microchannels have generally used higher nanoparticle concentrations and Reynolds numbers. However, the present study focuses on low Reynolds number flows requiring reduced pumping powers, and is therefore favorable for microchannel flow. In addition, the maximum concentration used is 1mg/mL (0.001% volume fraction) which is much lower than previously reported values ranging between 0.3 and 10% [46].

The experimentally determined heat transfer coefficients for a microchannel with 70 μm × 50 μm cross section are shown in Figure 23 – 25. The effects of different parameters such as, the particle size, volumetric concentration and volume flow rate on the heat transfer coefficient are investigated.

3.5.1. Effect of particle size

To investigate the effect of particle size on heat transfer coefficient, three different particle sizes: 10 nm, 50 nm and 100 nm of gold nanoparticles suspended in DI water at 0.0025% volumetric fraction have been tested. The corresponding heat transfer coefficient has been determined for each nanofluid. Throughout these experiments, all parameters other than the particle size have been kept constant.

Hence, DI water and PVP - DI water solution had a single, constant heat transfer coefficient as shown in Figure 23. The heat transfer coefficients by DI water and PVP – DI water solution are calculated by LMTD method. The heat transfer coefficient with each nanofluid is calculated using two different methods LMTD and the average method which are explained in Section 2.3.1. The LMTD method yielded a higher heat transfer coefficient compared to the average method. This is due to the large temperature difference between the wall temperature and fluid inlet temperature. LMTD method accounts for this difference in the calculation and therefore gives a better estimate for the heat transfer coefficient. Moreover, most of the studies in the literature use the LMTD method during the calculations. For this reason, in the rest of the figures, the LMTD results for DI water, PVP – DI water solution and nanofluid are presented to enable comparison.

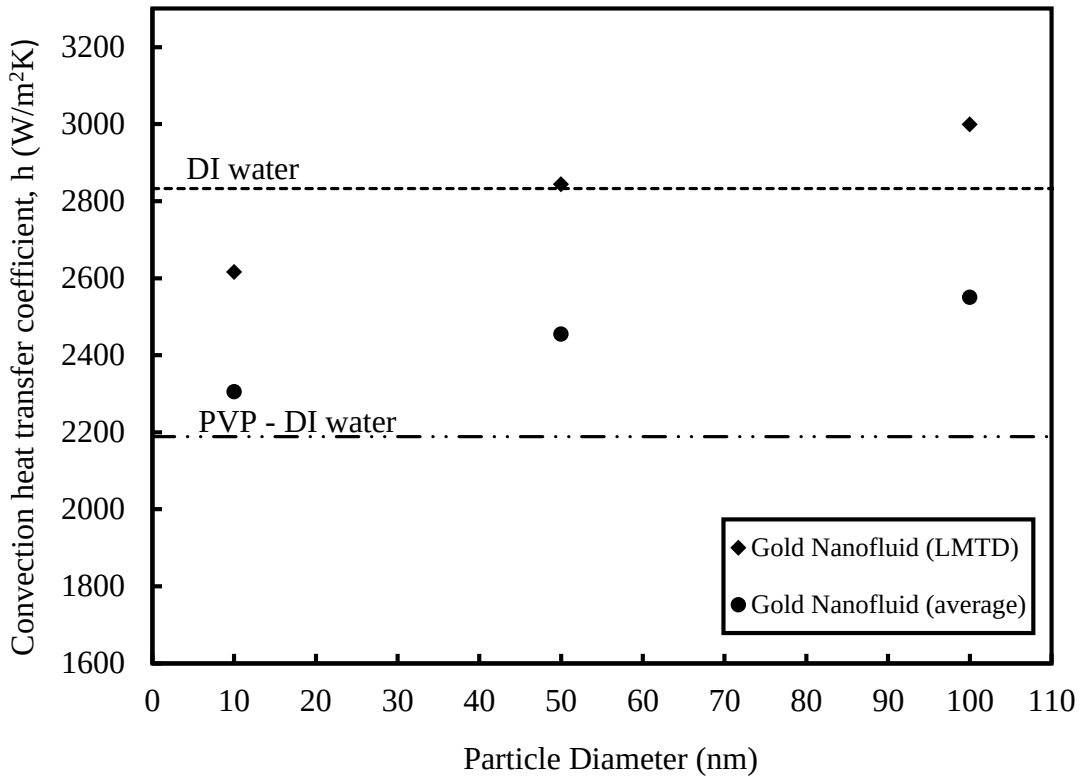

Figure 23. Heat transfer coefficient with respect to different diameter

From Figure 23, it is clearly seen that as the gold nanoparticle diameter increases, the heat transfer coefficient also increases. For all particle sizes, the heat transfer coefficient with the nanofluid is higher than that with the PVP - DI water solution. On the other hand, when a comparison is made between the gold nanofluid and DI water, the nanofluid with 50 nm gold nanoparticles yields a heat transfer coefficient overlapping with that for DI water. Nanoparticles greater than 50 nm in diameter lead to higher heat transfer coefficients than DI water as well.

The effect of nanoparticle size, on the heat transfer coefficient has not been examined as frequently as the other parameters. In addition, there are contradictions between the reported results. Anoop et al. [47] investigated the particle size effect on heat transfer coefficient in the entrance region.

Alumina-water nanofluids with average particle sizes of 45 and 150 nm are used in their study. It was reported that as the particle size increases, the heat transfer coefficient decreases which is just the opposite of the findings of the present study. This difference may be due to several reasons but the main reason maybe that in [47], the developing region is studied, whereas fully developed region is investigated in the present study. The relation between the particle size and heat transfer coefficient may depend on the flow region. Timofeeva et al. [48] presented results for SiC nanoparticles of 16, 29, 66 and 90 nm diameters suspended in water circulated in a closed loop in turbulent regime. The results indicated that nanofluids of 16 and 29 nm nanoparticle diameters yielded lower heat transfer coefficients than water, whereas nanofluids with 66 and 90 nm nanoparticles lead to higher heat transfer coefficients compared to water. Therefore, the results of the present study agree very well with those reported in [48]. In addition, the particle size after which the heat transfer coefficient with nanofluids exceeds that with the base fluid is nearly the same in both studies.

3.5.2. Effect of volumetric concentration

Nanofluids containing 50 nm gold nanoparticles with three different volumetric concentrations in the range of 0.00064% - 0.0052% have been tested to understand the effect of the volumetric concentration on the heat transfer coefficient.

The results are plotted in Figure 24. It has been expectedly observed that the heat transfer coefficient increased with an increase in the nanofluid volumetric concentration. There is a linear relation between the heat transfer coefficient and the volumetric concentration which can be formulated, with the experimental results of the present study, with a high R-squared value.

The nanofluid yielded a higher heat transfer coefficient than PVP - DI water solution for all tested concentrations, at concentrations higher than 0.0026% the heat transfer coefficient with the nanofluids could also exceed that with the DI water.

An error analysis has been performed on the volumetric concentration to understand the closeness of the volumetric concentration values. The gold nanofluids have been kept in 15 ml sealed bottles in the refrigerator during the last four years. In this time interval, partial evaporation of the base fluid might have occurred which will cause a change in the volumetric concentration of the nanofluid. For example, if evaporation causes a 2 mm height decrease in the bottle, which is hard to observe, it will cause a 5.88% error in the volumetric concentration of the nanofluid. With this error, it will be hard to exactly identify the volumetric concentration of the nanofluids.

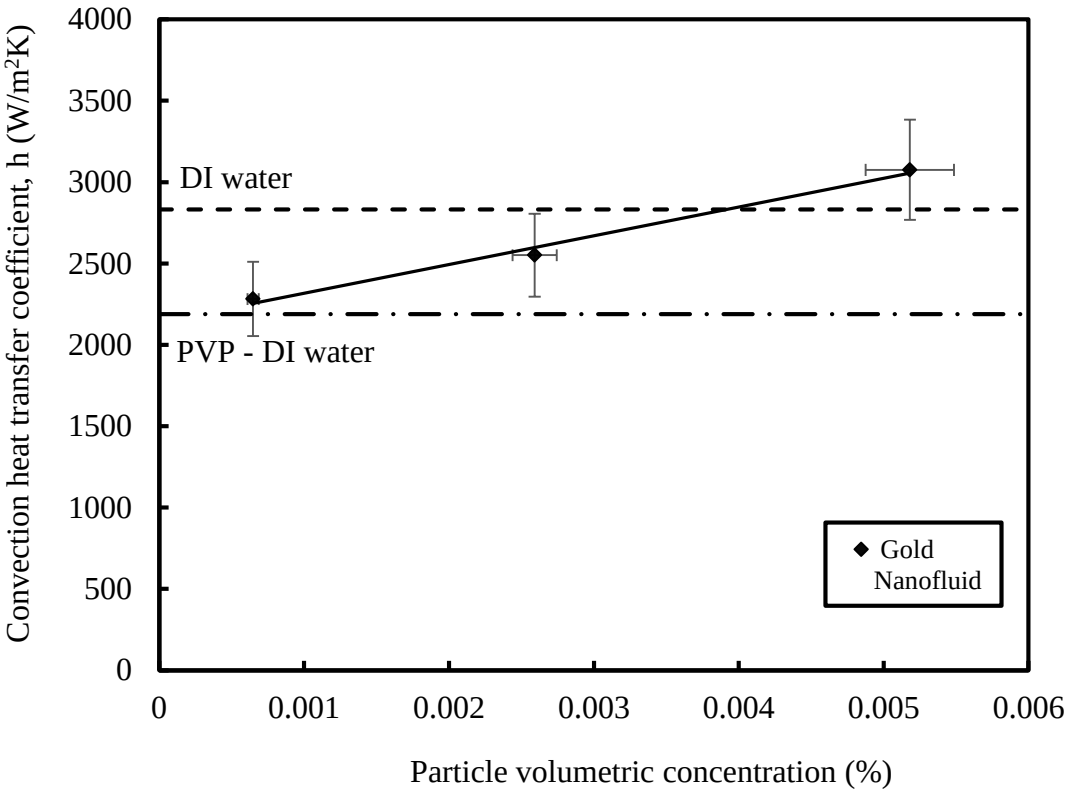

Figure 24. Heat transfer coefficient with respect to volumetric concentration of nanofluid using LMTD method

3.5.3. Effect of volumetric flow rate

One of the attractive parameters that has been investigated by several researchers is the heat transfer performance with respect to the flow rate. In the experiments, the flow rate has been changed in a range between 100 - 140 μL/min. A nanofluid with 10 nm gold nanoparticles at 0.0026% volumetric concentration has been used during the flow rate tests. An increase in the flow rate naturally caused an increase in the heat transfer coefficient as given in Figure 25**.**

Since the same voltage is applied to the microchannel heaters throughout the experiments, implying constant heat flux, an increase in the volumetric flow rate (hence *h*) caused a decrease in the temperature differences. All experiments have been performed with $70\,\mu m \times 50\,\mu m$ single channel chips with four side heating assumption, so that the heat transfer area were also equal for all experiments. These experimental results are parallel to the theoretical expectations which is important for the validation of experimental setup and the procedure. Although the flow rate range was not broad due to pumping power limitations, an obvious increase in heat transfer coefficient with respect to the flow rate is observed.

From Figure 25, some important conclusions can be drawn. For the 100 μL/min flow rate, the flow rate of gold nanofluid had significantly higher heat transfer coefficient than PVP - DI water solution. However, at higher flow rates, the heat transfer coefficient values of the gold nanofluid and PVP - DI water solution become very close to each other. A strict conclusion could not be drawn because the heat transfer coefficient values fell in the uncertainty band. The PVP - DI water solution had a steeper increase in the heat transfer coefficient with the flow rate than that for the nanofluid, therefore the two got closer with an increase in the flow rate.

Another remark can be made when the heat transfer coefficient obtained with the nanofluid is compared to that with DI water. The nanofluid with 10 nm gold nanoparticles never leads to a heat transfer coefficient greater than that with DI water at any flow rate.

During the flow rate experiments, due to the pressure drop limitations 10 nm nanoparticles have been used. However, as can be seen from Figure 23, the nanofluid with 10 nm gold nanoparticle led to the lowest heat transfer coefficient at 100 μL/min flow rate and only particle sizes higher than 50 nm yielded higher heat transfer coefficients than DI water. It can be concluded that if the particle size is lower than a limiting size, in this case 50 nm, increasing the flow rate does not bring any heat transfer enhancement above that obtained with water.

As a result, the particle size is concluded to be a more dominant factor than the flow rate in the enhancement of the heat transfer coefficient of the nanofluids.

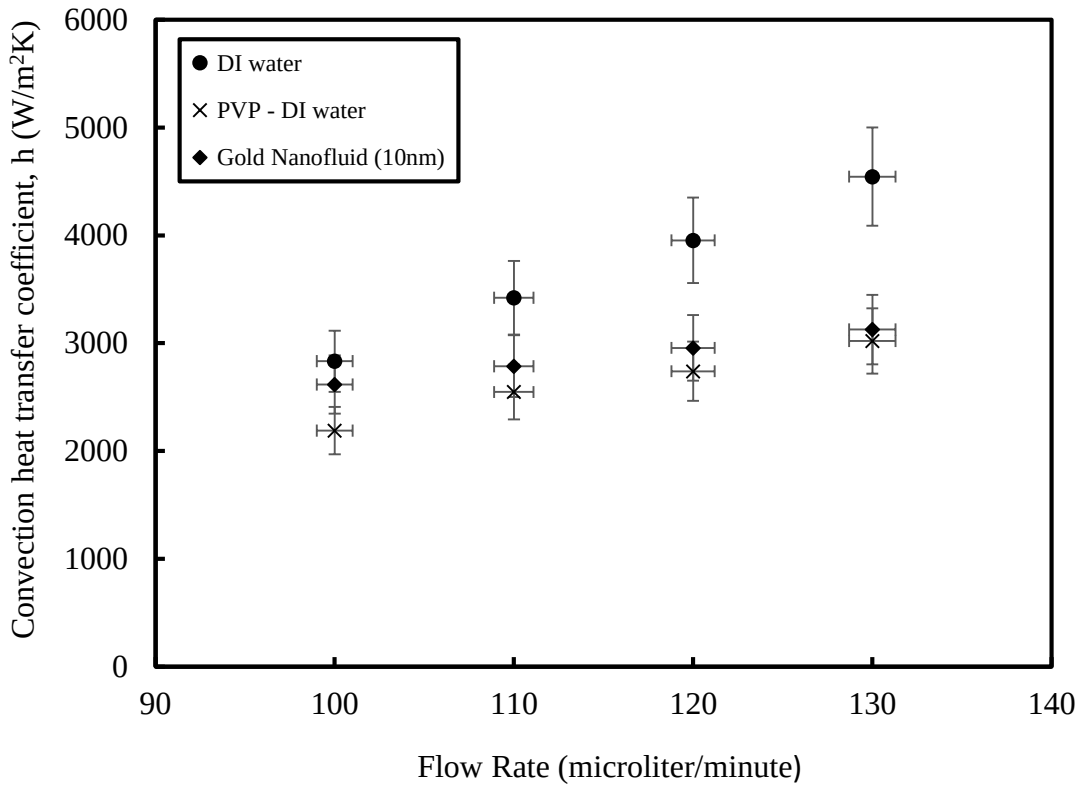

Figure 25. Convection heat transfer coefficient with respect to the flow rate

In the literature the heat transfer coefficient is usually plotted against the Reynolds number. In Figure 26, this variation is shown. At the same Reynolds number, the gold nanofluid has nearly the same heat transfer coefficient with PVP - DI water solution. Even though making a comparison using a nondimensional number seems logical, comparing different fluids at the same Reynolds number may not be correct. As stated in [48], a Reynolds number comparison is not fair enough due to the velocity/viscosity ratio. For example, a fluid flowing with a higher velocity and a higher viscosity can have the same Reynolds number with one having a lower velocity and a lower viscosity.

However higher velocity will result in a higher heat transfer performance. Secondly, there will be an uncertainty in the Reynolds number. Again, a comparison without indicating the uncertainty will not be accurate as higher uncertainties occur due to the accumulation of several uncertainties. For this reason that a comparison with respect to the flow rate given in Figure 25 has been preferred.

A comparison with the existing correlations has been made in Figure 26. It has been observed that the data obtained from experiments are between the correlations of Jung et al. [35] and Koyuncuoğlu et al. [34]. The correlation in [35] gives lower results and it is seen that this correlation's dependence on Reynolds number is relatively less than those of other correlations. The correlation in [34] considered 3-side heating and is developed using 100 μm × 50 μm single channel, 200 μm × 50 μm single channel, and 200 μm × 50 μm 10-channel test devices. It should be noted that four side heating (rather than three side heating used in [34,35]) is applicable to the channels in the present study. If three side heating was assumed in this study, the results get even closer to those by Koyuncuoglu et al. [34].

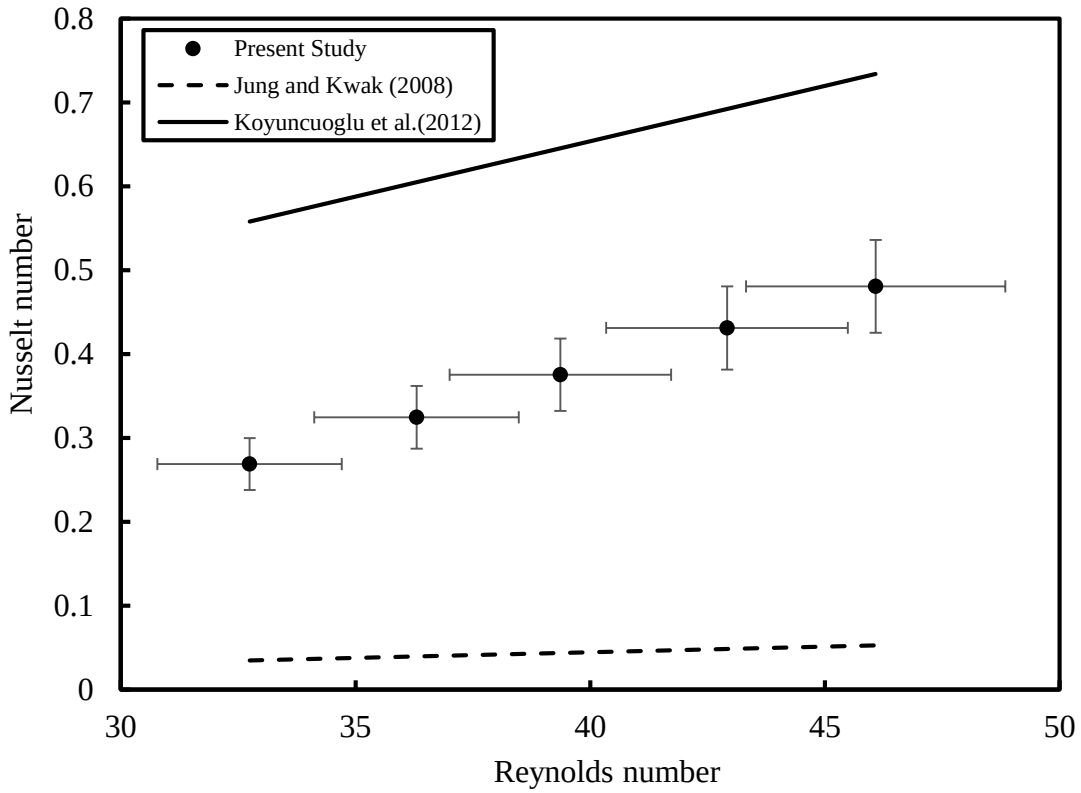

Figure 26. Nusselt number with respect to Reynolds number

3.6. Hydrodynamic Results

The experiments to determine the friction factor have been performed on a 70 μm × 50 μm microchannel with 10 nm gold nanofluid according to the previously discussed procedure. The ratio of experimentally determined friction factor to the theoretical one is shown in Figure 27. The measured friction factor is in good agreement compared with the theoretical friction factor for fully developed flow. The ratio is changing between 0.85 - 0.95 and it is close to 1 at different Reynolds numbers.

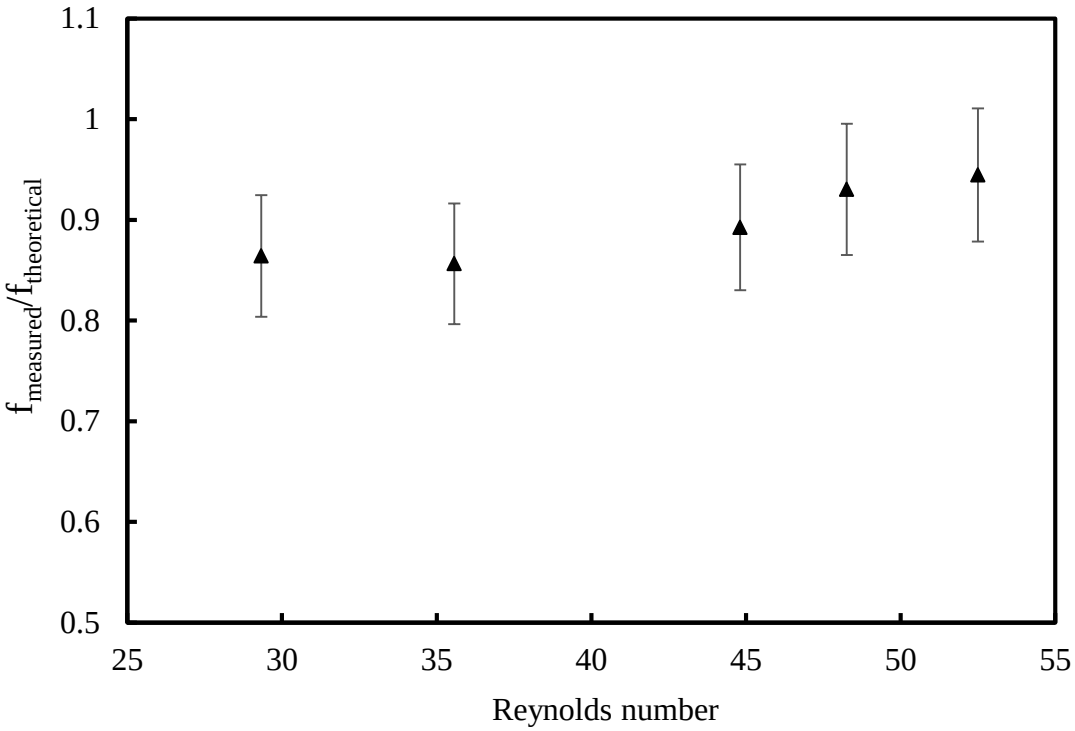

Figure 27. Measured friction factor/theoretical friction factor ratio for 10 nm nanofluid at different Reynolds numbers

The pumping power is another important parameter to evaluate the performance of a working fluid. High pumping power requirements should be precluded by selecting proper working fluids. In this work, the pumping powers required for DI water, PVP - DI water solution, and gold nanofluid are calculated and plotted against the volumetric flow rate in Figure 28. As the volumetric flow rate increases, the pumping power also increases linearly due to their linear relationship given in Equation (15). At the same flow rates, the gold nanofluid requires the highest pumping power as expected. However, the increase in the pumping power is not significant due to the very low volumetric concentrations of the investigated nanofluids

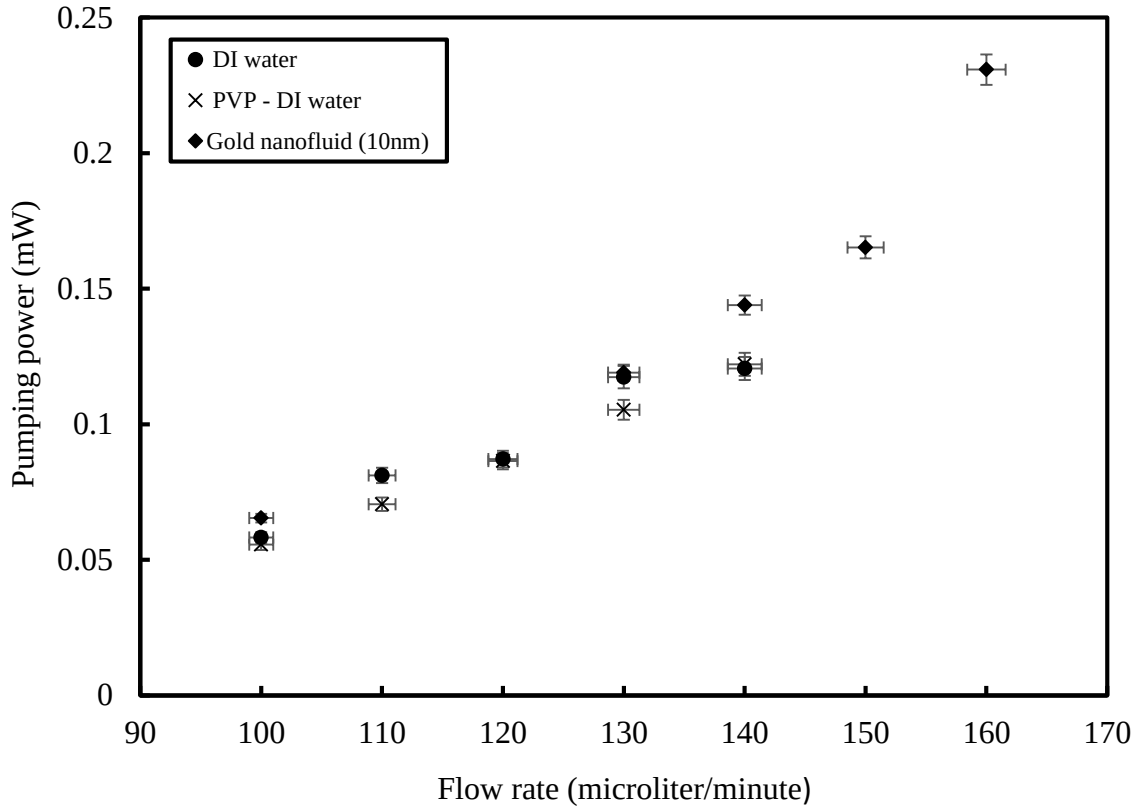

Figure 28. Pumping power of DI water, PVP - DI water solution and 10 nm gold nanofluid at different volumetric flow rates

A figure of merit has also been calculated in the present study. Koyuncuoglu et al. [32] introduce a figure of merit (FM) for the microchannel heat sink as the ratio of the cooling load to the pumping power. The FM has been defined as the ratio of the electrical heating to the pumping power as follows

$$FM = \frac{q_e}{\dot{P}} \tag{24}$$

From Table 3 and Table 4, it can be concluded that the FM values decrease with an increase in the flow rate. Since the electrical heating values are nearly the same, an increase in the flow rate causes an increase in the pumping power requirement.

The thermal resistance of the microchannel heat sink has been calculated from Equation (25)

$$R_{\mathrm{th}} = (T_{\mathrm{max}} - T_{\mathrm{f,in}})/q_{\mathrm{e}}^{''} \tag{25}$$

In this equation, T_{max} is the maximum chip temperature and $q_{\mathrm{e}}^{''}$ is the electrical heat flux. Similar FM and R_{th} values are tabulated in the literature [32,34]. The thermal resistance values obtained for DI water are in the range of the tabulated thermal resistances in [32]. From Table 3 and Table 4, although it seems that DI water has slightly lower thermal resistance values than PVP – DI water solution at same flow rate, the presented values are within the uncertainty band. In addition, during the flow of DI water, the maximum wall temperatures do not reach the maximum temperature values recorded during the flow of PVP – DI water solution. The difference between the maximum electrical heat flux and maximum heat flux removed by water is due to the heat loss to the substrate.

Table 3. DI water results

Flow rate (µl/min) (±1%)	**Electrical power (W)**	**Maximum electrical heat flux (W/cm^2)** (±5%)	**Maximum heat flux removed by water (W/cm^2)**	**Pumping power (mW)** (±4%)	**Pressure drop (kPa)** (±3.5%)	**Thermal resistance (cm^{2}K/W)** (±16%)	**FM** (±16%)
100	0.368	37.02	17.75	0.06	34.92	1.12	6318
110	0.368	37.02	19.62	0.08	44.23	1.08	4535
120	0.37	37.22	21.20	0.09	43.54	1.04	4245
130	0.37	37.22	22.68	0.12	54.14	1.01	3152

Table 4. PVP – DI water solution results

Flow rate (µl/min) (±1%)	**Electrical power (W)**	**Maximum electrical heat flux (W/cm^2)** (±5%)	**Maximum heat flux removed by water (W/cm^2)**	**Pumping power (mW)** (±4%)	**Pressure drop (kPa)** (±3.5%)	**Thermal resistance (cm^{2}K/W)** (±16%)	**FM** (±16%)
100	0.361	36.31	17.75	0.05	33.36	1.18	6491
110	0.363	36.52	19.61	0.07	38.48	1.16	5144
120	0.363	36.52	21.21	0.09	43.21	1.14	4200
130	0.365	36.72	22.68	0.11	48.61	1.11	3465

FM values of nanofluids for different flow rates, particle sizes and volumetric concentrations are tabulated in Table 5 - 7.

Table 5. Gold nanofluid with different volumetric flow rates

Flow rate (µl/min) (±1)	**Electrical power (W)**	**Maximum electrical heat flux (W/cm^2)** (±5%)	**Maximum heat flux removed by water (W/cm^2)**	**Pumping power (mW)** (±3%)	**Pressure drop (kPa)** (±2.45%)	**Thermal resistance (cm^{2}K/W)** (±16%)	**FM** (±16%)
100	0.288	28.97	18.57	0.0645	39.08	2.23	4401
130	0.288	29.07	23.52	0.119	54.66	2.06	2427
140	0.288	29.07	24.57	0.143	61.37	1.93	2083
150	0.29	33.19	29.79	0.165	65.71	1.72	1997
160	0.29	33.19	31.06	0.231	86.12	1.70	1429

In Table 5, the pumping power requirement, the pressure drop and the FM values of gold nanofluid are presented. The particle size of the gold nanofluid used in these experiments were 10 nm and its particle volumetric concentration was 0.0026%.

As the flow rate increased, the pressure drop between the inlet and outlet of the microchannel also increased. Since the flow through the experimental set up is open loop, the outlet pressure is equal to the atmospheric pressure which is 92 kPa during the experiments so that an increase in the pressure drop directly shows an increase in the inlet pressure of the microchannel.

As mentioned in Section 3.3, with an increase in the flow rate, the nanofluid heat transfer performance improves. However, there is a decline in the FM values as the flow rate increases.

An optimization should be made between the heat transfer performance and the FM so that without too much increase in the pumping power, better heat transfer performance can be achieved.

Table 6. Gold nanofluid with different nanoparticle sizes

Particle size (nm)	**Electrical Power (W)**	**Maximum electrical heat flux (W/cm^2)** (±5%)	**Maximum heat flux removed by water (W/cm^2)**	**Pumping power (mW)** (±3%)	**Pressure drop (kPa)** (±5%)	**Thermal resistance (cm^2K/W)** (±16%)	**FM** (±16%)
10	0.359	36.11	15.36	0.06	35.49	1.18	6064
50	0.36	36.22	16.62	0.06	36.37	1.08	5934
100	0.366	36.82	16.93	0.06	36.01	1.06	6083

In the present study, it was shown that as the particle size increases, better heat transfer performance can be obtained with the nanofluids relative to the base fluid. However, the pumping power and the FM values should also be examined with respect to the particle size alteration. The pumping power does not change with respect to the particle size which can be observed in Table 6 where particle size effect is investigated for the nanofluid with 0.0026% volumetric concentration. During these experiments, a constant volumetric flow rate of 100 μL/min has been used. The FM values are also nearly the same with respect to the particle size. This is an expected result because the electrical heat flux and pumping power values are nearly equal for different particle sizes. To sum up, the heat transfer performance of the gold nanofluid can be improved without any additional pumping power requirement by increasing the particle size of the nanoparticles.

Table 7. Gold nanofluid with different particle volumetric concentrations

Particle volumetric concentration (%) (±5.88%)	**Electric power (W)**	**Maximum electrical heat flux (W/cm^2)** (±5%)	**Maximum heat flux removed by water (W/cm^2)**	**Pumping power (mW)** (±3%)	**Pressure drop (kPa)** (±4%)	**Thermal resistance (cm^{2}K/W)** (±16%)	**FM** (±16%)
0.00065	0.365	36.72	25.7	0.074	44.37	1.07	4933
0.0026	0.37	37.42	25.8	0.067	40.41	1.06	5519
0.0052	0.37	37.22	26.2	0.064	38.00	1.05	5838

To determine the relation between the nanofluid volumetric concentration with the pumping power and FM, a nanofluid with 50 nm particles have been used at 100 μL/min volumetric flow rate. The changes in the pressure drop are very close to each other; the pressure drop values for the nanofluids with the highest volumetric concentrations are even in the uncertainty band. Due to the low volumetric concentration of the nanofluids used in this study, a distinct trend between pressure drop and nanofluid concentration could not be observed. Zhou et al. [11] also draw similar conclusion and report that at low concentrations, the effect of nanoparticle concentration on the pressure drop was not clear.

From Table 7, it can be observed that at higher volumetric concentrations an increase in concentration causes an increase in the FM value. It should be mentioned that this trend is observed in stable nanofluids so that there is not any agglomeration or sedimentation with an increase in the nanofluid concentration. In a well dispersed suspension, the volumetric concentration will cause an increase in the heat transfer coefficient without an increase in the pumping power. The results indicate the importance of the stability of nanofluids even at low volumetric concentrations.

CHAPTER 4

SILVER NANOFLUID EXPERIMENTS AND RESULTS

Convection heat transfer and pressure drop characteristics of water based silver nanowire suspensions flowing through CMOS compatible monolithic microchannel heat sinks are investigated experimentally. Three different rectangular channels of 200 μm × 50 μm, 100 μm × 50 μm and 70 μm × 50 μm cross-sectional area are used during the experiments. The stability of the silver nanofluids is established by the added polyvinylpyrrolidone (PVP) as the surfactant. To investigate the potential heat transfer enhancement by the silver nanofluids, the experiments are performed with DI water, PVP - DI water solution, and the silver nanofluid with added PVP. Silver nanofluids used in this study has 0.375 mg/ml concentration.

4.1. Preparation of the Coolants

For this study, again DI water, PVP - DI water solution and silver nanofluid have been prepared as the three coolants. The details of the synthesis of silver nanofluid is given in Section 4.1.1. In Section 4.1.2, preparation of the PVP – DI water solution is explained.

4.1.1. Synthesis of Silver Nanofluid

Silver nanofluid used in this study has been produced by Şahin Çoşkun and Doğa Doğanay in METU METE NANOLAB of Dr. H. Emrah Ünalan.

In the first stage, silver nanowires have been produced and then the suspension of the silver nanowires are prepared.Silver nanowires have been synthesized according to the procedure we reported elsewhere [49]. In a typical synthesis, 10 mL of 0.45 M (molarity) ethylene glycol (EG) solution of PVP (MW = 55 000 g/mol) is prepared and 7 mg of NaCl (99.5%) is added into the solution. Following this step, the solution is heated at 170°C in a two-necked round flask. In the meantime, a 0.12 M $AgNO_3$ (99.5%) solution in 5 mL of EG is prepared and added drop-wise into the PVP solution by an injection pump at a rate of 5 mL/h. The solution is stirred at a rate of 1000 rpm by a magnetic stirrer during the whole process. Upon the completion of drop-wise addition, the nanowire solution is annealed for further 30 min at 170°C and finally air-cooled to room temperature. Then, in order to separate polymer from the Ag nanowires, the solution is diluted with acetone (in a ratio of 1:5) and centrifuged two times at 8000 rpm for 20 min.

After that, the nanowires are dispersed in ethanol and again centrifuged at 8000 rpm for 20 min. The final product is dispersed in DI water for further characterization and processing. All chemicals used in this synthesis were purchased from Sigma-Aldrich were of analytical grade and used without further purification. Silver nanowires are dispersed in DI water and the nanowire concentration is determined via a micro balance.

After the synthesis of the silver nanofluid, its flow through the microchannel is tested. In the experiments with spherical gold nanoparticles, there was no problem with the flow of the nanofluid. However, the flow of silver nanowires through the microchannel was expected to be more problematic due to elongated shapes. Therefore before the experiments a flow test has been performed.

An initial microchannel test with the prepared silver nanofluid sample indicated an uncontrollable pressure increase at the inlet of the channel. The increased in the inlet pressure of the 100 μm × 50 μm channel while silver nanofluid with a 0.125 mg/ml concentration flowing is plotted in Figure 29.

This pressure increase implied a clogging problem which caused a blockage in the channel. The reason behind the blockage is found to be the length of the silver nanowires.

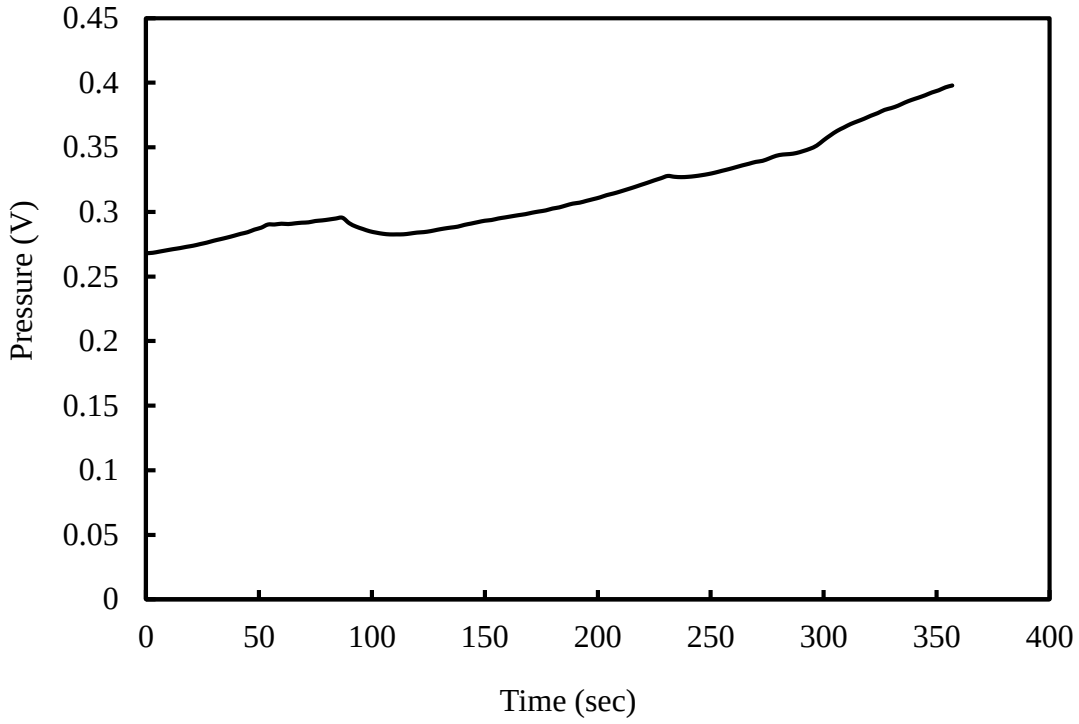

Figure 29. Pressure drop during the flow of the silver nanofluid

The diameters of the silver nanowires ranged between 50 nm – 100 nm which is illustrated in Figure 30. The length distribution of the nanowires was from 5 μm to 18 μm which is shown in Figure 31. The length of the silver nanowires may have caused the pressure increase in the smallest microchannel with a $70\,\mu m \times 50\,\mu m$ cross-sectional area. Any agglomeration or entangling of the silver nanowires will form a longer nanowire which will be close to the channel width and height. The agglomerated wires may stick on the channel walls and may cause a blockage at the channel inlet.

Again the silver nanowires may accumulate inside the microchannel which will act as a barrier to the fluid flow. As a solution to this problem, the usage of shorter nanowires seemed reasonable.

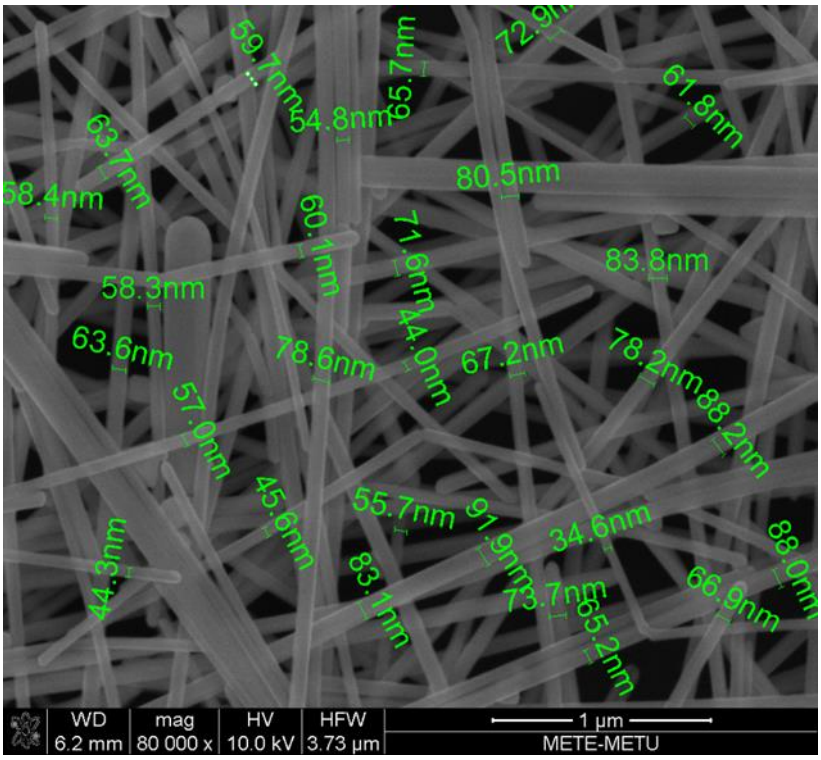

Figure 30. SEM images of dried silver nanowires after synthesis

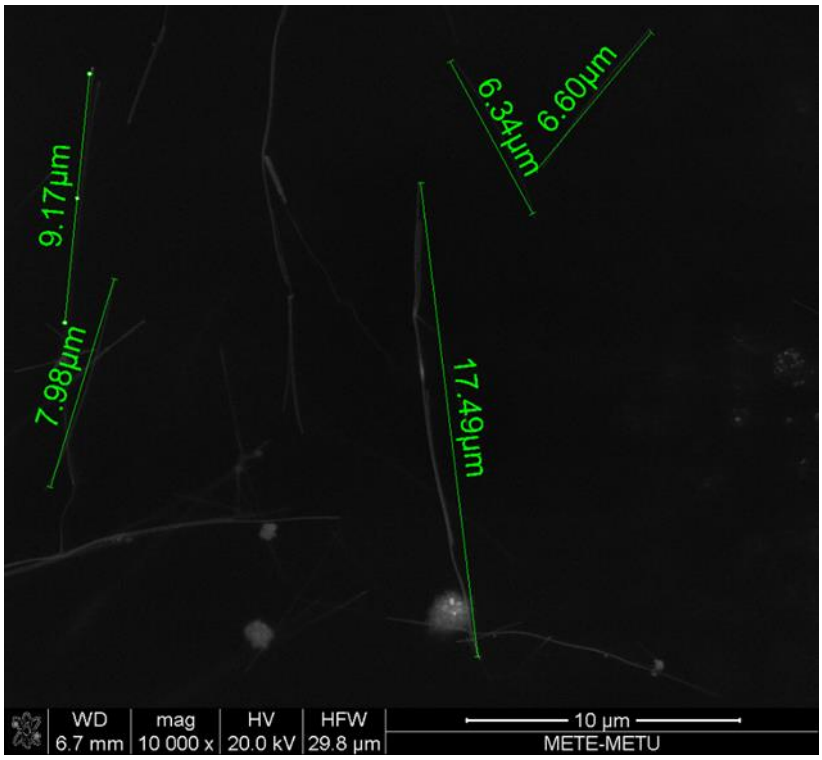

Figure 31. SEM image of dried silver nanofluid following synthesis

The silver nanowires can be shortened after the production step by using an ultrasonic tip. The ultrasonic tip not only serves for the homogenization of the suspension but it also breaks the wires so that shorter nanowires can be used in the experiments. The silver nanofluid is ultrasonicated by an ultrasonic tip for 2 hours. The SEM images of the broken silver nanowires following ultrasonication is given in Figure 32. The length distribution of the broken silver nanowires ranged between 400 nm to 2 µm. The repeated microchannel tests revealed that the shortened silver nanowires are suitable for use in the experiments as they did not cause any increase in the inlet pressure.

Initially silver nanowire concentration was 1 mg/ml, however during the tip ultrasonication, DI water has been added in the suspension to avoid overheating. The final concentration of the silver nanowires used in all experiments is 0.375 mg/ml.

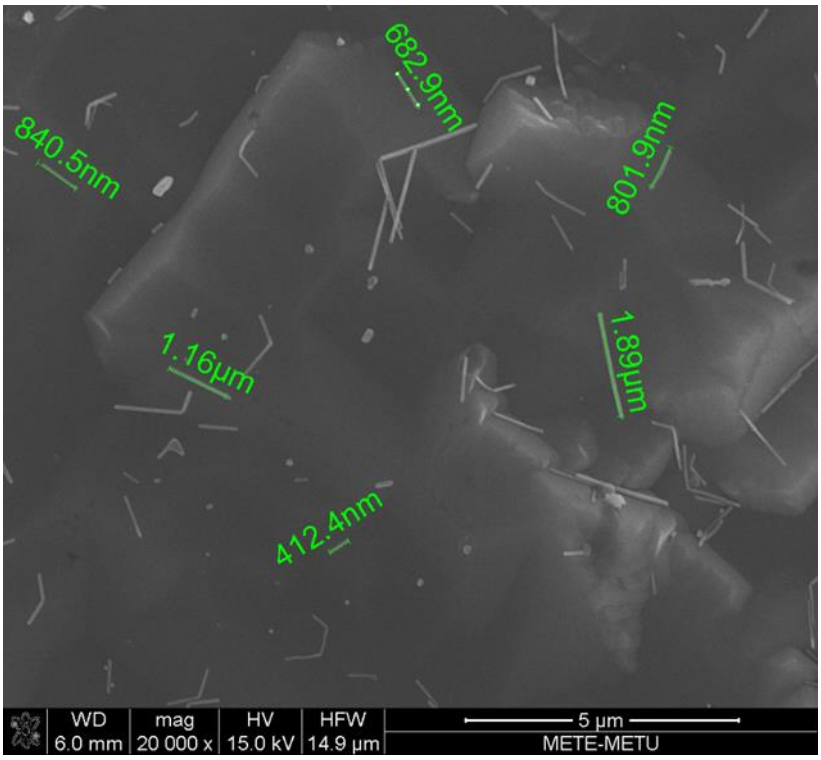

Figure 32. SEM image of broken dried silver nanowires

4.1.2. Synthesis of PVP – DI water solution

After the preparation of the silver nanofluids, the DI water - PVP solution has been prepared. As explained in Section 4.1.1, the PVP is added during the synthesis of the silver nanowires, and its amount is very little compared to the corresponding amounts reported in the literature [50,51]. The PVP layer that encapsulates the silver nanowires in the present study cannot be visualized in the SEM images as it is very thin. For silver nanowires produced with the present method the PVP layer thickness is visualized in [49] as 3 – 4 nm.

The PVP amount in the PVP - DI water solution to be prepared is calculated by assuming a 3 nm PVP layer thickness on the surface of the silver nanowires. The aim of the preparation of PVP - DI water solution is to investigate the effect of the surfactant on the heat transfer performance of the nanofluid, therefore the prepared solution contained the same amount of PVP as that in the silver nanofluid.

4.2. Stability of the silver nanofluid

The stability of the silver nanofluid is achieved by the addition of the PVP during the fabrication. In Figure 33, two nanowires that collide are seen. The wires are close to the each other, however they do not stick to each other and larger wires do not form. A similar trend is observed from the zoomed out view shown in Figure 34 so that even when more silver nanowires are screened, there is still not any agglomeration.

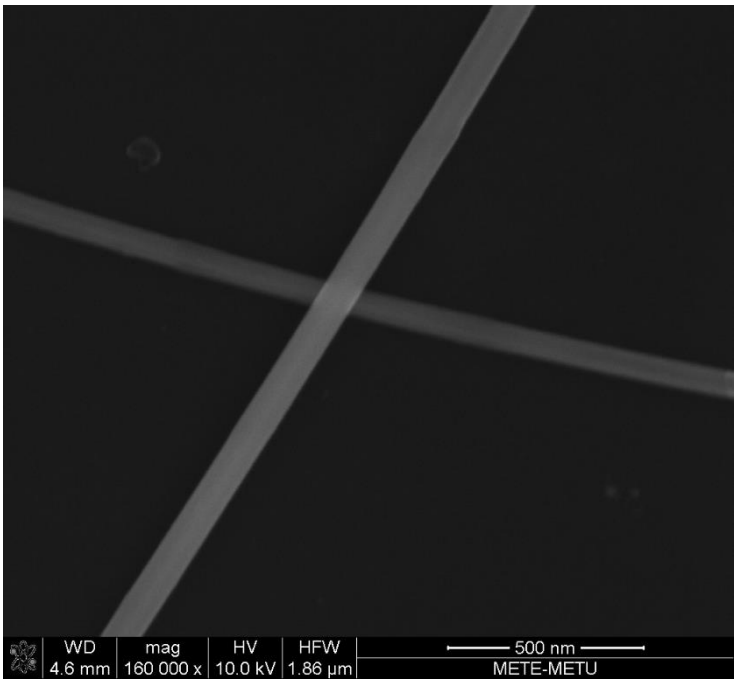

Figure 33. SEM images of the dried silver nanofluid (zoomed in view)

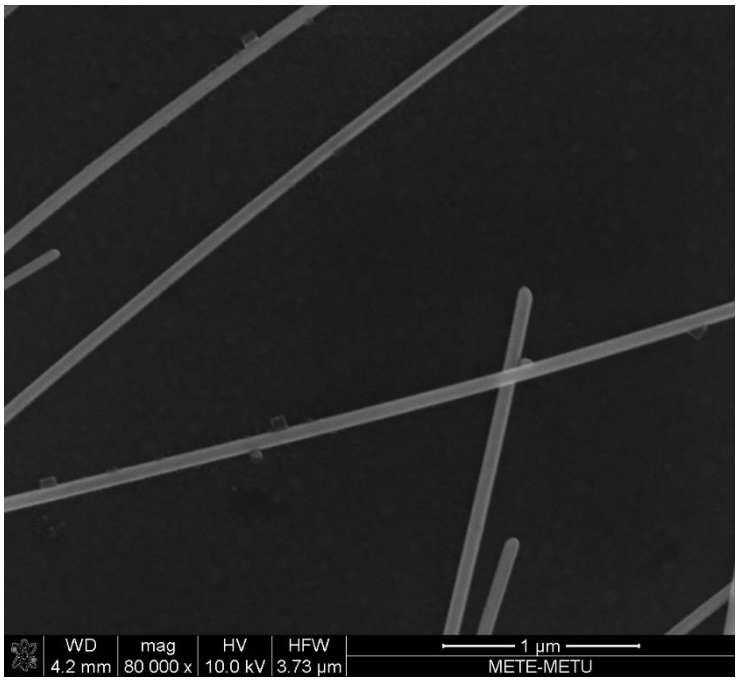

Figure 34. SEM images of the dried silver nanofluid (zoomed out view)

Sediment photography capturing method is also used in this study as a stability indicator. Photographs of the silver nanofluids before and after ultrasonication are shown in Figure 35. According to the SEM images and the sediment photography capturing, it can be concluded that the stability of the silver nanofluid is achieved with a little amount of PVP and sedimentation can be avoided just using an ultrasonic bath.

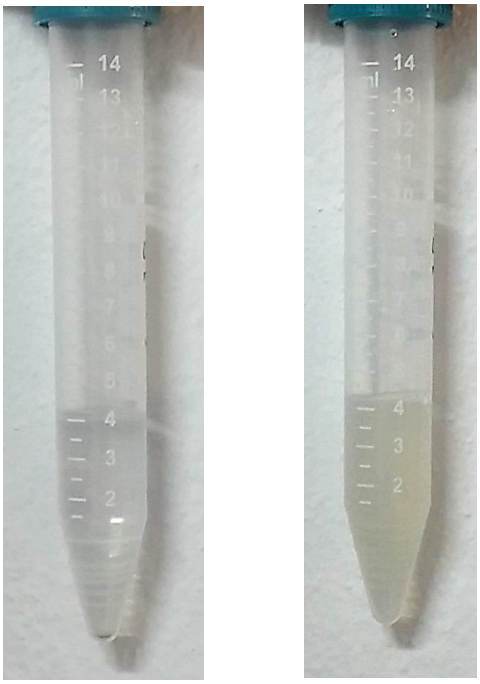

(a) (b)

Figure 35. Photographs of the silver nanofluid sediments

4.3. Assumptions

Assumptions made during the silver experiments and data analysis may be stated as follows:

- System is assumed to be at steady state and data is recorded when a stable outlet fluid temperature is reached to validate this assumption.
- Microchannel wall temperature is determined by assuming one dimensional heat conduction through the parylene layer.
- A uniform flow rate of the fluid through the microchannel is assumed.

- The flow is assumed to be fully developed both thermally and hydrodynamically. Hydrodynamic entry length and thermal entry length is calculated from Equation (18)-(19).

It is found that thermal entry length is only 9% and hydrodynamic length is 8% of the total microchannel length in silver experiments.

- For the 70 μm × 50 μm single channel microchannel four side heated area is assumed. However in the 100 μm × 50 μm and 200 μm × 50 μm single channel microchannels there is a gap in the top wall area, therefore during the calculation of the fourth area, the gap size is extracted.

- Silver nanowires uniform dispersion inside the DI water is assumed. This assumption is supported with the SEM images of the silver nanofluids given in the Figure 30 -34.

- Axial heat conduction in the fluid is neglected. This assumption is verified using Equation (26) [52].

$$\frac{l}{r_h} Pe < 20 \qquad (26)$$

In this equation, x is the axial distance, r_h is hydraulic diameter and Pe is Peclet number. Axial fluid conduction should be taken into account if this equation is satisfied. During the experiments, this equation is satisfied only in the first 15 μ of the channel length which very small compared to total channel length. Therefore, axial fluid conduction is neglected.

- During the calculations, it is assumed that pump has 100% efficiency.

4.4. Thermophysical properties of the silver nanofluid

Thermophysical properties of the silver nanofluid and PVP – DI water solution is calculated with the same procedure and the equations mentioned in Section 3.4. Only the thermal conductivity of the silver nanowires are calculated with a different equation because of their nonspherical shapes. The thermal conductivity of the nanowire suspension is calculated with the following equation [53]:

$$k_{\mathrm{nf}} = \frac{k_{\mathrm{np}} + (n-1)k_{\mathrm{bf}} - (n-1)\chi\,(k_{\mathrm{bf}} - k_{\mathrm{np}})}{k_{\mathrm{np}} + (n-1)k_{\mathrm{bf}} + \chi\,(k_{\mathrm{bf}} - k_{\mathrm{np}})}\,k_{\mathrm{bf}} \tag{27}$$

In this equation n is empirical shape factor and it is defined as

$$n = \frac{3}{\psi} \tag{28}$$

In this equation ψ is sphericity which is ratio of the surface area of the sphere at the same volume with particle to surface area of the particle.

4.5. Heat transfer coefficient results

Results of the experiments performed using the three different microchannels are presented in this section. The nanowire concentration in the silver nanofluid is 0.375 mg/ml concentration (0.00357% volume). A comparison of heat transfer coefficients obtained by DI water and the silver nanofluid is made.

4.5.1. Heat transfer results for the 200 μm × 50 μm channel

In the 200 μm × 50 μm channel, the experiments have been performed with all three coolants. The corresponding heat transfer coefficients are presented in Figure 36. All coolants are tested in volumetric flow rates between 140 μL/min to 220 μL/min. It is observed that the PVP - DI water solution yielded nearly the same heat transfer coefficient as that by DI water from 140 μL/minute to 180 μL/minute.

At higher volumetric flow rates, there is a slight difference between the two, however, the difference is within the uncertainty band. This is an expected result because of the very low PVP content of the silver nanofluid, thus the solution practically acts like DI water. Although this small amount of PVP prevented agglomeration of the nanowires, it did not cause a decrease in the heat transfer coefficient yielded by the solution. After this confirmation of the negligible effect of the surfactant, the tests are only performed using DI water and the silver nanofluids in the remaining microchannels.

In the tested flow rate range, it has been observed that the silver nanofluid has higher heat transfer coefficient than both DI water and the PVP - DI water solution. All coolants have a linear variation between the volumetric flow rate and the convective heat transfer coefficient. For the silver nanofluid, there is a steeper variation of the heat transfer coefficient with the volumetric flow rate. In this channel, a maximum heat transfer coefficient enhancement of 54% has been reached which occurred at 220 μL/min volumetric flow rate.

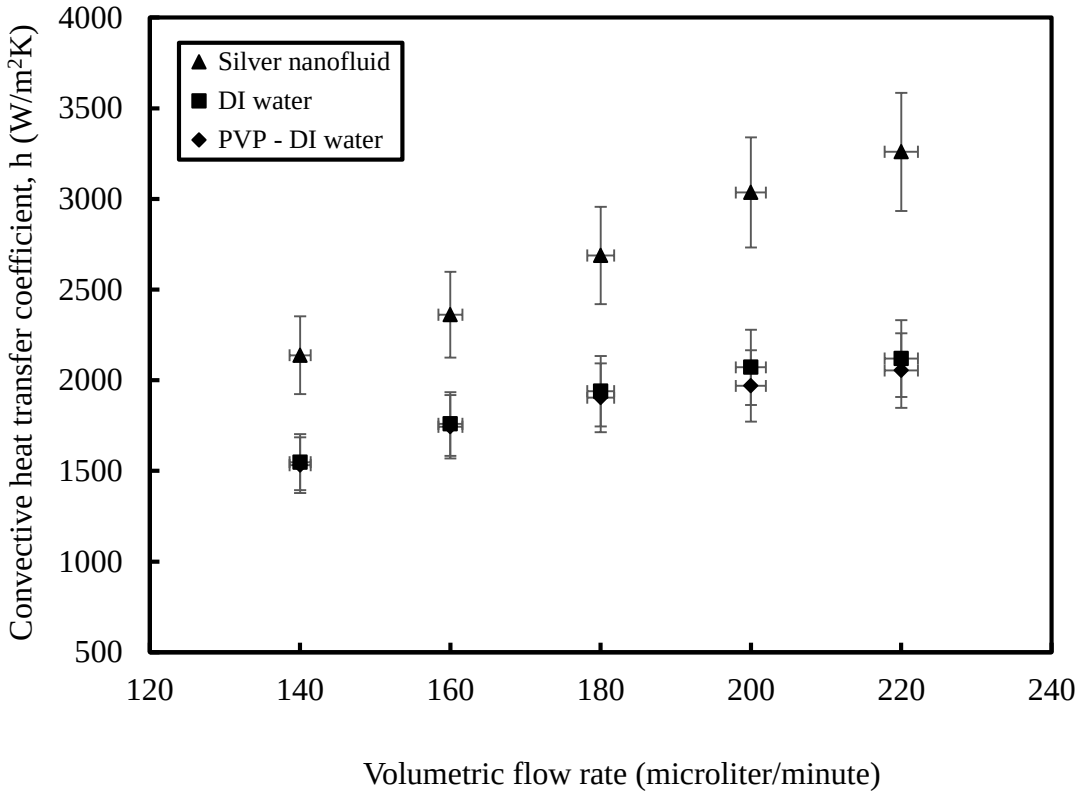

Figure 36. Convection heat transfer coefficient with respect to the flow rate for the 200 μm×50 μm channel

4.5.2. Heat transfer results for the 100 μm × 50 μm channel

In the 100 μm × 50 μm channel, experiments have been performed with DI water, and the silver nanofluid in the flow range between 140 μL/min to 220 μL/min. The respective heat transfer coefficients are plotted in Figure 37. Up to 180 μL/min flow rate, the silver nanofluid yields lower or equal heat transfer coefficient to that by DI water. This trend changes after 180 μL/min flow rate, where the silver nanofluid resulted in greater heat transfer coefficient. The maximum enhancement of 24% is observed at 220 μL/min volumetric flow rate.

The increase in the heat transfer coefficient with respect to an increase in the volumetric flow rate is steeper at lower flow rates, however, as the flow rate increases, less increase is observed in heat transfer coefficient. A limiting volumetric flow rate of around 200 μL/min could be pronounced beyond which no further improvement in the heat transfer coefficient could be attained.

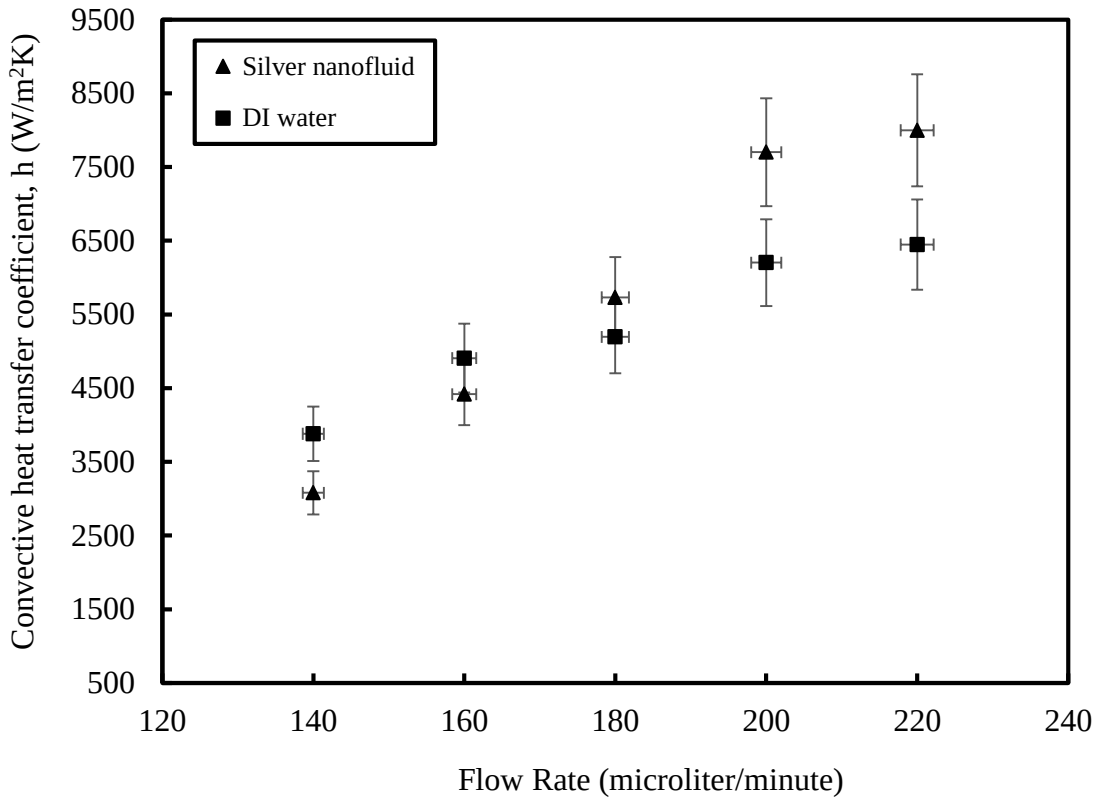

Figure 37. Convection heat transfer coefficient with respect to the flow rate for the 100 μm × 50 μm channel

4.5.3. Heat transfer results for the 70 μm × 50 μm channel

In the 70 μm × 50 μm channel, again DI water, and silver nanofluid have been tested in a flow range between 120 μL/min to 200 μL/min.

The upper limit of the volumetric flow rate decreased to 200 μL/min in this narrower channel due to the increased pumping power requirement. According to Figure 38, the silver nanofluid leads to higher heat transfer coefficients compared to DI water at all flow rates in the 70 μm × 50 μm channel. The maximum heat transfer coefficient enhancement has been 56% which is observed at 180 μL/min.

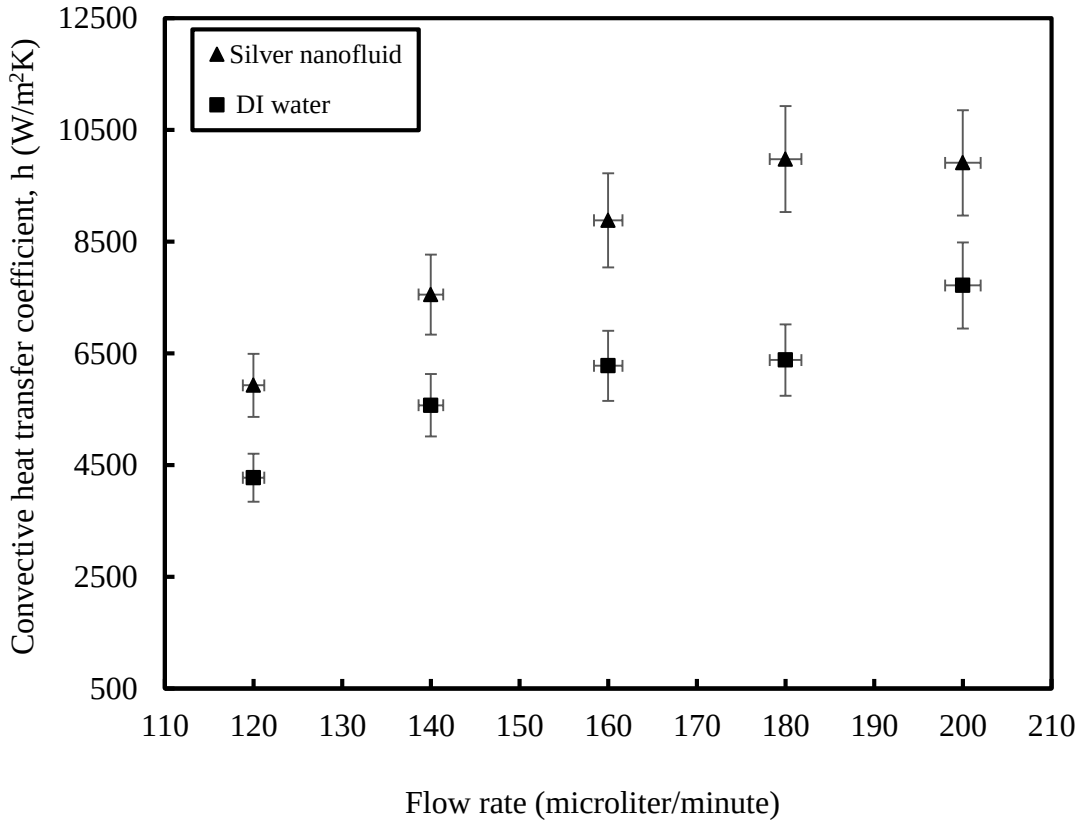

Figure 38. Convection heat transfer coefficient with respect to the flow rate for the 70 μm × 50 μm channel

4.5.4. Combined results heat transfer results for all microchannels

To understand the effect of different microchannel geometries, all experimental data for the silver nanofluid are plotted in Figure 39.

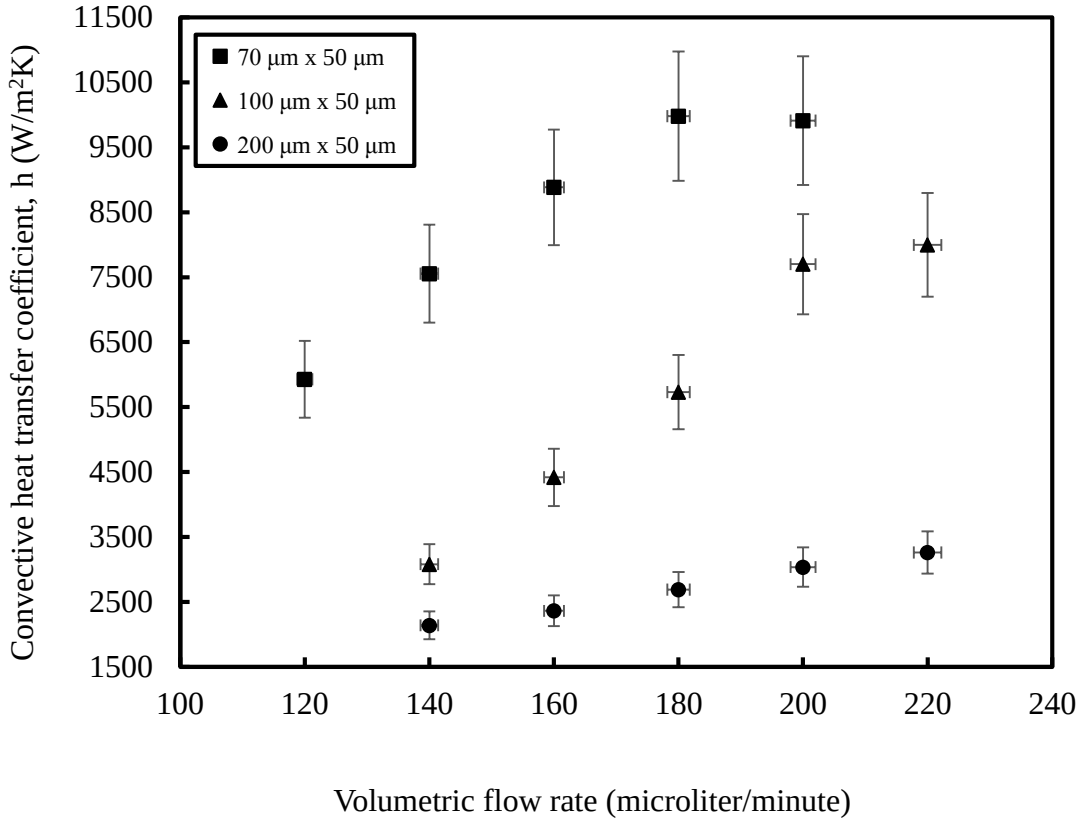

Figure 39. Convective heat transfer coefficient of different microchannel geometries

As mentioned in Section 4.5.3, the 220 μL/min flow rate could not be tested in 70 μm × 50 μm microchannel, however, the flow rate range of 140 μL/min – 200 μL/min have been tested in all microchannels.

According to Figure 39, as the cross- sectional area of the microchannel decreases, the convective heat transfer coefficient increases, expectedly ($h = Nu_D\, k\, /\, D_h$). It should be mentioned that the investigated flow rate range is relatively high for the 70 μm × 50 μm channel, while it is relatively low for the 200 μm × 50 μm. Higher flow rates can be provided to the 200 μm × 50 μm channel without damaging the channel or pump so that higher heat transfer coefficients are achievable in this channel. However, at the investigated flow rates, 70 μm × 50 μm channel led to the highest heat transfer coefficients.

The change in Nusselt number with Reynolds number is plotted in Figure 40 for all microchannel geometries. It is observed that as the Reynolds number increases, there is an increase in the Nusselt number. It is observed that at the same Reynolds number value, different channels have nearly equal Nusselt number values.

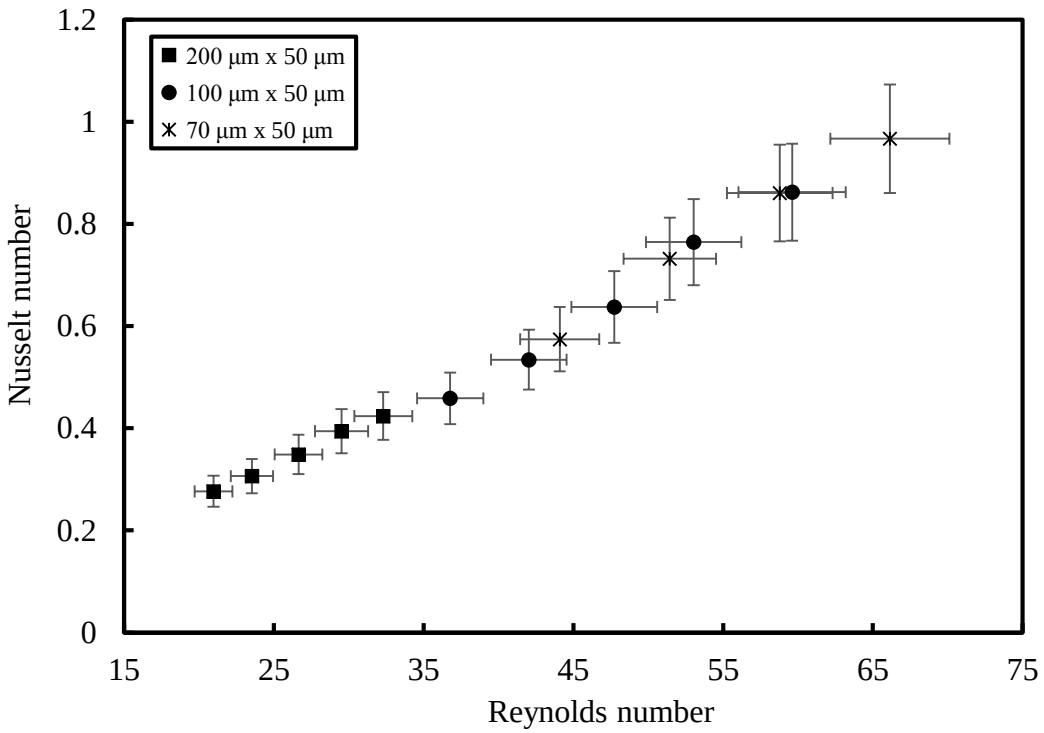

Figure 40. Nusselt number values of different microchannel geometries with respect to Reynolds number

In this study, experiments are performed in a relatively low Reynolds number range, therefore flow is assumed to be laminar. However, it is observed that Nusselt number is not constant, it changes with respect to Reynolds number. This behavior is observed in turbulent flow, rather than laminar flow. In an earlier study [54], Dittus-Boelter correlation was used as a reference for nanofluid flow through microchannels in low Reynolds number range. With the same reasoning, Nusselt number variation in the present study is compared with that estimated by Dittus-Boelter correlation given by [55] that is used for turbulent flow:

$$Nu = 0.023 Re_D^{4/5} Pr^{0.8} \quad (29)$$

The results are shown in Figure 41. It is seen that experimental results are parallel with those by Dittus Boelter equation. Nanoparticles may lead to turbulent-like flow due to the motion of the particles during the flow. However, there is difference between the experimental results and Dittus Boelter correlation results. This difference may be due to the overestimated thermal conductivity values of the nanofluids used to estimate the experimental Nusselt numbers. Thermal conductivity of the silver nanofluids is not measured experimentally, they are estimated using Equation (27) developed for nonspherical particles. These theoretical thermal conductivity values may be higher than their real values which cause a decrease in Nusselt number. If the measured thermal conductivity values can be used, experimental Nusselt number values will be closer to the Nusselt numbers obtained from Dittus Boelter correlation.

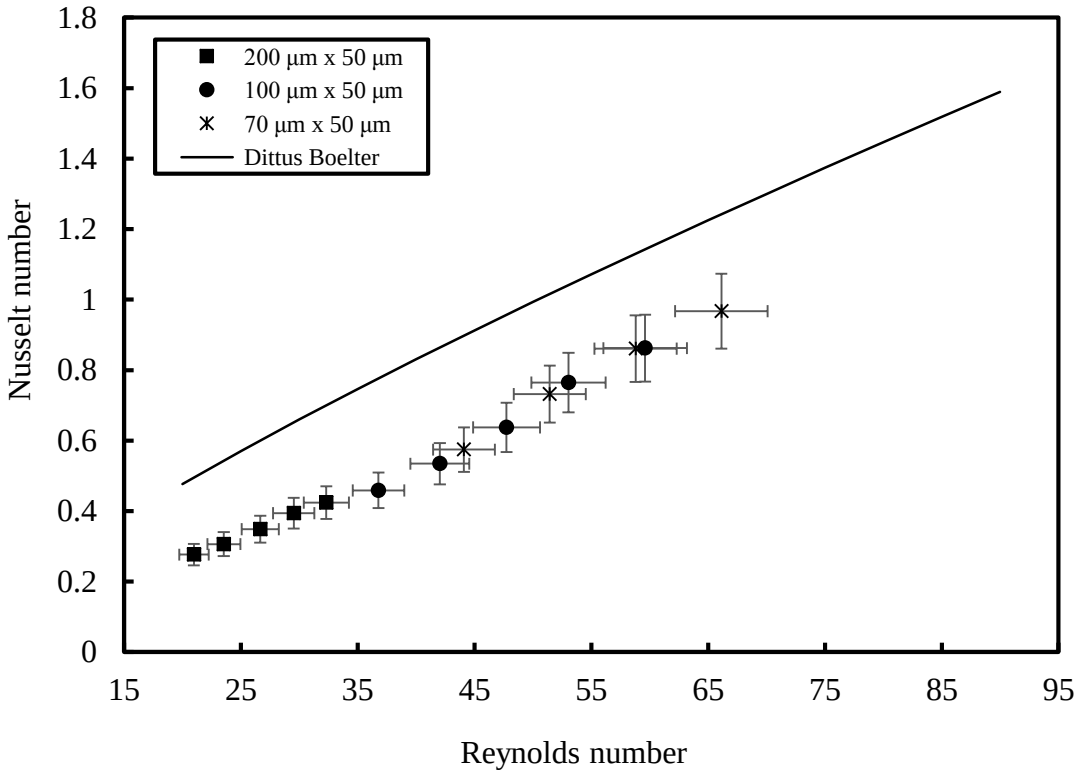

Figure 41. Nusselt number comparison with Dittus Boelter correlation results

4.6. Hydrodynamic performance

One major drawback of the nanofluid usage is the high pumping power requirements relative to the base fluid due to added nanoparticles and surfactants [56,57]. For this reason, the pumping power, friction factor, thermal resistance, pressure drop and FM values for each channel have been estimated.

4.6.1. Hydrodynamic performance of the 200 µm × 50 µm channel

In Figure 42, the pumping powers for the DI water, PVP - DI water solution and the silver nanofluid with respect to their volumetric flow rates are given. In the investigated flow rate range, all three coolants required equal pumping powers at a given flow rate.

This is a significant advantage of the silver nanofluids prepared in the present study. Although nanofluids are usually expected to require higher pumping powers, the silver nanofluid used in the present experiments did not as it has a very low surfactant and nanowire concentration. Lie et al. [58] also mentioned that at low volumetric concentrations, nanofluids did not cause an increase in the pumping power.

The pumping power values for the 200 μm × 50 μm channel are very small due to its large cross-sectional area especially relative to 70 μm × 50 μm channel but to make a comparison, the same flow rates have been applied regardless of the channel cross-sectional area.

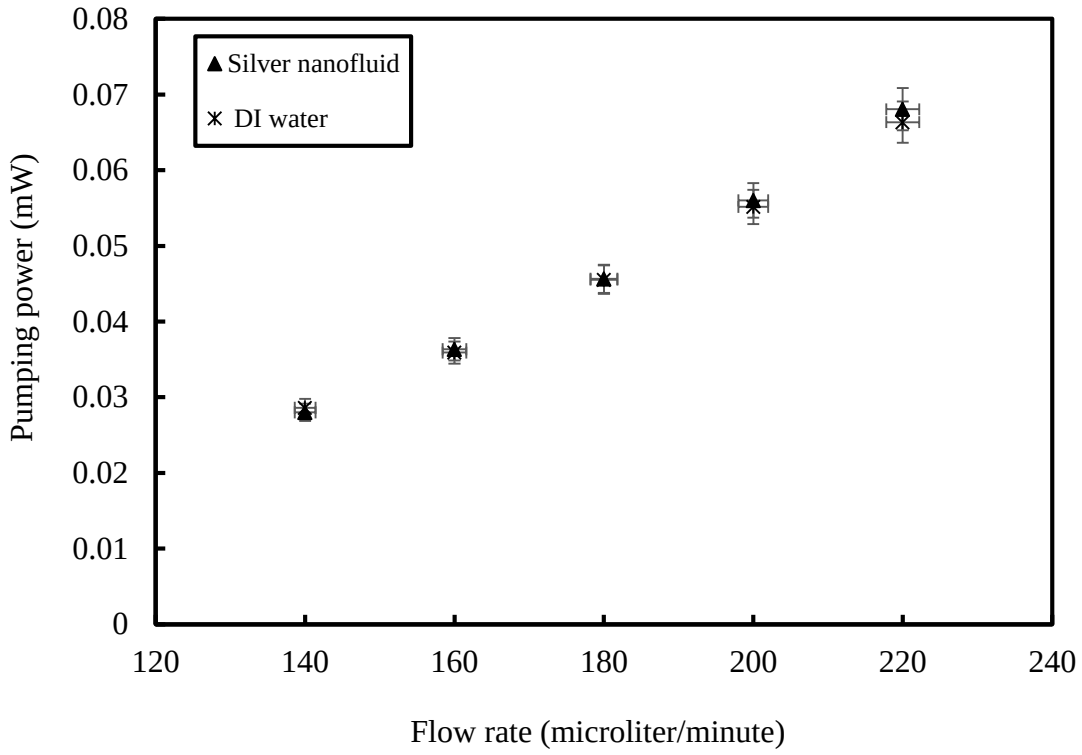

Figure 42. Pumping power with respect to volumetric concentration for 200 μm × 50 μm channel

The pressure drop, thermal resistance and FM values for the 200 μm × 50 μm channel have also been calculated. The results for DI water, PVP - DI water solution and silver nanofluid are tabulated in Table 8 –10, respectively.

It is observed that at a given flow rate the silver nanofluid has the highest, and the PVP - DI water solution has the lowest FM values. It should be noted, however, that the FM values are close to each other for the three coolants considering the uncertainty.

The same voltage has been applied across the heaters for each and every experiment, therefore, at a given pumping power, a variation in FM is purely due to the variation in electrical heating which changes only due to the current change through the resistance heaters. The current varies due to changes in the heater resistances, and that results from the temperature change of the heaters, hence the walls. A higher FM at a given pumping power, therefore, implies a higher electrical heating and lower thermal resistance.

As the flow rate increases, the thermal resistance, a commonly used comparison criterion, decreases because more heat is transferred reducing the maximum temperature along the channel wall.

For the comparison to be fair, the thermal resistance values should be compared at equal pumping powers. When the three coolants of the present study are considered, it can be concluded that the silver the nanofluid has the lowest thermal resistance at a given flow rate and pumping power. This indicates that if an equal pumping power is applied, the silver nanofluid will absorb more heat and reduce the working temperature of the system, therefore is more favorable than the base fluid.

Table 8. DI water results in single 200 μm × 50 μm channel

Flow rate (μl/min) (±1%)	**Electrical power (W)**	**Maximum electrical heat flux (W/cm^2)**	**Maximum heat flux removed by water (W/cm^2)** (±5%)	**Pumping power (mW)** (±8%)	**Pressure drop (kPa)** (±8%)	**Thermal resistance (cm^{2}K/W)** (±16%)	**FM** (±17%)
140	0.14	4.93	3.52	0.029	12.21	2.48	4894
160	0.14	4.93	3.85	0.036	13.41	2.41	3899
180	0.14	4.93	4.09	0.045	15.11	2.34	3074
200	0.14	4.93	4.33	0.055	16.46	2.33	2538
220	0.14	4.93	4.43	0.066	18.00	2.32	2110

Table 9. PVP – DI water solution results in 200 μm × 50 μm channel

Flow rate (μl/min) (±1%)	**Electrical Power (W)**	**Maximum electrical heat flux (W/cm^2)**	**Maximum heat flux removed by water (W/cm^2)** (±5%)	**Pumping power (mW)** (±8%)	**Pressure drop (kPa)** (±8%)	**Thermal resistance (cm^{2}K/W)** (±16%)	**FM** (±17%)
140	0.13	4.57	3.57	0.027	11.35	2.73	4764
160	0.13	4.57	3.80	0.035	13.18	2.59	3683
180	0.13	4.57	4.01	0.044	14.67	2.52	2939
200	0.13	4.57	4.12	0.054	16.10	2.51	2409
220	0.15	4.92	3.85	0.068	18.32	2.24	2220

Table 10. Silver nanofluid results in 200 μm × 50 μm microchannel

Flow rate (μl/min) (±1%)	**Electrical Power (W)**	**Maximum electrical heat flux (W/cm^2)**	**Maximum heat flux removed by water (W/cm^2)** (±5%)	**Pumping power (mW)** (±12%)	**Pressure drop (kPa)** (±12%)	**Thermal resistance (cm^{2}K/W)** (±16%)	**FM** (±19%)
140	0.13	4.93	4.12	0.028	11.96	2.07	4999
160	0.13	4.93	4.49	0.036	13.58	2.05	3851
180	0.15	5.28	4.87	0.046	15.15	1.98	3066
200	0.15	5.28	5.18	0.056	16.71	1.76	2678
220	0.15	5.63	5.42	0.068	18.45	1.61	2351

4.6.2. Hydrodynamic performance of the 100 μm × 50 μm channel

The pumping power values at different volumetric flow rates of DI water and silver nanofluid are shown in Figure 43. Although it seems that DI water requires higher pumping power compared to the nanofluid at the same flow rate, the presented values are within the uncertainty band. Therefore, the pumping power requirements of the two coolants may be considered equal.

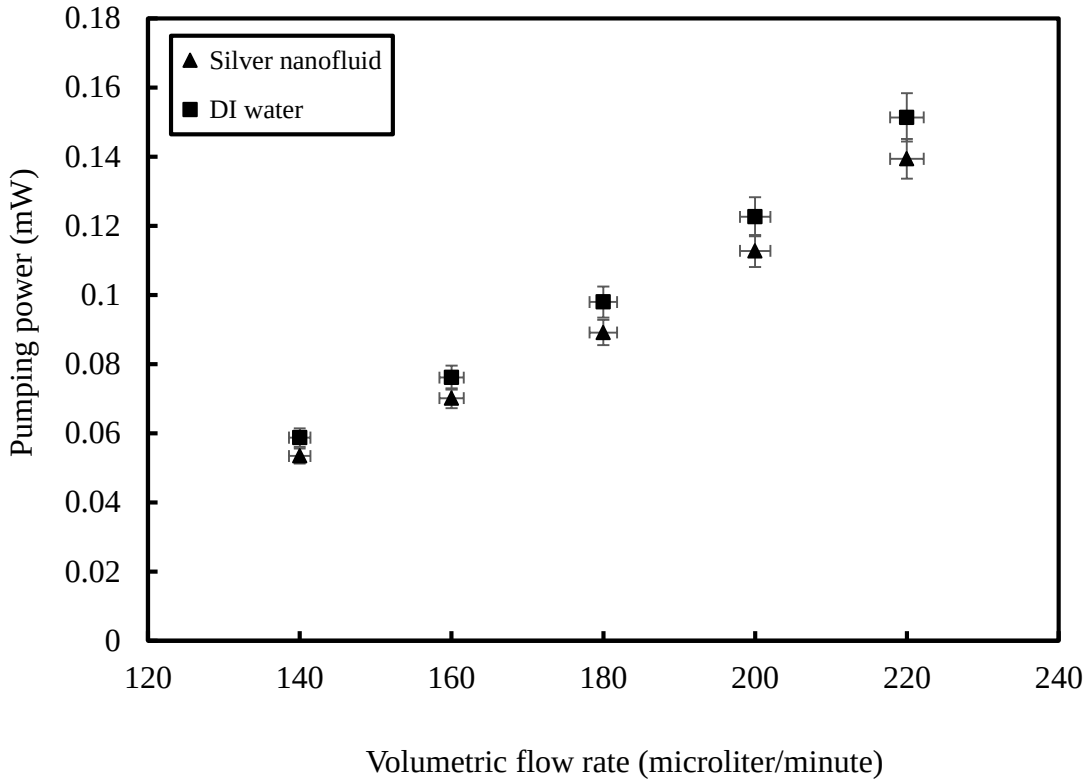

Figure 43. Pumping power with respect to volumetric concentration for 100 μm × 50 μm channel

Pressure drop values in the 100 μm × 50 μm channel are higher than those in 200 μm × 50 μm channel at the same flow rate due to reduced cross-sectional area. For the same reason, the pumping power is also higher for the 100 μm × 50 μm channel at the same flow rate.

Assuming nearly equal pumping power requirements for both DI water and silver nanofluid, the thermal resistance can become an important parameter to evaluate the performance of the working fluid. For the same pumping power, a low thermal resistance implies that the fluid will receive more heat from the system. A comparison of the thermal resistances with the two coolants can be made from Table 11 – 12.

Considering the uncertainties, the thermal resistance values with the silver nanofluid are still lower than those with DI water at the same flow rates and similar pumping powers. Furthermore, the silver nanofluid yielded higher FM values compared to DI water. These results prove that the silver nanofluid has superior thermal performance with similar hydrodynamic performance.

Table 11. DI water results in single 100 μm × 50 μm channel

Flow rate (μl/min) (±1%)	**Electrical Power (W)**	**Maximum electrical heat flux (W/cm^2)**	**Maximum heat flux removed by water (W/cm^2)** (±5%)	**Pumping power (mW)** (±4%)	**Pressure drop (kPa)** (±4%)	**Thermal resistance (cm^2K/W)** (±16%)	**FM** (±16%)
140	0.3	21.12	14.13	0.059	25	1.56	5109
160	0.3	21.12	15.28	0.076	28	1.40	3943
180	0.3	21.12	15.81	0.097	32	1.34	3063
200	0.3	21.12	16.86	0.122	36	1.27	2447
220	0.3	21.12	17.79	0.151	41	1.25	1982

Table 12. Silver nanofluid results at 100 μm × 50 μm channel

Flow rate (μl/min) (±1%)	**Electrical Power (W)**	**Maximum electrical heat flux (W/cm²)**	**Maximum heat flux removed by water (W/cm²)** (±5%)	**Pumping power (mW)** (±5%)	**Pressure drop (kPa)** (±5%)	**Thermal resistance (cm²K/W)** (±16%)	**FM** (±16%)
140	0.3	21.12	11.64	0.053	23	1.22	5617
160	0.3	21.12	13.93	0.070	26	1.18	4277
180	0.3	21.12	15.15	0.089	29	1.09	3366
200	0.3	21.12	15.94	0.113	34	0.99	2661
220	0.35	24.6	22.09	0.139	38	0.80	2152

4.6.3. Hydrodynamic performance of the 70 μm × 50 μm channel

The pumping power requirements of DI water and the silver nanofluid at different flow rates in the 70 μm × 50 μm channel are given in Figure 44. It can be concluded that to pump the silver nanofluid at the same flow rate with DI water, no additional pumping power is required. The 70 μm × 50 μm microchannel has the highest pressure drop and pumping power relative to 100 μm × 50 μm and 200 μm × 50 μm due to its smaller dimensions. Due to this limitation, the highest flow rate that could be achieved during the experiments with 70 μm × 50 μm channel was 200 μL/min.

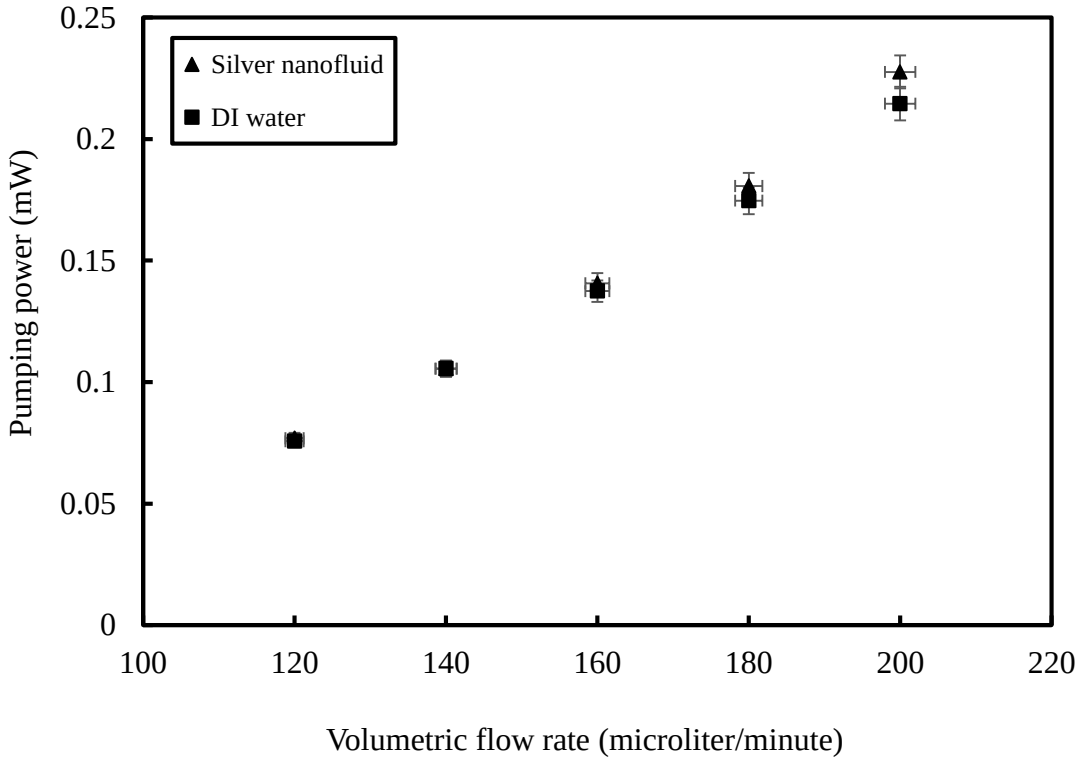

Figure 44. Pumping power with respect to flow rate for 70 μm × 50 μm channel

In Table 13 and Table 14, the thermal resistance and FM values for DI water and silver nanofluid are presented. The silver nanofluid has slightly lower thermal resistance and slightly higher FM values compared to DI water at the same flow rate. However, the differences are within the uncertainty band.

Table 13. DI water results of single 70 μm × 50 μm channel

Flow rate (μl/min) (±1%)	**Electrical power (W)**	**Maximum electrical heat flux (W/cm^2)**	**Maximum heat flux removed by water (W/cm^2)** (±5%)	**Pumping power (mW)** (±3%)	**Pressure drop (kPa)** (±3%)	**Thermal resistance (cm^{2}K/W)** (±16%)	**FM** (±16%)
140	0.3	30.18	22.90	0.075	37	1.21	3965
160	0.3	30.18	25.64	0.105	45	1.13	2842
180	0.3	30.18	28.06	0.137	51	1.09	2182
200	0.32	32.19	30.15	0.175	58	1.02	1832
220	0.32	32.19	31.82	0.215	64	0.95	1491

Table 14. Silver nanofluid results of single 70 μm × 50 μm channel

Flow rate (μl/min) (±1%)	**Electrical Power (W)**	**Maximum electrical heat flux (W/cm2)**	**Maximum heat flux removed by water (W/cm2)** (±5%)	**Pumping power (mW)** (±3%)	**Pressure drop (kPa)** (±3%)	**Thermal resistance (cm^{2}K/W)** (±16%)	**FM** (±16%)
140	0.3	30.18	23.89	0.077	38	1.16	3903
160	0.3	30.18	26.96	0.106	45	1.12	2843
180	0.35	35.21	29.51	0.141	52	0.92	2488
200	0.35	35.21	31.36	0.181	60	0.87	1937
220	0.35	35.21	33.35	0.227	68	0.86	1537

CHAPTER 5

CONCLUSIONS AND FUTURE WORK

5.1. Summary

In this study, the thermal and hydrodynamic performances of nanofluids through microchannels have been experimentally investigated. Two different nanofluids have been considered: dispersions of spherical gold nanoparticles, and silver nanowires in DI water. PVP is used as the surfactant in preparing both nanofluids. The gold nanofluid is a custom made commercial product of Nanocomposix Inc., and the silver nanofluid has been prepared at the METU METE Nanolab of Dr. H. Emrah Ünalan.

Experiments have been conducted using rectangular microchannels of 1.42 cm length and 50 μm height with three different widths of 70 μm, 100 μm and 200 μm. The microchannels have been fabricated by the Ph.D. student Aziz Koyuncuoğlu at METU-MEMS center under the guidance of Dr. Haluk Külah.

The experimental setup consisted of a syringe pump for the fluid circulation, two DC supplies to heat the channel walls, and to actuate the pressure transducers, and a DAQ system. Thermocouples and RTDs have been used for fluid and wall temperature detection, and absolute pressure transducers measured the pressure drop through the microchannels during the experiments.

The effects of the microchannel dimensions, surfactant, nanofluid concentration, nanoparticle size, and the volumetric flow rate on heat transfer coefficient, and pressure drop, hence pumping power have been explored. In addition, the stabilities of the gold and silver nanofluids have been investigated using sediment photography capturing as well as SEM and STEM imaging.

The results have been presented in two different chapters. In Chapter 3, results of the gold nanofluid are given. The experiments with gold nanofluid have been performed in a single channel of 70 μm width.

In Chapter 4, the results for silver nanofluid have been presented. In the silver nanofluid experiments, three different microchannels having different widths of 200 μm,100 μm and 70 μm have been tested.

The results obtained for the gold and silver nanofluids have been compared with those of the base fluid (DI water) and a PVP - DI water solution prepared to see the surfactant effect. DI water results have also been compared with those available in the literature.

The contribution of the present study and the main conclusions are presented in the next section.

5.2. Conclusions

Due to the improved heat transfer performance by the nanofluids compared to their base fluids, a large number of experimental and theoretical studies have been conducted on them. However, a consensus especially among the experimental results could not be obtained. Besides, experimental studies on pure metallic nanofluids are rare. Furthermore, no studies using a silver nanowire suspension has been reported in the literature. This thesis is unique in that regard.

In addition, the parameters affecting the heat transfer performance of the nanofluids are not investigated together and in detail. Moreover, the studies exploring nanofluid flow through microchannels lack the information on nanofluid stability and the surfactant effect on heat transfer of coefficient.

Interestingly, in most of the reported experimental work, uncertainty analyses have not been performed, therefore, a true assessment of the performance improvement could not be made in these studies.

In all experimental studies encountered in the literature, the performance of the nanofluid is compared with its pure base fluids rather than the surfactant added base fluid. On the other hand, it has been shown in the present study that the surfactants added for stability may significantly shade the heat transfer enhancement potential of the nanofluids. For a more fair comparison to reveal the true heat transfer enhancement by the added nanoparticles, comparisons have been made both with the base fluid and its solution with the surfactant in the present study. For this purpose, a base fluid and surfactant solution (PVP - DI water) has also been prepared. The amount of the PVP in the gold and silver nanofluids differed from each other, therefore different PVP - DI water solutions have been prepared for the gold and silver nanofluid experiments.

A given nanoparticle may conditionally improve the heat transfer performance as in the case of gold nanofluids in the present study. The particle size, shape, concentration, surfactant amount, flow conditions all affect the performance. This also explains the discrepancies among the results reported in the literature. Considering that the surfactants are essential for the long term maintenance of superior nanofluid properties, a wise judgement is needed in terms of the required conditions for heat transfer enhancement with respect to the pure base fluid which is the main motivation behind the nanofluid usage.

Experimental results indicated that microchannel cooling is an attractive option, if challenges related to fabrication and system integration can be overcome. The results of the nanofluid tests indicated that even low concentration nanofluids at a low Reynolds number range may yield heat transfer enhancement, and an optimum combination of the parameters can be found where nanofluids have better performance than their pure base fluids.

Further conclusions obtained from this study may be stated as follows:

- A comparison in the heat transfer behavior of DI water and PVP - DI water solution revealed that heat transfer coefficient changes with respect to the amount of the surfactant. The PVP amount was very high in the commercial gold nanofluid relative to the homemade silver nanofluid. For this reason, the base fluid always showed better heat transfer performance than the surfactant added solution (with the same surfactant amount in the gold nanofluid) at a given flow rate. Whereas the PVP - DI water solution prepared with the same amount of the PVP as in the silver nanofluid showed equal heat transfer performance compared to pure DI water. This is an expected results since the amount of the PVP in the silver nanofluid is very low. The amount of the PVP in the silver nanofluid is an optimum value that provides stability of the nanofluid while it does not cause any decrease in the heat transfer coefficient.

- Although it can be concluded that the gold nanofluids enhance heat transfer performance with respect to PVP - DI water solution, the same conclusion cannot always be drawn when a comparison is made with the pure base fluid. The particle size and the flow rate are two very important parameters affecting heat transfer enhancement.

- In the gold nanofluid, it has been observed that as the nanoparticle size suspended in the base fluid increases, the heat transfer coefficient also increases. The heat transfer coefficient with the gold nanofluid is greater than that with PVP - DI water solution for all sizes of the nanoparticles, however, it is greater than that with pure DI water for nanoparticle diameters greater than 50 nm.

- For very low volumetric concentrations of gold nanofluids, the heat transfer performance does not alter with respect to volumetric concentration. After a limiting value, an increase in the heat transfer coefficient with an increase in the volumetric concentration has been observed.

- During the gold nanofluid experiments, flow rates ranging from 100 μL/min to 160 μL/min have been applied. Even with a small increment in the flow rate, an enhancement in the heat transfer coefficient with the nanofluids could be achieved. Since nanofluids with 10 nm particles were used in the flow rate experiments, higher heat transfer coefficients relative to the pure base fluid could not be obtained. It is observed that in low volumetric concentrations, at low Reynolds numbers nanoparticle size is more dominant than the volumetric flow rate.

- For the gold nanofluid, the measured friction factor and the theoretical one are close to each other, their ratio being nearly 1.

- During the gold nanofluid experiments, it has been observed that the pumping power increases with an increase in the flow rate, and a decrease in the volumetric concentration. The pumping power and the FM values do not change with respect to the particle size.

- A long term stability of over 4 years has been demonstrated for the gold nanofluids due to the added surfactant PVP, the drawback being the case by case reduced thermal performance compared to pure DI water. An optimization study with the objective functions being a long stable life and enhanced heat transfer may be conducted for real and feasible applications of nanofluids outside laboratories.

- Owing to the low PVP concentration, the silver nanofluid always yielded higher heat transfer coefficient compared to both PVP - DI water solution, and to pure water at a given volumetric flow rate. Therefore, the results with the silver nanofluids are even more promising.

- A higher pumping power requirement is generally expected for nanofluids, especially for those with added surfactants due to increased viscosity. However, in this study it has been observed that the prepared silver nanofluid has nearly equal pumping power requirement to that of DI water due to very low nanowire and surfactant concentrations.

It should be mentioned that even at this low volumetric concentration, the silver nanofluid showed better thermal performance than DI water, and surely than PVP - DI water solution.

- The silver nanofluid led to lower thermal resistances compared to DI water for all microchannel sizes. This proved that the prepared silver nanofluid yielded the lowest wall temperatures along the microchannels.

- A maximum enhancement of 56% has been observed in the heat transfer coefficient at 180 μL/min flow rate in the 70 μm × 50 μm channel.

- The concentrations of the surfactant and the nanowires in the nanofluid are very important two parameters that alter the heat transfer coefficient. A high volumetric concentration of the nanoparticles may increase the heat removal with the penalty of increased pumping power, hence the nanofluid usage may be questionable. This study presented a justified usage of silver nanofluids by the enhanced heat transfer at no additional cost of pumping power.

- The silver nanowires used in the study were by products of a parallel solar cell fabrication process, hence are produced at no additional cost. The results indicate that silver nanowires may be considered as promising coolants. It is observed that the silver nanofluid has better heat transfer performance than gold nanofluid. This conclusion may be drawn due to higher thermal conductivity of the silver than gold and due to the wire shape of the silver nanofluid leading to increased surface area.

- Due to its high heat capacity, water is an effective fluid for cooling application.

5.3. Future Work

During this study, numerous difficulties have been faced that can be addressed in future studies. Firstly, experiments with the microchannels should better be performed in a clean room at the same temperature and the same humidity without any dust. Microchannels are very sensitive to dust, existence of any dust causes blockage in the microchannel, and the microchannel become useless. Doing experiments in a conditioned room could solve this problem. Moreover, it is better to conduct all experiments in the same environmental conditions for a fair comparison. Especially the temperature of the test room highly affects the inlet conditions of the fluid. Therefore, stabilization of the experimental conditions is needed.

In addition, the evaluation of thermophysical properties of the nanofluids are not straightforward. If thermophysical properties of the coolants such as their thermal conductivity and viscosity are measured experimentally, more reliable results can be obtained.

Due to the different parameters such as the volumetric concentration, particle size and the shape, it will be better to measure thermal properties of the coolants just before the experiments. For example, the validation of the specific heat and thermal conductivity of PVP - DI water solution by the experiments will help one calculate the Nusselt number for this solution without making any assumptions.

According to the results obtained from this study, it can be concluded that the surfactant has an effect on the heat transfer performance of the nanofluid. Therefore, more theoretical and experimental studies should be performed on the surfactants that may validate the results of this study. Furthermore, it is observed that as the amount of the surfactant increases, it generally causes a decrease in the heat transfer performance of the nanofluid. For this reason, different methods on the synthesis of the nanofluid should be introduced minimizing the amount of the surfactant without any change in the stability.

In this study it is shown that stability of the nanofluid is a very important parameter for experimental studies. However, limited studies give information about the stability of the nanofluid. During the studies, stability of the nanofluid should be investigated and should be reported, particularly before and after experiments.

Uncertainty analysis is an important part of experimental studies. In nanofluid experiments, enhancement in the heat transfer coefficient relative to the base fluid is reported. However, in the searched literature, error bars are not shown in the plots, hence it is hard to estimate the actual improvement percentage. Therefore, the uncertainties in each experiment should be calculated and shown in the plots.

There are discrepancies in the experimental results that are tabulated in the literature. For consistent experimental studies on nanofluid flow, a joint document which includes the experimental procedure should be prepared. By the usage of this joint document, future work results can be consistent with each other.

In a future work, the nanofluid flow through the microchannels can be visualized to understand how nanoparticles/nanowires act during the flow. This way, modifications can be done in the particles shapes or concentration to obtain a better cooling performance with nanofluids in microchannels. Especially the movement of the cylindrical silver nanowires inside the channel is an interesting topic since the alignment of the wires during the flow is unknown. Besides, the visualization will show whether any touch or agglomeration of the particles occur during heating in the channel. This may also lead to a better understanding of the heat transfer enhancement mechanism by the nanofluids.

Moreover, the use of hybrid nanofluids may be considered so that cost of the nanofluid production will decrease due to decreased amount of relatively expensive metallic particles.

Finally, base fluids with higher heat capacity may be tested to observe their effects on nanofluid performance.

REFERENCES

[1] D.B. Tuckerman, R.F.W. Pease, High-performance heat sinking for VLSI, IEEE Electron Device Lett. 2 (1981) 126–129. doi:10.1109/EDL.1981.25367.

[2] S.G. Kandlikar, W.J. Grande, Evolution of Microchannel Flow Passages--Thermohydraulic Performance and Fabrication Technology, Heat Transf. Eng. 24 (2003) 3–17. doi:10.1080/01457630304040.

[3] S.U.S. Choi, J.A. Eastman, Enhancing Thermal Conductivity of Fluids With Nanoparticles, Mater. Sci. 231 (1995) 99–105. http://www.osti.gov/energycitations/product.biblio.jsp?osti_id=196525.

[4] Q. Li, Y. Xuan, Convective heat transfer and flow characteristics of Cu-water nanofluid, Sci. China (Series E). 45 (2002).

[5] M. Rafati, A.A. Hamidi, M. Shariati Niaser, Application of nanofluids in computer cooling systems (heat transfer performance of nanofluids), Appl. Therm. Eng. 45-46 (2012) 9–14. doi:10.1016/j.applthermaleng.2012.03.028.

[6] S. Zeinali Heris, M. Nasr Esfahany, S.G. Etemad, Experimental investigation of convective heat transfer of Al_2O_3/water nanofluid in circular tube, Int. J. Heat Fluid Flow. 28 (2007) 203–210. doi:10.1016/j.ijheatfluidflow.2006.05.001.

[7] L. Godson, B. Raja, D. Mohan Lal, S. Wongwises, Convective Heat Transfer Characteristics of Silver-Water Nanofluid Under Laminar and Turbulent Flow Conditions, J. Therm. Sci. Eng. Appl. 4 (2012) 031001. doi:10.1115/1.4006027.

[8] P. Nitiapiruk, O. Mahian, A.S. Dalkilic, S. Wongwises, Performance characteristics of a microchannel heat sink using TiO_2/water nanofluid and different thermophysical models, Int. Commun. Heat Mass Transf. 47 (2013) 98–104. doi:10.1016/j.icheatmasstransfer.2013.07.001.

[9] S.M. Peyghambarzadeh, S.H. Hashemabadi, A.R. Chabi, M. Salimi, Performance of water based CuO and Al_2O_3 nanofluids in a Cu-Be alloy heat sink with rectangular microchannels, Energy Convers. Manag. 86 (2014) 28–38. doi:10.1016/j.enconman.2014.05.013.

[10] B. Rimbault, C.T. Nguyen, N. Galanis, Experimental investigation of CuO-water nanofluid flow and heat transfer inside a microchannel heat sink,Int. J. Heat Mass Transf. 84 (2014) 275–292.

[11] M. Zhou, G. Xia, L. Chai, J. Li, L. Zhou, Analysis of flow and heat transfer characteristics of micro-pin fin heat sink using silver nanofluids, Sci. China Technol. Sci. 55 (2012) 155–162. doi:10.1007/s11431-011-4596-5.

[12] K. Anoop, R. Sadr, J. Yu, S. Kang, S. Jeon, D. Banerjee, Experimental study of forced convective heat transfer of nanofluids in a microchannel, Int. Commun. Heat Mass Transf. 39 (2012) 1325–1330. doi:10.1016/j.icheatmasstransfer.2012.07.023.

[13] G. Duursma, K. Sefiane, A. Dehaene, S. Harmand, Y. Wang, Flow and Heat Transfer of Single-and Two-Phase Boiling of Nanofluids in Microchannels, Heat Transf. Eng. 36 (2014) 1252–1265. doi:10.1080/01457632.2014.994990.

[14] R. Nimmagadda, K. Venkatasubbaiah, Conjugate heat transfer analysis of micro-channel using novel hybrid nanofluids (Al_2O_3 + Ag / Water), Eur. J. Mech. B/Fluids. 52 (2015) 19–27. doi:10.1016/j.euromechflu.2015.01.007.

[15] P.K. Singh, P. V. Harikrishna, T. Sundararajan, S.K. Das, Experimental and numerical investigation into the hydrodynamics of nanofluids in microchannels, Exp. Therm. Fluid Sci. 42 (2012) 174–186. doi:10.1016/j.expthermflusci.2012.05.004.

[16] E. Simsek, E.B. Elcioglu, T. Okutucu-Özyurt, Stability of nanofluids- a critical review, CONV-14: International Symposium on Convective Heat and Mass Transfer, 314 (2014).

[17] Y. Hwang, J.K. Lee, C.H. Lee, Y.M. Jung, S.I. Cheong, C.G. Lee, et al., Stability and thermal conductivity characteristics of nanofluids, Thermochim. Acta. 455 (2007) 70–74. doi:10.1016/j.tca.2006.11.036.

[18] Y. Li, J. Zhou, S. Tung, E. Schneider, S. Xi, A review on development of nanofluid preparation and characterization, Powder Technol. 196 (2009) 89–101. doi:10.1016/j.powtec.2009.07.025.

[19] J. Lee, K. Han, J. Koo, A novel method to evaluate dispersion stability of nanofluids, Int. J. Heat Mass Transf. 70 (2014) 421–429. doi:10.1016/j.ijheatmasstransfer.2013.11.029.

[20] H. Setia, R. Gupta, R.K. Wanchoo, Stability of nanofluids, Mater. Sci. Forum. 757 (2013) 139–149. doi:10.4028/www.scientific.net/MSF.757.139.

[21] V. Trisaksri, S. Wongwises, Critical review of heat transfer characteristics of nanofluids, Renew. Sustain. Energy Rev. 11 (2007) 512–523. doi:10.1016/j.rser.2005.01.010.

[22] A. Ghadimi, R. Saidur, H.S.C. Metselaar, A review of nanofluid stability properties and characterization in stationary conditions, Int. J. Heat Mass Transf. 54 (2011) 4051–4068. doi:10.1016/j.ijheatmasstransfer.2011.04.014.

[23] E.B. Haghighi, N. Nikkam, M. Saleemi, M. Behi, S. a Mirmohammadi, H. Poth, et al., Shelf stability of nanofluids and its effect on thermal conductivity and viscosity, Meas. Sci. Technol. 24 (2013) 105301. doi:10.1088/0957-0233/24/10/105301.

[24] Y. Hwang, J.K. Lee, J.K. Lee, Y.M. Jeong, S. ir Cheong, Y.C. Ahn, et al., Production and dispersion stability of nanoparticles in nanofluids, Powder Technol. 186 (2008) 145–153. doi:10.1016/j.powtec.2007.11.020.

[25] R. Mondragon, J.E. Julia, A. Barba, J.C. Jarque, Characterization of silica-water nanofluids dispersed with an ultrasound probe: A study of their physical properties and stability, Powder Technol. 224 (2012) 138–146. doi:10.1016/j.powtec.2012.02.043.

[26] J. Lee, I. Mudawar, Assessment of the effectiveness of nanofluids for single-phase and two-phase heat transfer in micro-channels, Int. J. Heat Mass Transf. 50 (2007) 452–463. doi:10.1016/j.ijheatmasstransfer.2006.08.001.

[27] C.Y. Tso, S.C. Fu, C.Y.H. Chao, A semi-Analytical model for the thermal conductivity of nanofluids and determination of the nanolayer thickness, Int. J. Heat Mass Transf. 70 (2014) 202–214. doi:10.1016/j.ijheatmasstransfer.2013.10.077.

[28] H. Xie, M. Fujii, X. Zhang, Effect of interfacial nanolayer on the effective thermal conductivity of nanoparticle-fluid mixture, Int. J. Heat Mass Transf. 48 (2005) 2926–2932. doi:10.1016/j.ijheatmasstransfer.2004.10.040.

[29] L. Yang, K. Du, A thermal conductivity model for low concentrated nanofluids containing surfactants under various dispersion types, Int. J. Refrig. 35 (2012) 1978–1988. doi:10.1016/j.ijrefrig.2012.07.013.

[30] K.C. Leong, C. Yang, S.M.S. Murshed, A model for the thermal conductivity of nanofluids - The effect of interfacial layer, J. Nanoparticle Res. 8 (2006) 245–254. doi:10.1007/s11051-005-9018-9.

[31] W. Rashmi, M. Khalid, A.F. Ismail, R. Saidur, A.K. Rashid, Experimental and numerical investigation of heat transfer in CNT nanofluids, J. Exp. Nanosci. 10 (2013) 545–563. doi:10.1080/17458080.2013.848296.

[32] A. Koyuncuoglu, G. Türkakar, M. Redmond, T. Okutucu-Özyurt, H. Külah, S. Kumar, An experimental study on performance enhancement of CMOS compatible monolithic microchannel heat sinks, CONV-14: International Symposium on Convective Heat and Mass Transfer, 317 (2014).

[33] A. Koyuncuoglu, Design, fabrication, and experimental evaluation of microchannel heat sinks in CPU cooling, Thesis submitted to the graduate school of natural and applied sciences of METU, (2010).

[34] A. Koyuncuolu, R. Jafari, T. Okutucu-Özyurt, H. Külah, Heat transfer and pressure drop experiments on CMOS compatible microchannel heat sinks for monolithic chip cooling applications, Int. J. Therm. Sci. 56 (2012) 77–85. doi:10.1016/j.ijthermalsci.2012.01.006.

[35] J.-Y. Jung, H.-Y. Kwak, Fluid flow and heat transfer in microchannels with rectangular cross section, Heat Mass Transf. 44 (2008) 1041–1049. doi:10.1007/s00231-007-0338-4.

[36] X.F. Peng, G.P. Peterson, Convective heat transfer and flow friction for water flow in microchannel structures, Int. J. Heat Mass Transf. 39 (1996) 2599–2608. doi:10.1016/0017-9310(95)00327-4.

[37] H.S. Park, J. Punch, Friction factor and heat transfer in multiple microchannels with uniform flow distribution, Int. J. Heat Mass Transf. 51 (2008) 4535–4543. doi:10.1016/j.ijheatmasstransfer.2008.02.009.

[38] S.G. Kandlikar, Single-Phase Liquid Flow in Minichannels and Microchannels, Heat Transf. Fluid Flow Minichannels Microchannels. (2013) 103–174. doi:10.1016/B978-0-08-098346-2.00003-X.

[39] E. B. Elcioglu, E.Simsek, T. Okutucu-Ozyurt, Chapter 6 - Stability of nanofluids: Fundamentals, state-of-the-art and potential applications, in Microscale and Nanoscale Heat Transfer: Analysis, Design, and Appl., Editors M. Rebay and S. Kakaç, (2016) 155–181.

[40] R. Sadeghi, M.T. Zafarani-Moattar, Thermodynamics of aqueous solutions of polyvinylpyrrolidone, J. Chem. Thermodyn. 36 (2004) 665–670. doi:10.1016/j.jct.2004.04.008.

[41] D. Bolten, T. Michael, Experimental Study on the Surface Tension , Density , and Viscosity of Aqueous Poly (vinylpyrrolidone) Solutions, J. Chem. Eng. Data. 56 (2011) 582–588.

[42] A. Einstein, Eine neue Bestimmung der Molekul-dimensionen, Ann. D. Phys. 19 (1906) 289–306. doi:10.1002/andp.19063240204.

[43] R. Prasher, D. Song, J. Wang, P. Phelan, Measurements of nanofluid viscosity and its implications for thermal applications, Appl. Phys. Lett. 89 (2006). doi:10.1063/1.2356113.

[44] J.C. Maxwell, A treatise on electricity and magnetism, Oxford Clarendon Press. (1873) 360–366. doi:10.1016/0016-0032(54)90053-8.

[45] R. L. Hamilton, O. K. Crosser, Thermal conductivity of heterogeneous two-component systems, Industrial and Engineering Chemistry Fundamentals 1 (1962), 187-191.

[46] J. Sarkar, A critical review on convective heat transfer correlations of nanofluids, Renew. Sustain. Energy Rev. 15 (2011) 3271–3277. doi:10.1016/j.rser.2011.04.025.

[47] K.B. Anoop, T. Sundararajan, S.K. Das, Effect of particle size on the convective heat transfer in nanofluid in the developing region, Int. J. Heat Mass Transf. 52 (2009) 2189–2195. doi:10.1016/j.ijheatmasstransfer.2007.11.063.

[48] E. V Timofeeva, D.S. Smith, W. Yu, D.M. France, D. Singh, J.L. Routbort, Particle size and interfacial effects on thermo-physical and heat transfer characteristics of water-based alpha-SiC nanofluids., Nanotechnology. 21 (2010) 215703. doi:10.1088/0957-4484/21/21/215703.

[49] S. Coskun, B. Aksoy, H.E. Unalan, Supporting Information Polyol Synthesis of Silver Nanowires : An extensive parametric study, Cryst. Growth Des. 2 (2011) 2–5. doi:10.1021/cg200874g.

[50] W. Yu, H. Xie, L. Chen, Y. Li, Investigation on the thermal transport properties of ethylene glycol-based nanofluids containing copper nanoparticles, Powder Technol. 197 (2010) 218–221. doi:10.1016/j.powtec.2009.09.016.

[51] K.S. Suganthi, K.S. Rajan, Temperature induced changes in ZnO-water nanofluid: Zeta potential, size distribution and viscosity profiles, Int. J. Heat Mass Transf. 55 (2012) 7969–7980. doi:10.1016/j.ijheatmasstransfer.2012.08.032.

[52] G. Hetsroni, A. Mosyak, E. Pogrebnyak, L.P. Yarin, Heat transfer in micro-channels: Comparison of experiments with theory and numerical results, Int. J. Heat Mass Transf. 48 (2005) 5580–5601. doi:10.1016/j.ijheatmasstransfer.2005.05.041.

[53] S. Ozerinc, S. Kakac, A. G. Yazicioglu, Chapter 5 - Thermophysical Properties of Nanofluids, in Microscale and Nanoscale Heat Transfer: Analysis, Design, and Appl., Editors M. Rebay and S. Kakaç, (2016) 125–154.

[54] A. Sivakumar, N. Alagumurthi, T. Senthilvelan, Investigation of Heat Transfer in Serpentine Shaped Microchannel Using Al_2O_3/Water Nanofluid, Heat Transf. Res. 45 (2016) 424–433. doi:10.1002/htj.21169.

[55] T. L. Bergman, A. S. Lavine, F. P. Incropera, D. P. Dewitt, Fundamentals of Heat and Mass Transfer,7th ed. John Wiley & Sons Inc.; 2012.

[56] I. Gherasim, G. Roy, C.T. Nguyen, D. Vo-ngoc, International Journal of Thermal Sciences Heat transfer enhancement and pumping power in con fi ned radial fl ows using nanoparticle suspensions (nanofluids), 50 (2011) 369–377. doi:10.1016/j.ijthermalsci.2010.04.008.

[57] M. Mital, Analytical analysis of heat transfer and pumping power of laminar nanofluid developing flow in microchannels, Appl. Therm. Eng. 50 (2013) 429–436. doi:10.1016/j.applthermaleng.2012.07.040.

[58] J. Li, C. Kleinstreuer, Thermal performance of nanofluid flow in microchannels, Int. J. Heat Fluid Flow. 29 (2008) 1221–1232. doi:10.1016/j.ijheatfluidflow.2008.01.005.

APPENDIX A

UNCERTAINTY ANALYSIS

An uncertainty analysis has been performed for this study. Calculation of the uncertainty for an experimental study is very important during the interpretation of the results. Especially plots should have the uncertainty of the results so that uncertainty band of the results can be seen clearly. There are mainly two sources that may cause an uncertainty during the experiments: instrumentation and random variation uncertainties. Instrumentation uncertainties occur due to the instruments used during the experiments. This type of uncertainty can be calculated from the information supplied by the producer of the instruments. Random variation uncertainty may occur due to many reasons therefore it is more complicated than instrumentation uncertainties. Random variation uncertainty can be calculated from the recorded data.

Instrumentation uncertainties of the Agilent DAQ is calculated from an equation that is provided in its' user guide, pressure transducer uncertainty is calculated from the data sheet. Also pump instrumentation uncertainty is calculated by an equation. All thermocouples used in this study are T-type thermocouple and the absolute uncertainty of T-type thermocouple is 1^{o}C which is provided by the manufacturer. These instrumentation absolute uncertainties can be calculated directly.

Random variation uncertainty calculations depend on the number of sample and the standard deviation of the data.

During the calculation of the random variation uncertainty, data that is recorded when the system reaches steady state is used. Random variation uncertainty is calculated from Equation (30).

$$U_{random} = k \times \left(\frac{s}{\sqrt{n}}\right) \tag{30}$$

In this equation, s is the standard deviation, n is sample number and k is coverage factor. Coverage factor depend on the confidence level and number of the data points. Confidence level is selected as 95% but number of the data points are different in different experiments.

After calculating instrumentation and random variation uncertainty, total absolute uncertainty can be calculated from Equation (31).

$$U = U_{instrument} + U_{random} \tag{31}$$

The uncertainty values that are calculated from Equation (31) are shown in Table A.1. These values are calculated from the experiment results of a DI water flow at 220 μL/minute in the 100 μm × 50 μm channel.

Table A.1 Experimental uncertainty values for DI water flow at 220 μL/minute in the 100 μm × 50 μm channel

Variable	Measured value	Absolute uncertainty	Relative uncertainty
Flow Rate (μL/min)	220	2.2	1%
V_{PCB1} (V)	0.11	2.054×10^{-5}	0.018%
V_{PCB2} (V)	0.11	1.988×10^{-5}	0.018%
V_{PCB3} (V)	0.12	2.068×10^{-5}	0.018%
V_{PCB4} (V)	0.11	1.997×10^{-5}	0.018%
V_{PCB5} (V)	0.11	2.057×10^{-5}	0.018%
V_{PCB6} (V)	0.12	2.0969×10^{-5}	0.017%
V_{PCB7} (V)	0.11	1.142×10^{-5}	0.0104%
V_{H1} (V)	0.81	0.000182	0.0225%
V_{H2} (V)	0.82	0.000186	0.0228%
V_{H3} (V)	0.81	0.000183	0.0227%
V_{H4} (V)	0.81	0.000182	0.0224%
V_{H5} (V)	0.81	0.000183	0.0226%
V_{H6} (V)	0.81	0.000180	0.0224%
V_{H7} (V)	0.78	0.000191	0.0244%
P_{in} (kPa)	133.16	1.376	1.034%
P_{out} (kPa)	91.88	0.931	1.0128%
I_3 (mA)	24.25	0.0161	0.066%
I_5 (mA)	24.53	0.0162	0.066%

Uncertainty can propagate during the calculation of other variables. Uncertainty calculation of these variables depends on the mathematical operation that is needed to find that variable. Uncertainty of the variables that is formed by the summation or subtraction of the other variables can be found from Equation (32).

$$U_{variable} = \sqrt{\sum_{i=1}^{n} U_i^2} \tag{32}$$

In this equation U_{variable} is the absolute uncertainty of the desired variable, U_{i} is the absolute uncertainty of the used variables and n is the number of the variables.

If the variable is formed by the multiplication of division of the other variables, it will be more straightforward to use relative uncertainties of that variables during the uncertainty calculation. Relative uncertainty will be calculated from Equation (33). In this equation u_{variable} is the relative uncertainty of the desired variable, u_{i} is the relative uncertainty of the used variables and *n* is the number of the variables.

$$u_{variable} = \sqrt{\sum_{i=1}^{n} u_i^2} \tag{33}$$

The relative uncertainties that are calculated by the uncertainty propagation equations are tabulated in Table A.2. These tabulated values are for DI water flow at 220 μL/minute in the 100 μm × 50 μm channel.

During the uncertainty calculations, uncertainty in the thermophysical properties of the fluid is neglected.

Table A.2 Uncertainty analysis

	Relative Uncertainty (%)
Pressure Drop, ΔP	2.0
Hydraulic Diameter, D_h	2.5
Mass Flow Rate, $\dot{m}$	1.0
Friction Factor, f	7.3
Reynolds Number, Re	5.9
Convection Coefficient, h	9.9
Nusselt number, Nu	10.7
Pumping power, $\dot{P}$	4.1
Thermal resistance, R_{th}	16
Figure of merit, FM	16